Aus dem Institut für Biochemie und Molekularbiologie II

der Heinrich-Heine-Universität Düsseldorf

Direktor: Univ.-Prof. Dr. rer. nat. Jürgen Scheller

The Interactions of Lymphotoxin β with ADAM Proteases and Lymphotoxin α

Dissertation

Zur Erlangung des Grades eines Doktors der Humanmedizin

der Medizinischen Fakultät der Heinrich-Heine-Universität Düsseldorf

Vorgelegt von

Stephan Pieper

2026

Als Inauguraldissertation gedruckt mit der Genehmigung der

Medizinischen Fakultät der Heinrich-Heine-Universität Düsseldorf

gez.

Dekan: Univ.-Prof. Dr. med. Nikolaj Klöcker

Erstgutachter: Univ.-Prof. Dr. rer. nat. Jürgen Scheller

Zweitgutachterin: Univ.-Prof. Dr. rer. nat. Stefanie Scheu

It's all success if it's what you need. Do what you like, and do it honestly.

- Tom DeLonge

Teile dieser Arbeit wurden veröffentlicht in:

1) Gesiorowski A, Ettich J, Werner J, Wittich C, **Pieper S**, Padrini G, Behnke K, Floss DM, Lang PA, Moll JM, Scheller J. *Bispecific soluble cytokine receptor-nanobody fusions inhibit Interleukin (IL-)6 trans-signaling and IL-12/23 or tumor necrosis factor (TNF) signaling.* J Biol Chem. 2023 Nov;299(11):105343. doi: 10.1016/j.jbc.2023.105343. Epub 2023 Oct 13. PMID: 37838173; PMCID: PMC10652096.

Zusammenfassung

Zytokine sind eine vielfältige Gruppe regulatorischer Proteine. Sie beeinflussen die zelluläre Kommunikation, Entzündungsprozesse, Zellproliferation sowie -differenzierung. Die Tumor-Nekrose-Faktor (TNF)/ Tumor-Nekrose-Faktor-Rezeptor (TNFR)-Superfamilie besteht aus 19 Zytokinen und 29 Rezeptoren, die wichtige Regulatoren des Immunsystems sind. Eine Fehlregulierung dieser Superfamilie trägt zu genetischen, autoimmunen und onkologischen Krankheiten bei. Biologika, die auf die TNF/TNFRSF wirken, waren ein Meilenstein in der Behandlung schwerer Krankheiten und erforderten ein detailliertes Verständnis der betreffenden Zytokine und Prozesse. Um das therapeutische Potential der TNF/TNFRSF weiterzuentwickeln, konzentriert sich diese Arbeit auf die Charakterisierung drei spezifischer Aspekte der Lymphotoxine α und β, die zwei zentrale Mitglieder der TNF/TNFRSF sind.

Zunächst wurde die Aminosäuresequenz des murinen LTβ (mLTβ) identifiziert, die die Überführung von membrangebundenem in gelöstes mLTβ ermöglicht. Ein möglicher zugrundeliegender Mechanismus, die Interaktion mit *A Desintegrin A Metalloproteinase* (ADAM)-Proteasen (*Shedding*), wurde dabei gesondert untersucht. Außerdem wurde festgestellt, dass vier Aminosäuren (R53, R54, V55 und K57) aufgrund ihrer Ladungseigenschaften innerhalb der Sequenz besonders relevant für den Prozess sind. Positive Ladung der Aminosäuren begünstigte die Freisetzung, während negative Ladung den Prozess inhibiert. Valin, an Position 55, wurde als wichtiger Faktor identifiziert, aber auch die Nähe der Interaktionsstellestelle zur Zellmembran kann ein entscheidender Faktor sein.

Darüber hinaus wurde das induzierte und konstitutive *Shedding* von mLTβ differenziert betrachtet. Dabei zeigte sich, dass die zwei Proteasen, ADAM10 und ADAM17, eine entscheidende Rolle unter verschiedenen Bedingungen einnehmen könnten. ADAM10 ist dabei vermutlich wesentlich für das *Shedding* von mLTβ innerhalb von 24 Stunden unter konstitutiven Bedingungen, während ADAM17 mLTβ mutmaßlich innerhalb von 2 Stunden nach der Stimulation von der Zellmembran ablöst.

Zuletzt wurde der Einfluss von LTβ auf die Synthese von LTα untersucht. mLTβ scheint die Expression von mLTα zu stimulieren und somit zur Dynamik der TNF/TNFRSF beizutragen.

Zusammenfassend beleuchtet diese Arbeit die extrazelluläre Freisetzung von LTβ und den Einfluss das Zytokinnetzwerk. Die Ergebnisse tragen dabei zur Weiterentwicklung therapeutischer Strategien zur Behandlung TNF/TNFRSF-assoziierter Erkrankungen bei.

Summary

Cytokines are a diverse group of regulatory proteins. They mediate cellular communication and affect cell proliferation as well as differentiation. The Tumor Necrosis Factor (TNF)/ Tumor Necrosis Factor Receptor (TNFR) Superfamily consists of 19 cytokines and 29 corresponding receptors, which are important regulators of the immune system. Dysregulation of this superfamily contributes to genetic, autoimmune, and oncological diseases. *Biologicals* (antagonistic monoclonal antibodies) addressing the TNF/TNFRSF were a milestone in the treatment of severe diseases and demanded a detailed understanding of the regarding cytokines and processes. To further develop the therapeutic potential of the TNF/TNFRSF this work aims to characterize three specific aspects of the lymphotoxins α and β, two key members of the TNF/TNFRSF.

Firstly, the amino acid sequence of murine LTβ (mLTβ) that enables the conversion of the membrane-bound to a soluble cytokine was identified. A potential underlying mechanism, the interaction with A Desintegrin A Metalloproteinase (ADAM) proteases (shedding) was examined more closely. Furthermore, charge properties of four amino acids (R53, R54, V55, and K57) within the sequence were found to be particularly relevant in the process. Positive charge of amino acids increased the transfer of extracellular domains, while negative charge attenuated it. Valine at position 55 was identified as an important factor. But also, the proximity of the interaction sequence to the cell membrane seems to be a crucial regulatory factor.

Secondly, the induced and constitutive shedding of mLTβ was analyzed. Two proteases, ADAM10 and ADAM17, can play a crucial role for transferring membrane-bound mLTβ to its soluble form under different conditions. ADAM10 potentially mediated shedding of LTβ within 24 hours under constitutive conditions, whereas ADAM17 putatively separated mLTβ from the cell membrane within 2 hours after stimulation.

Lastly, the study investigated the influence of LTβ on the synthesis of LTα. mLTβ seems to stimulate the expression of mLTα and thereby contributes to the plasticity of TNF/TNFRSF.

In conclusion, this work provides further insights into the mechanisms of the extracellular release of LTβ and the impact of LTβ on the dynamic of the TNF/TNFRSF. The results contribute to the further development of therapeutic strategies for the treatment of TNF/TNFRSF-associated diseases.

Table of Contents

Abbreviations

Word Abbreviations

In this work, abbreviations facilitate legibility and coherence according to the following table.

Abbreviation	**Full name**
A	Adenin
ADAM10/17	A Disintegrin A Metalloproteinase 10/17
ALCAM	Activated leukocyte cell adhesion molecule (CD166)
BCA	Bicinchoninic acid
C	Cytosin
CV	Charge variant
CD	Cluster of differentiation
cDNA	Complementary DNA
Cf.	*Conferatur* (Latin “to be compared”)
CL	Cell culture lysate
Da	Dalton
DMEM	Dulbecco’s modified Eagle medium
DMSO	Dimethyl sulfoxide
dsDNA	Double Strand DNA
DV	Deletion variant
e.g.	*exempli gratia* (Latin “for example”)
ECD	Extracellular domain
EDTA	Ethylenediaminetetraacetic acid
EGF	Epidermal growth factor
ER	Endoplasmic reticulum
ERK	Extracellular signal-related kinase
ES	Embryonic stem cells
FACS	Fluorescence activated cell sorting
FADD	Fas-associated protein with death domain
FBS	Fetal bovine serum
Fig.	Figure
G	Guanin
GFP	Green fluorescent protein
h	Hour
ddH_2O	Double-distilled, autoclaved H_2O
HA	Haemagglutinin
HCl	Hydrochloric acid
HRP	Horseradish peroxidase
HVEM	Herpes virus entry mediator

Abbreviation	Full name
ICD	Intracellular domain
IG	Immunoglobulin
IKK	Inhibitor of NFκB kinase
iRhom	Inactive rhomboid-like protein
JNK	c-Jun-N-terminal kinase
LB	Lysogeny broth
LN	Lymph node
LPA	Lysophosphatidic acid
LTα	Lymphotoxin α (if not stated otherwise $LT\alpha_3$)
LTβ	Lymphotoxin β (if not stated otherwise $LT\alpha_1\beta_2$)
LTβR	Lymphotoxin β receptor
Min	Minute/-s
mLTα	Murine lymphotoxin α
mLTβ	Murine lymphotoxin β
MM	Marimastat
MW	Molecular weight
Myc	Protein tag sequence derived from human c-Myc protein (primary structure: N-EQKLISEEDL-C)
n.d.	Not detectable
NC	Negative control
NFκB	Nuclear factor kappa B
ORF	Open reading frame
p	*post* (lat. for "after"; if not stated otherwise time in hours)
p.	Page
PBS	Phosphate buffered saline
PC	Positive control
PCR	Polymerase chain reaction
pEGFP	Plasmid enhanced green fluorescent protein
PI3K	Phosphoinositide 3-kinase
PLAD	Preligand assembly domain
PMA	Phorbol 12-myristate 13-acetate
POD	Peroxidase
Rpm	Rounds per minute
RT	Room temperature; ~ 18 to 20°C
Second(-s)	s
SDM	Site-directed mutagenesis
sLTβ	Soluble lymphotoxin β
s.c.	So-called

Abbreviation	Full name
SN	Cell culture supernatant
ssDNA	Single stranded DNA
T	Thymin
TACE	TNFα converting enzyme/ ADAM17
Table	Table
TEMED	Tetramethylethylendiamine
THD	TNF homology domain
TIM	TRADD interacting motif
TM	Transmembrane
tmLTβ	Transmembrane bound lymphotoxin β
TNFR	Tumor necrosis factor receptor
TRADD	TNFR-associated death domain
TRAIL	TNF-related apoptosis-inducing ligand receptor
Tris	Trishydroxymethylaminomethane
TBS(-T)	Tris-buffered saline (with tween)
WB	Western (Immuno-)blot
WT	Wild-type
$\bar{x}$	Arithmetic mean

Amino Acid Base Code

In this work including continuous text, tables and figures amino acids are abbreviated according to the following table. Furthermore, exchanges in an amino acid sequence of proteins are abbreviated like this: X10Y (amino acid X is changed to amino acid Y at sequence position 10).

Amino acid	**Three letters amino acid code**	**One letter code**
Alanine	Ala	A
Arginine	Arg	R
Asparagine	Asn	N
Aspartic acid	Asp	D
Cysteine	Cys	C
Glutamine	Gln	Q
Glutamic acid	Glu	E
Glycine	Gly	G
Histidine	His	H
Isoleucine	Ile	I
Leucine	Leu	L
Lysine	Lys	K
Methionine	Met	M
Phenylalanine	Phe	F
Proline	Pro	P
Serine	Ser	S
Threonine	Thr	T
Tryptophan	Trp	W
Tyrosine	Tyr	Y
Valine	Val	V

List of Tables

All tables imbedded in this work can be found in the following list:

List of Figures

All figures imbedded in this work can be found in the following list:

1 Introduction

1.1 Cytokines – Function and Classification

Cytokines are an inhomogeneous group of small (~5 to 20 kDa) regulatory proteins. They are predominantly expressed by immune cells but can be synthesized by nearly all nucleated cells of the body. Cytokines mediate the cellular environment and communication by affecting cell proliferation and differentiation. They occur in a picomolar to nanomolar range and can increase up to a 1000-fold concentration upon cellular stimulation [1]. Physiologically, cytokines can be considered as messenger molecules same as tissue hormones that develop their effects in an autocrine, paracrine and endocrine manner. Cytokine receptors bind to their extracellular ligands, initiating intracellular cascades which influence protein expression and cellular behavior (Fig. 1) [2].

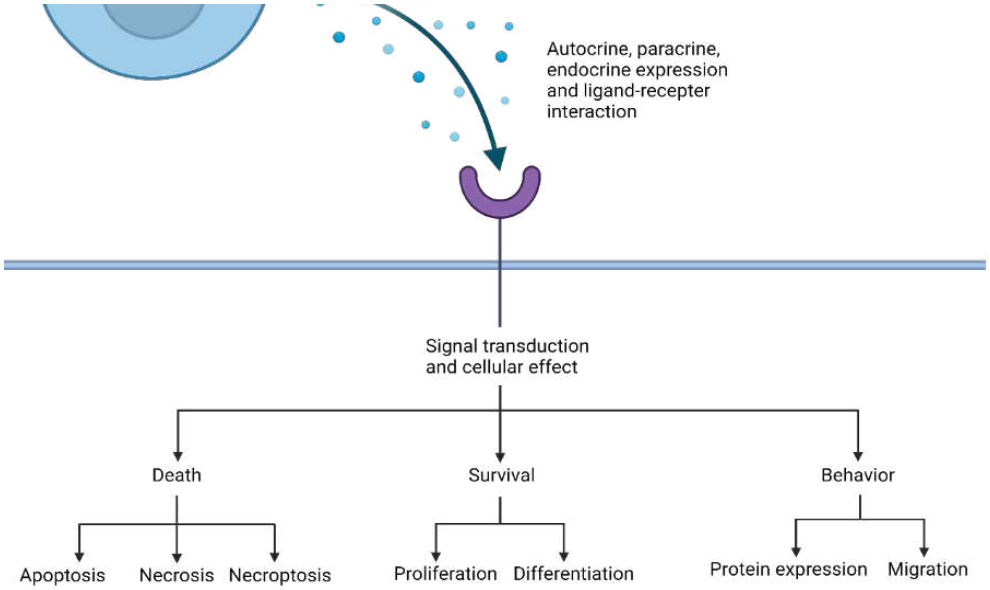

Fig. 1 ***Schematic representation of signal transduction via ligand-receptor interaction.*** *A ligand or cytokine (blue dots) is secreted by a signaling cell and binds to a specific membrane receptor (purple U-shaped structure) on the target cell. This binding event triggers the activation of intracellular signaling cascades, depicted as branching pathways below the receptor. The cascades diverge to represent the activation of various downstream signaling molecules. Each branch indicates distinct signaling pathways, potentially leading to different cellular responses. These responses may include gene expression, metabolic changes, cell proliferation, differentiation, or apoptosis, depending on the cellular context. The illustration highlights the concepts of signal amplification and pathway specificity in cellular communication through cytokines. Created with biorender.com.*

A single cytokine has numerous effects, and different cytokines can share functional as well as structural properties working in cellular homeostatic networks. Five major functional groups of cytokines have been identified: interferons, interleukins, colony-stimulating factors, chemokines, and tumor necrosis factors. They play pivotal roles in the antiviral immune response, immunological cellular communication, as hematopoietic growth factors, mediating

cellular migration and inflammatory responses. Furthermore, cytokines are classified by their chemical three-dimensional structure, their biological pro- or anti-inflammatory properties and by corresponding receptor network [2-4]. This work focusses on messenger molecules of the group of tumor necrosis factors called lymphotoxin α (LTα) and β (LTβ).

1.2 The TNF/TNFR-Superfamily

The Tumor Necrosis Factor (TNF)/ Tumor Necrosis Factor Receptor (TNFR) superfamily (TNF/TNFRSF) is a group of 19 ligands and 29 corresponding receptors [5]. The receptors are TNFRI, TNFRII, LTβR, Herpes Virus Entry Mediator (HVEM) and Decoyreceptors (DcR) [2]. Up to six extracellular cysteine-rich domains are characteristic to form the TNFR Family. The cysteine-rich domains serve as structuring elements of the receptors and enable highly specific ligand interaction [6]. Depending on the presence and function of the preligand assembly domain the receptors can form a trimer either before or after ligand binding [7]. Following ligand binding, higher-ordered oligomerization of receptor-ligand complexes occurs, initiating the formation of supramolecular signaling platforms that recruit intracellular signaling molecules [8]. The signaling cascade is mediated by adapter molecules that associate with the activated intracellular domain (ICD) of the receptor. Consequently, the TNFR superfamily can be divided into three groups, characterized by two major modes of signaling [6]. Death receptors (*e.g.*, TNFRI, TRAIL-R 1, 2, 4 and CD95/Fas) carry an intracellular death domain. This domain associates with further adapter molecules. Upon stimulation TNFR-associated death domain (TRADD) either leads to cellular apoptosis, necroptosis or promitogenic pathways [1]. The other group carries a TNFR-associated factor (TRAF) interacting motif (TIM). Different signal pathways are initiated depending on the certain TRAF. The cellular effects of this group promote cell differentiation and survival as well as immune responses[9]. The TNFRII, the LTβR and HVEM are representatives of this group [1]. The third group is made up of receptors with regulatory functions. Decoyreceptors 1 and 3 (DcR), and Osteoprotegerin are members of this group. These receptors are characterized by missing a functional ICD. Still, they compete with the receptors of the other groups for the promiscuous ligands [10].

Important ligands of the TNF Superfamily are TNFα, LTα, LTβ, Lymphotoxin homolog exhibits Inducible expression and competes with herpes simplex virus Glycoprotein D for HVEM, a receptor expressed on T cells (LIGHT; CD258) and B and T lymphocyte attenuator (BTLA). These cytokines signal via specific interaction with the TNF receptor family [10, 11] and are structurally homolog type II transmembrane proteins containing the TNF homology domain (THD). This 20 to 30% amino acid homology enables the cytokines to form non-covalently bound trimers [6]. The majority of these proteins are expressed as a membrane-bound homotrimer which can be shed by A Disintegrin A Metalloproteases (ADAMs) [12, 13]. Shed cytokines develop different functions than their bound counterparts and contribute to a variable expression profile [5]. This work focuses on LTα and LTβ, their shedding mechanism and their corresponding receptors. Fig. 2 provides an overview of the ligands and receptors of the TNF/TNFRSF and their intracellular pathways.

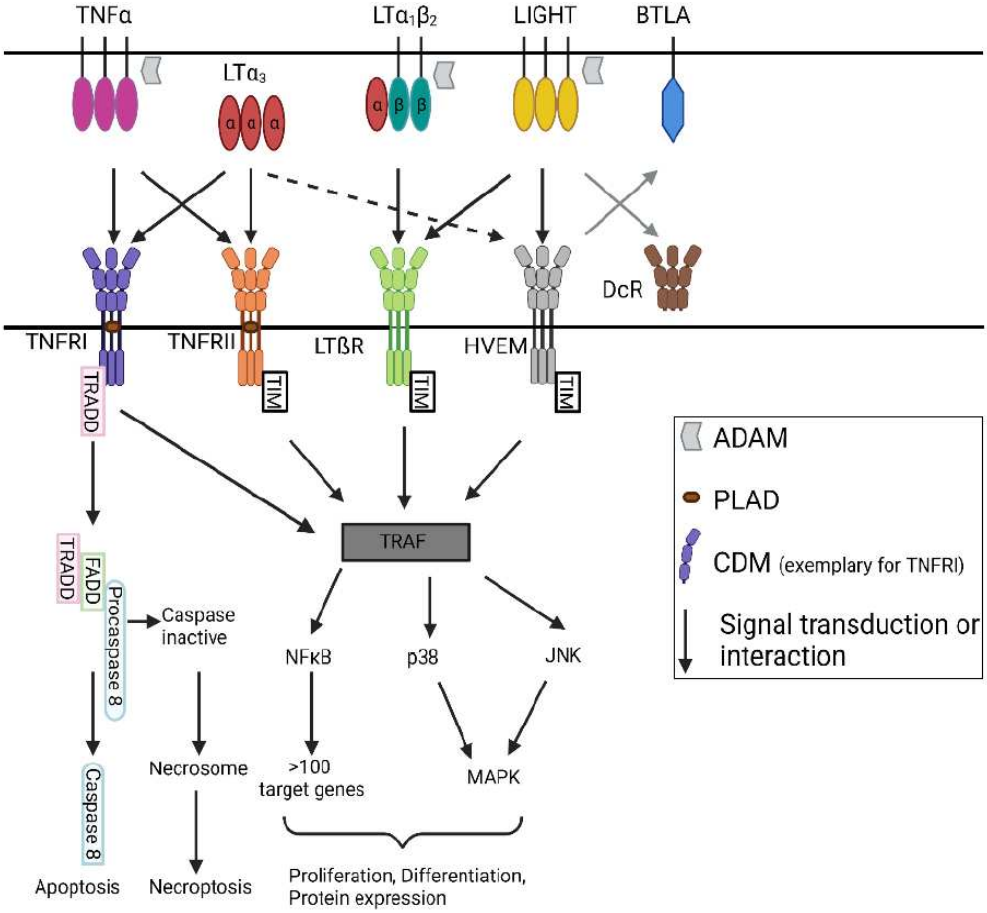

Fig. 2 ***Overview of the TNF superfamily receptor-ligand interactions and downstream signaling pathways.*** *The figure illustrates the binding of ligands (TNFα, LTα₃, LTα₁β₂, LIGHT, and BTLA) to their respective receptors (TNFRI, TNFRII, LTβR, HVEM, and DcR) on the cell surface. Upon ligand binding, receptor-specific signaling cascades are activated. TNFRI initiates apoptosis through the recruitment of TRADD, FADD, and the activation of caspase-8, while necroptosis is triggered via the formation of the necrosome. TNFRII, LTβR, and HVEM signaling primarily involve the recruitment of TRAF proteins, leading to the activation of NFκB, p38, JNK, and MAPK pathways. These pathways regulate various cellular responses, including gene expression, cell proliferation, differentiation, and survival. The figure also highlights the role of specific regulatory elements such as ADAM (a disintegrin and metalloprotease), PLAD (Pre-ligand Assembly Domain), and CDM (Cytoplasmic Domain Motif) in receptor function and signaling. Created with biorender.com.*

1.3 TNF/TNFRSF in Human Disease and Therapy

As the TNF/TNFRSF is known to essentially regulate immunity in humans, its dysregulation contributes to the development of hereditary and non-hereditary disorders[14]. Genetic studies found that mutations in the gene loci of the TNF/TNFRSF are responsible for TNF receptor-associated periodic syndrome [15, 16], type I autoimmune lymphoproliferative syndrome [17] and hyper IgM syndrome [18]. In non-hereditary diseases, the TNF/TNFRSF have been proven to play relevant roles in many autoimmune diseases [19], such as inflammatory bowel disease [20], rheumatoid arthritis [21], multiple sclerosis [14] or systemic lupus erythematosus [22]. So far, therapeutic approaches targeting the TNF/TNFRSF have presented themselves to be highly potential [19]. Table 1 presents biologicals targeting the TNF/TNFRSF, along with their respective clinical indications and the status of the clinical trial based on each indication.

TNFSF Ligand	TNFRSF Receptor	Pharmaceutical Name	Type of Molecule	Indications	Trial Status
TNFα	TNFRI, TNFRII	Infliximab	Chimeric anti-TNF mAb	Crohn's disease, ulcerative colitis, psoriasis, rheumatoid arthritis	Approved
		Adalimumab	Human anti-TNF mAb	Crohn's disease, juvenile idiopathic arthritis, psoriasis, rheumatoid arthritis	Approved
		Certolizumab	Human PEGylated F_{ab} anti-TNF mAb	Crohn's disease, rheumatoid arthritis psoriasis, ulcerative colitis	Approved Phase III Phase II
		Golimumab	Human anti-TNF mAb	Rheumatoid arthritis ulcerative colitis	Approved Phase IV
TNFα, LTα	TNFRI, TNFRII	Etanercept	Human TNFRII-F_c fusion protein	Juvenile idiopathic arthritis, psoriasis, rheumatoid arthritis	Approved
LTα	TNFRI, TNFRII, HVEM	Pateclizumab	Human anti-LTα mAb	Rheumatoid arthritis	Phase II
LTβ	LTβR	Baminercept	Human LTβR-Ig fusion protein	Rheumatoid arthritis	Cancelled in Phase II

Table 1 ***Biologicals targeting the TNF/TNFRSF, their clinical indications and trail status,*** *adapted from[23].*

1.4 The Lymphotoxin System

The ligands of the lymphotoxin subfamily are the trimeric proteins $LT\alpha_3$, $LT\beta_3$, $LT\alpha_1\beta_2$, $LT\alpha_2\beta_1$ and LIGHT. The most prominent role plays $LT\alpha_3$, which was identified as a factor produced by T lymphocytes upon viral or tumor antigen contact. It is synthesized and secreted by activated T-cells, resting B-cells, myeloid cells and to a small amount by non-hematopoietic cells. $LT\alpha_3$ is an exception of the TNF/TNFRSF because it is secreted as a soluble homotrimer, therefore it is not subject to shedding nor bound to the membrane [24]. If not stated otherwise LTα refers to the predominant homotrimer $LT\alpha_3$.

In 1992 LTβ was described as p33- a membrane anchoring protein of LTα [25]. As characteristic member of the TNF/TNFRSF it is expressed by naive splenic B-cells, $CD4^+$ T-cells and mature dendritic cells. On the cell's surface, it assembles to either a homotrimer or a heterotrimer with LTα monomers [5]. The $LT\alpha_1\beta_2$ heterotrimer is the predominant isomer over $LT\alpha_2\beta_1$ and $LT\beta_3$ and is commonly referred to as LTβ [26]. All LTβ isomers can be shed from the cell membrane and be transferred to the soluble form by ADAM17 [13]. The LTβ homotrimer and the $LT\alpha_1\beta_2$ heterotrimer have a high affinity to their receptor LTβR, while LTα and the $LT\alpha_2\beta_1$ homotrimer rather engage with the TNFRI and II (*cf.* 1.2) as well as with HVEM with a low affinity [26].

LIGHT is also a ligand of the LTβR and constitutively expressed on myeloid cells and immature DCs and can be induced by active T-cells and monocytes [27]. Its HVEM receptor can be expressed by Natural Killer (NK) cells and naive CD4+ and CD8+ T-cells. LIGHT is essential for T-cell proliferation, differentiation, and homeostasis as well as DC maturation [28].

The respective receptors of the lymphotoxins are LTβR, HVEM, TNFRI and II as well as DcR3. TNFRI is subject to LTα. The receptor is expressed constitutively and ubiquitously [5]. Signal transduction is started by the recruitment of TRADD which is an adapter molecule for further signaling complexes and can initiate contrary pathways. The TNFRI/TRADD complex leads to the assembly of various mediator proteins which predominantly initiate the canonical NFκB pathway [29]. Depending on the metabolic environment of the cell the NFκB activation is not available, and the TNFRI/TRADD complex is internalized. This leads to the recruitment of Fas-associated death domain protein (FADD) instead. FADD activates caspase 8 which either leads to apoptosis or necroptosis of the cell. Alternatively, a different mediator complex can bind to the TNFRI/TRADD complex and activate the c-Jun-N-terminal-kinase (JNK) or the p38 pathway. Even though the TNFRI belongs to the death receptors, its activation results in

promitogenic effects more often than in proapoptotic effects [5, 30, 31]. TNFRI plays a central role in the immune defense of the entire body by inducing the death of damaged cells and local as well as systemic mediation of an inflammatory response [32, 33].

TNFRII is found only on immune, neuronal and endothelial cells[34]. The receptor recruits its mediator complex without interacting with TRADD but still recruits the same signalosome as TNFRI that activates the canonical NFκB pathway. Besides that, TNFRII is able to persistently and non-canonically activate the NFκB pathway. Because of its specific expression pattern and a lower binding affinities TNFRII is suspected to play a regulatory role in local homeostasis and reinforcement of TNFRI responses [35, 36].

The LTβ Receptor (LTβR) is expressed on stromal fibroblasts, epithelial cells, hepatocytes, endothelial cells, DCs and mast cells but not on lymphocytes [37]. The signaling of LTβR can be described homologically to the signaling of TNFRII.

1.4.1 The Domains of LTα and LTβ

A mLTβ monomer is made up of four domains. The N-terminus is in the intracellular compartment (M1-T27). The following single-pass helical transmembrane domain anchors the cytokine to the cell membrane (S28-P48). After the stalk region (Q49-P154), the C-terminal extracellular part (A155-G306) is the functional domain of the cytokine [38]. Predominantly a mLTβ monomer assembles with another mLTβ and mLTα monomer to form a functional cytokine [5] (Fig. 3).

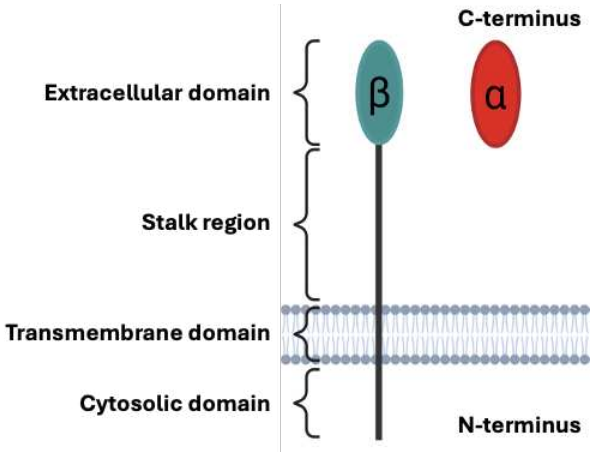

Fig. 3 ***Schematic representation of a membrane-bound mLTβ and a non-membrane-bound mLTα monomer.*** *mLTβ contains a stalk region, a transmembrane domain, and a cytosolic domain, while mLTα features a signal peptide and is localized extracellularly. created with biorender.com.*

A mLTα monomer is made up of two domains. A signal peptide (M1-G33) and a functional domain (L34-L202) [38]. It misses the stalk, transmembrane and cytosolic domain. mLTα either assembles with two mLTα monomers to form a secreted $mLT\alpha_3$ homotrimer or with two mLTβ monomers to form a $mLT\beta_2\alpha_1$ heterotrimer which can be membrane-bound or shed [5] (Fig. 3).

LTβ in its predominant and most bioactive form occurs as $LT\alpha_1\beta_2$ heterotrimer. It signals exclusively via the LTβR (Fig. 2) [39]. The $LT\beta_3$ homotrimer binds the cognate receptor but fails to induce apoptosis in the absence of LTα domains [40]. $LT\alpha_2\beta_1$ shows low affinity to LTβR but is functionally active, therefore, the β domain interacts with the receptor while the α domain regulates the structural conformation of the β domain necessary for signal transduction [40]. Mutated LTα (D50N and Y108F) is dysfunctional as LTα homotrimer. However, a $LT\alpha_1\beta_2$ heterotrimer with a mutated LTα domain is functional presuming that these α domains have two independent functions [40, 41].

LTα and LTβ are structurally and functionally connected (*cf.* 1.2). The fact that $LT\alpha_3$ homotrimer is only secreted and LTβ occurs in three isoforms ($LT\beta_3$, $LT\alpha_1\beta_2$, $LT\alpha_2\beta_1$) leads to the question of how the trimers assemble and how LTβ influences the LTα synthesis and vice versa. The heterotrimeric complexes $LT\alpha_2\beta_1$ and $LT\alpha_1\beta_2$ assemble intracellularly before post-translational modification without cell surface assembly or domain exchange [26]. Moreover, LTα monomers have a faster expression kinetic [25]. After stimulation of T-cells, the mRNA of LTα prevails LTβ mRNA. 4 h after stimulation the LTβ prevails LTα and $LT\alpha_1\beta_2$ becomes abundantly predominant [26]. Knock-out cell lines have shown that LTβ synthesis is crucially influenced by the presence of LTα. The LTβ amount decreases, and the trimer shows altered affinity to antibodies and its LTβR due to structural differences when LTα is knocked out [26, 40].

1.4.2 Functional Aspects of Lymphotoxins in Mice

Functional properties of the lymphotoxins cannot be narrowed to a single ligand-receptor interaction nor one signal pathway. Targeted deletions in mice have helped to examine the unique and complementary functions of this cytokine system [42].

LTβR$^{-/-}$ mice develop an entirely lymph-node deficient phenotype [43]. LTβ$^{-/-}$ mice always have functional but disrupted intestinal (Peyer's patches) and cervical lymph nodes while lymph nodes in other parts are completely missing. This suggests that LTβ plays a role in lymph organogenesis but its signal via the LTβR can be partly substituted [44]. Interestingly, an isolated genetic deficiency in the gen locus of LIGHT does not cause pathogenic phenotypes. Nevertheless, LIGHT is suspected to be responsible for the rescue of cervical and mesenteric lymph nodes in a LTβ$^{-/-}$ genotype since LTβ-LIGHT$^{-/-}$ double knockout mice miss all lymph nodes and LIGHT is a subordinated ligand of LTβR [45]. Moreover, the application of a LTβR-fusion protein, which blocks the interaction of LTβ and LTβR, into pregnant mice affects the lymphoid organogenesis in the offspring [46]. LTα$^{-/-}$ genotypes rarely develop any lymph follicles [47]. This shows that all lymphotoxins are involved in the lymphoid organogenesis, have redundant functions, and can partly substitute each other.

The LTβ-LTβR interaction is also critically involved in the maintenance of secondary lymphoid tissue and its function such as splenic architecture and antibody maturation [43, 48]. Anders *et. al* [49] found that LTβ, LTα and LIGHT induce hepatomegaly and heavily affect liver regeneration and DNA synthesis after partial hepatectomy (70% resection of hepatic parenchyma as a model of acute liver damage [50]). Especially T-cell LTβ was proven to be crucial for liver regeneration after partial hepatectomy. A transfer of wild-type (WT) splenocytes into T-cell-deficient mice significantly improved survival after partial hepatectomy [51]. While B-cells are essential for liver regeneration after partial hepatectomy due to their induction of CD169-positive macrophages [52], B-cell LTβ has no regenerative effect [51]. Instead, B-cell LTβ is especially important for the maintenance of splenic architecture while T-cell LTβ fulfills only a complementary role in this regard [53]. Concludingly, lymphotoxin β fulfills different functions according to the expressing cell. Table 2 shows the impact of different knockouts in the lymphotoxin system on the murine immune system.

Gene deletion (-/-)	Lymph-nodes	Peyer's patches	Splenic architecture	Liver regeneration**	Antibody maturation
Wild type (none)	+	+	+	+	+
LTα	-	-	-	-	-
LTβ	-*	-	-	-	-
LIGHT	+	+	+	+***	n.r.
LTβ, LIGHT	-	-	n.r.	n.r.	n.r.
B-cell LTβ	+****	+****	-	+	n.r
T-cell LTβ	+****	+****	+	-	n.r.
LTβR	-	-	-	-	-

Table 2 ***The lymphotoxins and the murine immune system****; absent lymph nodes, impaired antibody maturation or disrupted splenic compartmentalization, -; physiological/as WT, +; not reported, n.r; * except cervical and mesenteric lymph nodes; **10-day survival after 70% partial hepatectomy[54]; *** higher total mass in transgene animals, **** physiological but reduced in size[53]; adapted and modified from[42-44, 49, 52, 55-58].*

1.5 ADAM Proteases and Shedding of LTβ

ADAMs are a group of membrane metalloendopeptidases that belong to the metzincin superfamily. They are characterized by a particular domain organization [59]. They contain a N-terminal propeptide, followed by a metalloproteinase and the structuring disintegrin, cysteine-rich and epidermal-growth-factor-like domain. The single transmembrane domain anchors the ADAM and ends with an intracellular C-terminal tail [60]. In contrast to other metzincin proteases, ADAMs are active while membrane-bound [61]. The human genome carries 21 genes encoding for ADAMs. 13 harbor a zinc-binding site with a Met-turn which is indispensable for proteolytical activity [62, 63]. ADAMs without functional protease domains work with protein interaction. In contrast, active ADAMs are called sheddases as they shed extracellular domains of transmembrane proteins (s.c. "ectodomain shedding"). ADAM10 and ADAM17 are the two major human sheddases [63]. Protein kinase C (PKC) phosphorylation and furin-type proprotein convertase cut off the propeptide upon stimulation, thereby switching the cation orientation to the metalloproteinase domain and activating the catalytical activity [64] (Fig. 4). In the case of ADAM17 activation takes place in the trans-Golgi network and leaves it packed in lipid rafts in a submembrane standby mode [65, 66]. Upon stimulation, ADAM17 is translocated to the cell's membrane, and ectodomain shedding is initiated [67].

Stimulating factors are *e.g.*, Phorbol 12-myristate 13-acetate (PMA) *in vitro* or thrombin, TNFα, lipopolysaccharides, or caspase 3 *in vivo* [67]. The intracellular translocation and modification of ADAM17 is controlled by the inactive rhomboid protein 2 [68]. ADAM17 also has a constitutive activity but unfolds a much stronger effect upon stimulation [69, 70]. ADAM10 instead, is primarily constitutively active and does not rely on stimulation [71, 72].

Ectodomain shedding through ADAMs increases the functional abundance of cytokines and their receptors [73]. Upon shedding, cytokines can change their mode of action from autocrine to paracrine or endocrine. Regarding receptors, it can unfold a decoy mechanism in which cytokines are bound and neutralized by shed receptors [74]. Additionally, shedding decreases the cell's reactivity to ligands [75]. Remaining cellular parts can be subject to γ-secretase-dependent regulated intramembrane proteolysis (RIP) which influences gene expression [73, 76, 77].

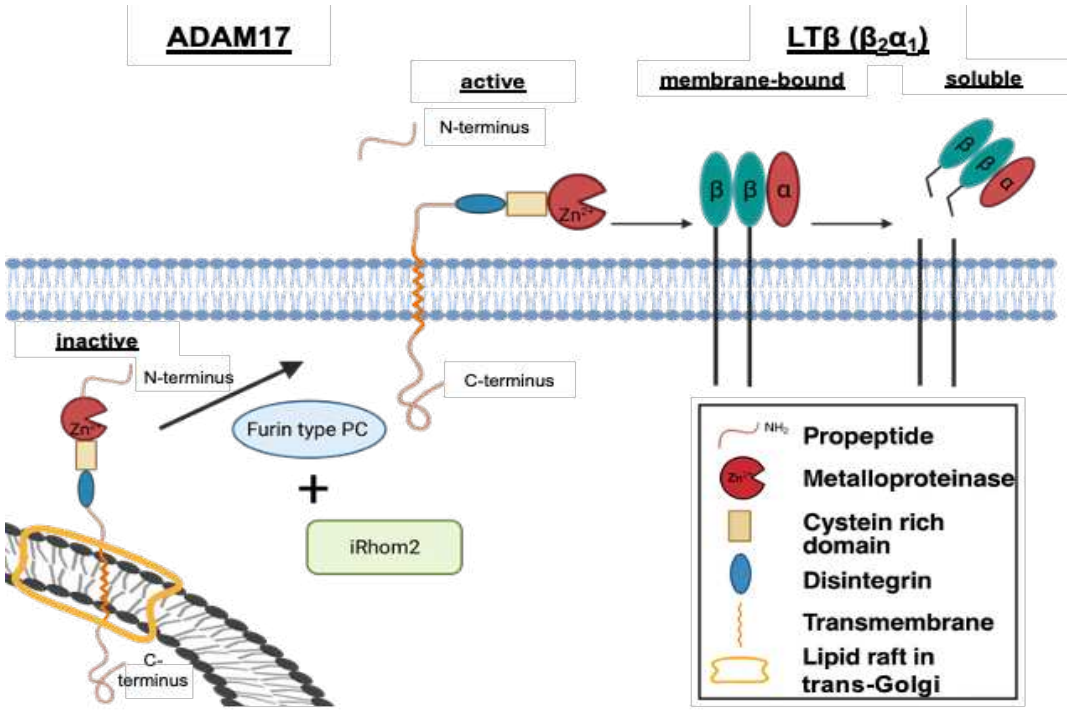

Fig. 4 ***Processing of ADAM17 and shedding of mLTβ.*** *Initially, pro-ADAM17 is processed by Furin-type PC within the trans-Golgi network, while iRhom2 regulates its maturation and trafficking. Upon cellular stimulation, the mature ADAM17 is translocated to the cell membrane. At the membrane, active ADAM17 facilitates ectodomain shedding of various substrates, exemplified here by the shedding of the membrane-bound LTβ2α1 heterotrimer. This shedding process is critical for the release of soluble signaling molecules and the modulation of receptor-ligand interactions, playing a central role in cell signaling and communication [1-3]. Created with biorender.com.*

LTβ is subject to ADAM17 and potentially to further ADAMs [13]. Since the shedding mechanism of ADAM17 was first described in the context of TNFα it is also called TNFα converting enzyme (TACE). LTβ occurs in a soluble (sLTβ) and a membrane-bound (tmLTβ) form. sLTβ has been found to activate primary synovial fibroblasts in patients with rheumatoid arthritis and contribute to the adaptive immune system in a proinflammatory way. In contrast, tmLTβ has been proven to be essential in the physiological processes of lymphoid organogenesis and liver regeneration [51, 53]. Functional differences in the two isoforms continue to be poorly understood. Fig. 4 shows the shedding mechanism of LTβ through ADAM17.

Since ADAM17 has more than 80 and ADAM10 more than 40 substrates, an approach targeting ADAM17 and its regulators has extensive effects [78, 79]. Clinical trials testing ADAM-inhibiting drugs have presented promising results but still call for a more specific approach addressing selected protease-ectodomain interactions [79]. The identification of the LTβ shedding site can therefore open new roads for highly specific and potent therapeutic use [80].

1.6 Aim of the Work

In the last decades biologicals addressing the TNF/TNFRSF significantly improved therapeutic opportunities for genetic, autoimmune and oncological diseases [81]. The development required a precise molecular understanding. The lymphotoxins, being part of the TNF/TNFRSF, possess molecular peculiarities that have been identified but not fully explored. This work aims to characterize three specific aspects. Firstly, the amino acid sequence of murine LTβ that enables to transfer of membrane-bound to the soluble cytokine will be identified. Thereby the role of ADAM proteases and certain amino acids will be examined. Analyzing changes in the protein's properties will help to understand the functional differences between bound and shed LTβ. Previous studies found that cell type-specific expression and domain composition influence the cytokines' function. Secondly, induced and constitutive LTβ shedding will be analyzed in a time-dependent manner. Lastly, the influence of LTβ on the synthesis of LTα will be investigated. LTα and LTβ monomers interact and rely on each other to form heterotrimers and extend their functions. However, a comprehensive investigation into their regulatory and synthetic interaction has not been conducted so far. As preliminary works have been conducted in mice, the cellular examination of LTβ and LTα will also be conducted with the murine isoforms of the cytokine. By delving into these aspects, this work aims to contribute to a more comprehensive understanding of the lymphotoxins α and β and their therapeutic potential.

2 Material and Methods

2.1 Material

2.1.1 Antibodies

All antibodies used in this work are shown in the following table.

Antibody	**Description**	**Manufacturer/ Reference**
α-HA	Monoclonal rabbit IgG which detects the peptide sequence C-YPYDVPDYA-N	Cell Signaling, Danvers, Massachusetts, USA
α-hIL6R 4-11	Murine monoclonal IgG antibody directed against human IL-6R ([38], P08887)	[82]
α-hIL6R BAF 227	Biotinylated goat anti-human IL-6R antibody	R&D Systems, Minneapolis, Minnesota, USA
α-LTβ	Monoclonal mouse IgG antibody directed against full-length human lymphotoxin β ([38], Q06643)	Abcam, Cambridge, UK
α-mLTβ	Polyclonal rabbit IgG antibody directed against a peptide derived from the C-terminal region of human LTβ ([38], P41155)	MyBioSource, San Diego, California, USA
α-mouse POD	Polyclonal horseradish peroxidase-conjugated goat anti-mouse IgG	Thermo Fisher Scientific Bioscience GmbH, St. Leon-Rot, Germany
α-Myc	Monoclonal mouse IgG antibody which detects the peptide sequence N-EQKLISEEDL-C	Cell Signaling, Danvers, Massachusetts, USA
α-rabbit F_c Alexa Fluor 488	Alexa Fluor 488 conjugated polyclonal goat IgG directed against rabbit F_c	Cell Signaling, Danvers, Massachusetts, USA
α-rabbit POD	Polyclonal horseradish peroxidase-conjugated goat anti-rabbit IgG	Thermo Fisher Scientific Bioscience GmbH, St. Leon-Rot, Germany

2.1.2 Antibiotics

All antibiotics used in this work are shown in the following table.

Antibiotic	Working Solution	Manufacturer
Ampicillin	Agar plate: 200 µg/ml Liquid media: 100 µg/ml	Carl Roth GmbH, Karlsruhe, Germany
Kanamycin	50 µg/ml	Carl Roth GmbH, Karlsruhe, Germany
Penicillin	60 µg/ml	Genaxxon, Ulm, Germany
Puromycin	1,5 µg/ ml	Carl Roth GmbH, Karlsruhe, Germany
Streptomycin	100 µg/ml	Genaxxon, Ulm, Germany

2.1.3 Buffers and Solutions

All buffers and solutions used in this work are shown in the following table. If not stated otherwise buffers and solution were mixed in ddH_2O and autoclaved for 20 min at 120°C and 2 bar.

Buffer/Solution	Composition
Ammonium peroxide sulfate (APS)-solution	10% (w/v) APS
Collecting gel buffer (CGP)	500 mM tris-HCl pH 6.8 0.4% (w/v) sodium dodecyl sulfate
dNTP	10 mM dATP 10 mM dCTP 10 mM dGTP 10 mM dTTP
FACS buffer	5% (w/v) BSA in PBS
GI-Solution (GI)	3 mM GI in DMSO
GW-Solution (GW)	3 mM GW in DMSO
IL-6R ELISA blocking solution	5% (w/v) sucrose 1% (w/v) BSA in PBS
IP buffer	20 mM tris 150 mM NaCl 1 mM EDTA 1 mM EGTA
Jak2- lysis buffer	10 mM tris-HCl

Buffer/Solution	Composition
	150 mM NaCl 0.5 mM EDTA 0.5% NP40 1 mM $NaVO_3$ 10 mM $MgCl_2$ Complete protease inhibitor cocktail tablet (1/50 ml)
Laemmli buffer (5x)	10% (w/v) SDS 50% (v/v) Glycerol 50 mM tris-HCl pH 6.8 5% (v/v) β-Mercaptoethanol 0.5% (w/v) Bromophenol blue
Orange G loading dye buffer (6x)	30% (v/v) glycerol 50 mM EDTA 0.25% (w/v) Orange G
PBS-T	PBS 0.05% tween
Phorbol 12-myristate 13-acetate (PMA)-Solution	100 µM PMA in DMSO
Phosphate buffered saline (PBS)	137 mM NaCl 8.1 mM Na_2HPO_4 (pH 7.4) 1.5 mM KH_2PO_4 (pH 7.4) 2.7 mM KCl
SDS-page running buffer	25 mM tris-HCl pH 8.3 192 mM glycine 1% (w/v) SDS
SDS-page transfer buffer	25 mM tris 192 mM glycine 20% (v/v) methanol 0.01% (w/v) SDS
Separating gel buffer (SGP)	1.5 M tris-HCl pH 8.8 0.4% (w/v) SDS
Solution 1 (S1) for DNA-minipreparation	50 mM Glucose 25 mM Tris-HCl pH 8 10 mM EDTA 0.1% (v/v) RNAse
Solution 2 (S2) for DNA-minipreparation	0.2 M NaOH 1% (w/v) SDS
Solution 3 (S3) for DNA-minipreparation	5 M CH_3COOK_2, 2 M CH_3COOH
Streptavidin-horseradish peroxidase (HRP)	R&D Systems, Minneapolis, Minnesota, USA

Buffer/Solution	Composition
Stripping buffer	62.5 mM Tris-HCl pH 6.8 2% (w/v) SDS 0.1% (v/v) β-Mercaptoethanol
TAE-buffer	40 mM tris-HCl pH 8.8 10 mM EDTA 20 mM acetic acid
TBS-T	0.05% (v/v) Tween-20 in TBS
Tris buffered saline (TBS)	50 mM Tris-HCl pH 7.5 150 mM NaCl
Trypsin/EDTA-solution	10% (v/v) trypsin/EDTA (10x) in PBS
Western blot blocking solution	5% (w/v) skim milk powder in TBS-T

2.1.4 Cell Lines

All cell lines and bacteria used in this work are shown in the following tables.

Bacterium	Strain	Genotype
E. coli	XL-1 Blue	recA1, endA1, gyrA96, thi-1, hsdR17, supE44, relA1, lac [F'proAB lacIqZΔM15 Tn10 (TetR)]

Cell line	Culture medium	Origin
Ba/F3-gp130	DMEM+/+ + Hyper IL6 + Puromycin	Immunex, Seattle, Washington, USA
CHO-K1	DMEM +/+	DMSZ GmbH, Brunswick, Germany
HEK293T	DMEM +/+	DMSZ GmbH, Brunswick, Germany
Phoenix Eco	DMEM +/+	DKFZ, Heidelberg, Germany

2.1.5 Chemicals

All chemicals used in this work are shown in the following table.

Chemical	Manufacturer
Acetic acid	Carl Roth GmbH & Co. KG, Karlsruhe, Germany
Acrylamide mix 30%	Carl Roth GmbH, Karlsruhe, Germany
Agar	AppliChem GmbH, Darmstadt, Germany
Agarose	Biozym Scientific GmbH, Oldendorf, Germany
Albumin fraction V (8076.3) (BSA)	Carl Roth GmbH & Co. KG, Karlsruhe, Germany
Ammonium persulfate (APS)	Merck KGaA, Darmstadt, Germany
Bromophenol blue	Sigma-Aldrich Chemie GmbH, Steinheim, Germany
Citric acid	Sigma-Aldrich Chemie GmbH, Steinheim, Germany
Complete protease inhibitor cocktail tablets (EDTA-free)	Roche Diagnostics, Mannheim, Germany
Deoxyadenosine triphosphate (dATP)	Thermo Fisher Scientific Bioscience GmbH, St. Leon-Rot, Germany
Deoxycytidine triphosphate (dCTP)	Thermo Fisher Scientific Bioscience GmbH, St. Leon-Rot, Germany
Deoxyguanosine triphosphate (dGTP)	Thermo Fisher Scientific Bioscience GmbH, St. Leon-Rot, Germany
Deoxythymidine triphosphate (dTTP)	Thermo Fisher Scientific Bioscience GmbH, St. Leon-Rot, Germany
Dimethyl sulfoxide (DMSO)	Sigma-Aldrich Chemie GmbH, Munich, Germany
Disodium hydrogen phosphate	Merck KGaA, Darmstadt, Germany
Dulbecco's modified eagle's medium (DMEM)	Thermo Fisher Scientific Bioscience GmbH, St. Leon-Rot, Germany
Ethanol	Sigma-Aldrich Chemie GmbH, Munich, Germany
Ethidium bromide	Carl Roth GmbH & Co. KG, Karlsruhe, Germany
Ethylenediaminetetraacetic acid (EDTA)	Sigma-Aldrich Chemie GmbH, Munich, Germany
GI254023X (GI; (2R)-N-[(1S)-2.2-dimethyl-1-[(methylamino)carbonyl]propyl]-2-[(1S)-	Glaxo Smith Kline, Stevenage, UK

Chemical	Manufacturer
1-(N-hydroxyformamido)ethyl]-5-phenylpentanamide)	
Gibco® fetal bovine serum (FBS)	Thermo Fisher Scientific Bioscience GmbH, St. Leon-Rot, Germany
Glycerol	Carl Roth GmbH & Co. KG, Karlsruhe, Germany
Glycine	Merck KGaA, Darmstadt, Germany
GW280264X (GW; phenylmethyl N-[(5S)-5-[[(2R.3S)-3-(formylhydroxyamino)-2-(2-methylpropyl)-1-oxohexyl]amino]-6-oxo-6-(2-thiazolylamino)hexyl]carbamate)	Glaxo Smith Kline, Stevenage, UK
Immobilon Western HRP-substrate	Merck KGaA, Darmstadt, Germany
Isopropanol	AppliChem GmbH, Darmstadt, Germany
Loading-dye solution (6x)	Thermo Fisher Scientific Bioscience GmbH, St. Leon-Rot, Germany
Lysogeny broth-medium (LB-Medium)	Carl Roth GmbH & Co. KG, Karlsruhe, Germany
Marimastat (MM; (2S.3R)-N4-[(1S)-2.2 dimethyl-1-[(methylamino)carbonyl] propyl]-N1.2-dihydroxy-3-(2-methylpropyl)butanediamide)	Sigma-Aldrich Chemie GmbH, Munich, Germany
Methanol	Merck KGaA, Darmstadt, Germany
Nonidet® P 40 substitute (NP40)	Sigma-Aldrich Chemie GmbH, Munich, Germany
Phorbol 12-myristate 13-acetate (PMA)	Sigma-Aldrich Chemie GmbH, Munich, Germany
Polybrene infection/ transfection reagent	Sigma-Aldrich Chemie GmbH, Munich, Germany
Polysorbate 20 (Tween-20)	Sigma-Aldrich Chemie GmbH, Steinheim, Germany
Potassium acetate	Merck KGaA, Darmstadt, Germany
Potassium chloride	VWR International BVBA, Leuven, Belgium
Potassium dihydrogen phosphate	Carl Roth GmbH & Co. KG, Karlsruhe, Germany
Protein A-sepharose® beads	Sigma-Aldrich Chemie GmbH, Munich, Germany
RNase A	QIAGEN, Hilden, Germany

Chemical	Manufacturer
Skim milk powder	Carl Roth GmbH & Co. KG, Karlsruhe, Germany
Sodium chloride	AppliChem GmbH, Darmstadt, Germany
Sodium citrate	Sigma-Aldrich Chemie GmbH, Steinheim, Germany
Sodium dodecyl sulfate	Carl Roth GmbH & Co. KG, Karlsruhe, Germany
Sodium hydroxide	Merck KGaA, Darmstadt, Germany
Sodium vanadate	Sigma-Aldrich Chemie GmbH, Munich, Germany
Streptomycin	Genaxxon, Ulm, Germany
Sucrose	Merck KGaA, Darmstadt, Germany
Sulfuric acid	AppliChem GmbH, Darmstadt, Germany
Tetramethylethylendiamine (TEMED)	Sigma-Aldrich Chemie GmbH, Munich, Germany
Trishydroxymethylaminomethane (TRIS)	Bethesda Research Laboratories, Washington D.C., USA
TriTrack DNA-charging dye (6x)	Sigma-Aldrich Chemie GmbH, Munich, Germany
Trypan Blue Dye, 0.4%	Bio-Rad Laboratories GmbH, Munich, Germany
Trypsin/EDTA (10x)	Genaxxon, Ulm, Germany
TurboFect™ transfection reagent	Thermo Fisher Scientific Bioscience GmbH, St. Leon-Rot, Germany
β-mercaptoethanol	Sigma-Aldrich Chemie GmbH, Munich, Germany

2.1.6 Consumables

All consumables used in this work are listed in the following table.

Consumable	Manufacturer
Amersham™ protram™ 0.45 µm Western blotting membrane	GE LifeScience, Boston, USA
Cell culture dish TC dish 100	Sarstedt AG & Co. KG, Nümbrecht, Germany
Cell culture six wells VWR® tissue culture	VWR International, Radnor, USA
DERMAGRIP® nitrile examination Gloves	REMESCO Handelsges.m.b.H, Wien, Austria
ELISA plate 96-well medium binding F	Sarstedt AG & Co. KG, Nümbrecht, Germany
Eppendorf type graduated macro tip	Starlab International GmbH, Hamburg, Germany
Glass pasteur pipette	Brand GmbH + Co. Kg, Wertheim, Germany
Greiner Bio-One™ tube 15 ml	Greiner Bio-One, Kremsmünster, Austria
Greiner Bio-One™ tube 50 ml	Greiner Bio-One, Kremsmünster, Austria
Nunc-immuno™ microwell™ 96 well solid plates highly absorbent	Sigma-Aldrich Chemie GmbH, Munich, Germany
Petri/ suspension cell dishes 10 cm	Sarstedt AG & Co. KG, Nümbrecht, Germany
Pipette tips, neutral 10, 200, 1000 µl	Sarstedt AG & Co. KG, Nümbrecht, Germany
PVDF membrane 0.45 µm	Carl Roth GmbH + Co, Kg, Karlsruhe, Germany
SafeSeal tube 1.5 ml and 2 ml	Sarstedt AG & Co. KG, Nümbrecht, Germany
Sterile stripette costar® 10 ml, 25 ml, 50 ml	Corning Inc., New York City, USA
TC10 system counting slides, dual chamber	Bio-Rad Laboratories GmbH, Munich, Germany
Whatman paper	VWR International GmbH, Darmstadt, Germany

2.1.7 Devices

All devices used in this work are shown in the following table.

Device	Manufacturer
Analytical scale precisa 100M-300C	Hartenstein GmbH, Würzburg, Germany
Autoclave Laboklav 25	SHP Steriltechnik AG, Haldensleben, Germany
Cell culture vacuum pump N811KN.18	NeoLab Migge GmbH, Heidelberg, Germany
Centrifuge 5424, 5810 and 5810 R	Eppendorf GmbH, Hamburg, Germany
Centrifuge Heraeus Fresco 17	Thermo Fisher Scientific Bioscience GmbH, St. Leon-Rot, Germany
Centrifuge Heraeus megafuge 40	Thermo Fisher Scientific Bioscience GmbH, St. Leon-Rot, Germany
Chamber for gel electrophoresis	Bio-Rad Laboratories GmbH, Munich, Germany
CO_2 incubator BF400	Binder GmbH, Tuttlingen, Germany
CO_2 incubator HERACell VIOS S250i	Thermo Fisher Scientific Bioscience GmbH, St. Leon-Rot, Germany
Duran erlenmeyer flasks of different sizes	Schott AG, Mainz, Germany
ECL chemocam Imager	INTAS Science Imaging Instruments GmbH, Goettingen, Germany
Flow cytometer BD FACS canto II	BD Bioscience, Heidelberg, Germany
Fluorometer Infinite® M200 PRO reader	Tecan GmbH, Maennedorf, Switzerland
Fridge freezer	Liebherr GmbH, Bulle, Switzerland
Gel iX imager	INTAS Science Imaging Instruments GmbH, Goettingen, Germany
Heating bath memmert WNB7	Memmert GmbH + Co.KG, Schwabach, Germany
Incubation shaker infors HT multitron	Infors AG, Bottmingen, Switzerland
Labsolute® pipetting assistant	Th. Geyer Ingrenediernt GmbH & Co. KG, Hoexter, Germany
Magnetic stirrer with heating	Heidolph Instruments GmbH, Schwabach, Germany
Micropipette research® plus	Eppendorf GmbH, Hamburg, Germany
Microscope primovert	Carl Zeiss Microscopy GmbH, Jena, Germany
Microwave Siemens AM925ESW	Siemens AG, Munich, Germany
Milli Q® Direct 16 water cleansing system	Merck KGaA, Darmstadt, Germany

Device	Manufacturer
Minicentrifuge neoLab D-6015	neoLab® Migge GmbH, Heidelberg, Germany
Mini-PROTEAN tetra system	Bio-Rad Laboratories GmbH, Munich, Germany
Odyssey Fc dual-mode imaging system	LI-COR Bioscience GmbH, Bad Homburg, Germany
pH meter	Sartorius AG, Goettingen, Germany
Spectrophotometer NanoDrop 2000c	Thermo Fisher Scientific Bioscience GmbH, St. Leon-Rot, Germany
Sterile bench safe 2020	Thermo Fisher Scientific Bioscience GmbH, St. Leon-Rot, Germany
TC10™ automated cell counter	Bio-Rad Laboratories GmbH, Munich, Germany
Tempered shaking table Titramax 1000	Heidolph Instruments GmbH 6 Co.KG, Schwabach, Germany
Thermocycler PeqStar 2x gradient	PEQLAB Biotechnologie GmbH, Erlangen, Germany
Thermomixer® comfort	Eppendorf GmbH, Hamburg, Germany
Trans-blot® turbo™	Bio-Rad Laboratories GmbH, Munich, Germany
Tube roller RM 5-30V CAT	neoLab® Migge GmbH, Heidelberg, Germany
UniINCU 20 mini incubator	Lab Logistics Group GmbH, Meckenheim, Germany
UV-table	Bio-Budget Technologies GmbH, Munich, Germany
Voltage source power pac™ basic	BioRad Laboratories GmbH, Hercules, USA
Vortex mixer neoLab D-6012	neoLab® Migge GmbH, Heidelberg, Germany

2.1.8 Enzymes and Corresponding Buffers

All enzymes used in this work were manufactured by Thermo Fisher Scientific Bioscience GmbH and are listed below.

Enzyme type	**Enzyme**
Serine protease /cell detachment	Trypsin
DNA restriction enzyme	AflII (BspTI)
	BamHI
	DraIII (AdeI)
	Eco147I
	Eco72I (PmlI)
	EcoRI
	HindII
	NheI
	PmeI (Eco721)
DNA restriction enzyme buffer	Blue
	Green
	Orange
	Red
	SpeI (BcuI)
	Tango
	XbaI
	Yellow
Enzymes relevant to PCR and buffers	50% (w/v) polyethyleneglycol 4000
	DPNI
	DreamTaq polymerase
	DreamTaq polymerase buffer
	Fast-AP-thermosensitive alkaline phosphatase
	Phusion ® high-fidelity polymerase + HF buffer
	T4 ligase
	T4 polynucleotide kinase
	T4-DNA-ligase buffer

2.1.9 Kits and Pre-assembled Chemicals

All pre-assembled kits used in this work are shown in the following table.

Kit	Manufacturer
Complete protease EDTA free inhibitor cocktail tablet	Roche Diagnostics GmbH, Mannheim, Germany
GeneRuler™ express DNA ladder, ready-to-use	Thermo Fisher Scientific Bioscience GmbH, St. Leon-Rot, Germany
Immobilon Western HRP substrate	Merck KGaA, Darmstadt, Germany
Intercept® protein-free blocking buffer	LI-COR Bioscience GmbH, Bad Homburg, Germany
Mouse LTA ELISA kit (EML0288)	ABclonal Biotechnology Co., Wuhan, China,
Mouse lymphotoxin beta ELISA kit (MBS732001)	MyBioSource, San Diego, USA
NucleoBond® Xtra midi (740410.100)	Machery-Nagel, Dueren, Germany
NucleoSpin® gel and PCR clean-up (740609.250)	Machery-Nagel, Dueren, Germany
NucleoSpin® plasmid (740588.250)	Machery-Nagel, Dueren, Germany
PageRuler™ prestained protein ladder, 10 to 180 kDa	Thermo Fisher Scientific Bioscience GmbH, St. Leon-Rot, Germany
Pierce BCA™ protein assay kit	Thermo Fisher Scientific Bioscience GmbH, St. Leon-Rot, Germany
Signal fire™ elite ECL reagent	Cell Signaling Technology Europe B.V., Frankfurt a.M., Germany

2.1.10 Media

All media used for the cultivation of either bacteria or eukaryotic cells in this work are listed in the following table. If not stated otherwise bacterial media were mixed in ddH_2O and autoclaved for 20 min at 120°C and 2 bar.

Used for	Medium	Composition
Bacteria	Lysogeny-broth-(LB)-medium	1% NaCl, 0.5% yeast extract, 1% Trypton
Bacteria	LB-Amp-medium	1% NaCl, 0.5% yeast extract, 1% Trypton, 100 µg/ml Ampicillin
Bacteria	LB-Agar	1% NaCl, 0.5% yeast extract, 1% Trypton, 1.5% Agar
Bacteria	LB-amp-agar	1% NaCl, 0.5% yeast extract, 1% Trypton, 1.5% Agar, 200 µg/ml Ampicillin

Used for	Medium	Composition
Bacteria	LB-kanamycin-agar	1% NaCl, 0.5% yeast extract, 1% Trypton, 1.5% agar, 100 µg/ml Kanamycin
Cryo conservations of eukaryotic cells	Cryo medium	10% (v/v) DMSO, 90% (v/v) FBS
Eukaryotic cells	DMEM-/-	Dulbecco's modified eagle's medium, high glucose (4.5 g/l), with stable glutamine
Eukaryotic cells	DMEM+/+	Dulbecco's modified eagle's medium, high glucose (4.5 g/l), with stable Glutamine, 10% FBS, 1% penicillin/streptomycin
Retrovirally transduced eukaryotic cells	DMEM+/+ + Hyper-IL-6 + puromycin	Dulbecco's modified eagle's medium, high glucose (4.5 g/l), with stable glutamine, 10% FBS, 1% penicillin/streptomycin, 0.15% (w/v) puromycin, 0.02% (v/v) hyper IL-6

2.1.11 Oligonucleotides

All oligonucleotides used in this work are shown in the following table.

Name	Sequence (5'-3')
DF 86 (3' pMOWS)	AGCAATAGCATGATACAAAGG
DF16fw (pcDNA3.1 fwd)	AAATTAATACGACTCACTATAGG
DF17 (pcDNA3.1 rev)	AGGCACAGTCGAGGCTG
DF37rw (pcDNA3.1 rev3)	GCGATGCAATTTCCTCATT
DF38 (pCR-Script fwd 1)	TGCTGCAAGGCGATTAAG
DF39 (pCR-Script rev1)	ATGCTTCCGGCTCGTATG
DF85 (5'pMOWS)	AGCCCTTTGTACACCCTAAGC
DF87/T7 (T7 Promoter)	TAATACGACTCACTATAGGG
K57D_fw	AGGGCGATGATGTGGAAGATATCATCGGCTCTG GCG
K57D_rv	CGCCAGAGCCGATGATATCTTCCACATCATCGCC CT
LTA_EcoRI_RP	CTCGAATTCCAGAGCGAAGGCGCCAAAGAACAC AGAG

Name	Sequence (5'-3')
LTB_SpeI_RP	GACACTAGTTCCGACCATCACGGCGCCGAAGAAG
mLTA-EcoRV-FW	GACGATATCCTTAAGGCCACCATGACCCTGCTGGGCAGACTGCATC
pcDNA3.1_SpeI_FP	GATTATTGACTAGTTATTAATAGTAATCAATTACGGGGTCATTAG (45)
R53DR54D-fw	CACTGGTGCCTCAGGACCAGGGCGATGATGTGGAAAAGATCATCGGCTCTGG
R53DR54D-rv	CCAGAGCCGATGATCTTTTCCACATCATCGCCCTGGTCCTGAGGCACCAGTG
R54DV55D_fw	GTGCCTCAGGACCAGGGCAGAGATGATGAAAAGATCATCGGCTCTGGC
R54DV55D-rv	GCCAGAGCCGATGATCTTTTCATCATCTCTGCCCTGGTCCTGAGGCAC

2.1.12 Plasmids

All plasmids used in this work are shown in the following table.

Name	Description	Reference
pcDNA3.1	Vector for expression via transient transfection in eukaryotic cells carrying cytomegalovirus enhancer-promotor, cloning sites for forward and reverse orientation, ampicillin resistance gene and pUC origin	Thermo Fisher Scientific Bioscience GmbH, St. Leon-Rot, Germany
pcDNA3.1_mLTα_WT_HA	pcDNA3.1 vector with an insert encoding for WT murine LTα ([38], P09225) linked with a HA tag	Previous work
pcDNA3.1_mLTα_WT_myc	pcDNA3.1 vector with an insert encoding for WT murine LTα ([38], P09225) linked with a myc protein tag	This work
pcDNA3.1_mLTβ_CV1_myc	pcDNA3.1 vector with an insert encoding for mLTβ charge variant 1 (R53D;R54D) linked with a myc protein tag	This work
pcDNA3.1_mLTβ_CV2_myc	pcDNA3.1 vector with an insert encoding for mLTβ charge variant 2 (R53D;R54D;R57K) linked with a myc protein tag	This work
pcDNA3.1_mLTβ_CV3_myc	pcDNA3.1 vector with an insert encoding for mLTβ charge variant 3	This work

Name	Description	Reference
	(R53DV55D) linked with a Myc protein tag	
pcDNA3.1_mLTβ_DV1_HA	pcDNA3.1 vector with an insert encoding for mLTβ deletion variant 1 (ΔD50-Q66) linked with a HA protein tag	This work
pcDNA3.1_mLTβ_DV1_myc	pcDNA3.1 vector with an insert encoding for mLTβ deletion variant 1 (ΔD50-Q66) linked with a myc protein tag	Previous work
pcDNA3.1_mLTβ_DV2_myc	pcDNA3.1 vector with an insert encoding for mLTβ deletion variant 2 (ΔQ66-P135) linked with a myc protein tag	Previous work
pcDNA3.1_mLTβ_DV3_myc	pcDNA3.1 vector with an insert encoding for mLTβ deletion variant 3 (ΔT87-L153) linked with a myc protein tag	Previous work
pcDNA3.1_mLTβ_WT_2A_mLTα_HA	pcDNA3.1 vector with two inserts in one open reading frame encoding for WT murine LTβ ([38], P41155) linked with a myc protein tag and WT murine LTα ([38], P09225) linked with a HA protein tag	Previous work
pcDNA3.1_mLTβ_WT_HA	pcDNA3.1 vector with an insert encoding for WT murine LTβ ([38], P41155) linked with a HA protein tag	This work
pcDNA3.1_mLTβ_WT_myc	pcDNA3.1 vector with an insert encoding for WT murine LTβ ([38], P41155) linked with a myc protein tag	Previous work
pCR-Script	Bacterial expression vector carrying Iac promotor, cloning sites for forward and reverse orientation, ampicillin resistance gene and pUC origin	Addgene, Watertown, USA
pCR-Script_mLTα_WT_HA	pCR-Script vector with an insert encoding for WT mLTα ([38]; UniProt P09225) linked with a HA protein tag	This work

Name	Description	Reference
pCR-Script_mLTβ_DV1_myc	pCR-Script vector with an insert encoding for mLTβ deletion variant 1 (ΔD50-Q66) with a myc protein tag	This work
pCR-Script_mLTβ_WT_myc	pCR-Script vector with an insert encoding for WT mLTβ ([38]; P41155) linked with a myc protein tag	This work
pMOWS_puro	Hybrid retroviral vector carrying a puromycin resistance for cell selection	[83]
pMOWS_puro_mLTβ_CV1_myc	pMOWS_puro vector with an insert encoding for mLTβ charge variant 1 (R53D;R54D) linked with a myc protein tag	This work
pMOWS_puro_mLTβ_CV2_myc	pMOWS_puro vector with an insert encoding mLTβ charge variant 2 (R53D;R54D;R57K) linked with a myc protein tag	This work
pMOWS_puro_mLTβ_CV3_myc	pMOWS_puro vector with an insert encoding for mLTβ charge variant 3 (R53D;V55D) with a myc protein tag	This work
pMOWS_puro_mLTβ_DV1_myc	pMOWS_puro vector with an insert encoding for mLTβ deletion variant 1 (ΔD50-Q66) linked with a myc protein tag	This work
pMOWS_puro_mLTβ_DV2_myc	pMOWS_puro vector with an insert encoding for mLTβ deletion variant 2 (ΔQ66-P135) linked with a myc protein tag	This work
pMOWS_puro_mLTβ_DV3_myc	pMOWS_puro vector with an insert encoding for mLTβ deletion variant 3 (ΔT87-L153) linked with a myc protein tag	This work
pMOWS_puro_mLTβ_WT_myc	pMOWS_puro vector with an insert encoding for WT mLTβ ([38]; P41155) linked with a myc protein tag	Previous work

2.1.13 Recombinant Proteins

All recombinant proteins used in this work are shown in the following table.

Protein	Description	Origin
Hyper-IL-6	Fusion protein of Interleukin 6 and soluble Interleukin 6 receptor, which associates with gp130	Purified cell culture supernatant of transfected cells

2.1.14 Software and Websites for Data Analysis and Evaluation

The softwares used for the analysis and evaluation of the data of this work are shown in the following table.

Software	Used for	Developer
ChatGPT-4	Linguistic accuracy and brevity	OpenAI LP, San Francisco, USA
Clustal Omega Multiple Sequence Alignment	Alignment of Sanger sequencing data	EMBL-EBI, Hinxton, UK
DeepL Translator	Translation assistance	DeepL GmbH, Cologne, Germany
FlowJo	Analysis and evaluation of flow cytometry data	FlowJo LLC, Ashland, USA
GraphPad Prism	Analysis and evaluation of ELISA data	GraphPad Software Inc., San Diego, USA
Image Studio Lite Ver5.2	Evaluation of Western blot data	LI-COR Bioscience GmbH, Bad Homburg, Germany
ImageJ 1.53e; Java 1.8.0_172	Quantification of Western blot signals	Wayne Rasband, National Institute of Health, Bethesda, USA
Microsoft Office 365	Writing, compilation of figures, regression analysis and quantification	Microsoft Corp., Redmond, USA
SnapGene™ 1.3.3.	*In silico* gene analysis	GSL Biotech LCC, San Diego, USA
www.healthtech.dtu.dk	Prediction of protein size and glycosylation susceptibility	Department of Health Technology, Lyngby, Denmark

2.2 Molecular Biological Methods

2.2.1 Transformation of Chemically Competent Cells

The uptaking process of plasmid DNA into chemically competent *E. coli* XL-1 Blue for subsequent DNA amplification is called transformation. Chemically competent *E. coli* were cultured at 37°C shaking in 500 ml LB-Medium until the culture reached an optical density of 0.5-0.8 at 600 nm. The cell suspension was centrifuged (4°C, 5000 x g, 15 min), resuspended in 140 ml ice-cold 50 mM calcium chloride, and incubated for 20 min After repetition, the cells were resuspended in 25 ml 50 mM calcium chloride with 10% glycerol. Before the cells were aliquoted at 30 µl each and stored at -80°C they were centrifuged a third time and resuspended in 2 ml ice-cold 50 mM calcium chloride with 10% glycerol. The cells were defrosted on ice and mixed with either 1 µl plasmid DNA for transformation or 10 µl ligation solution for cloning strategies, and incubated for 5 min on ice. Afterward, the heat shock was performed by a 1 min incubation at 42°C. 500 µl prewarmed (37°C) LB-Medium was added and the suspension was incubated for 1 h at 37°C. Subsequently, 100 µl of the medium was spread out on a LB agar plate containing the corresponding antibiotic to select successfully transformed cells carrying the antibiotic resistance. The plate was incubated overnight at 37°C.

2.2.2 DNA Mini Preparation

For DNA analysis after cloning procedures, plasmid DNA was extracted from previously transformed *XL-1 blue* cells. A bacterial colony was picked and transferred to 1.5 ml LB-medium. The medium contained the corresponding selective antibiotic depending on the target plasmid. The tube was punctured at the lid to secure sufficient oxygen supply, and incubated overnight at 37°C. The culture was centrifuged at 5000 x g at RT and resuspended in 100 µl S1 buffer. By adding 200 µl S2 buffer and inverting the tube five times alkaline lysis was initiated and stopped by adding 150 µl acetic acid. The suspension was incubated for 10 min at 4°C and afterward centrifuged at 18,000 g, at 4°C for 10 min The DNA in the 450 µl SN was transferred to a tube with 900 µl 100% ethanol and incubated for 5 min at 4°C. The ethanol precipitated the DNA in the solution, which was centrifuged afterward at 18,000 x g, 4°C for 15 min The DNA pellet was resuspended in 30 µl ddH2O and quantified using spectrophotometry.

2.2.3 DNA Midi Preparation

For plasmid DNA amplification in large amounts transformation was utilized and a single colony was picked into 100 ml LB-medium with the selective antibiotic (100 µg/ml). After overnight incubation overnight (37°C, 140 rpm) the bacterial suspension was centrifuged (3,200 g, 4°C, 15 min). Subsequently, DNA was extracted via Midi preparation according to the protocol of NucleoBond® Xtra plasmid purification Midi/Maxi.

2.2.4 DNA Quantification

After DNA purifications and before cell biological experiments DNA was quantified via spectrophotometry using the NanoDrop 2000c. DNA was 1:10 diluted in ddH_2O when the expected concentration was >1000 ng/µl. Optical density (O.D.) was measured at 230 nm wavelength for polysaccharides, 260 nm for nucleic acids, and 280 nm for proteins. DNA solutions were considered to be pure when the quotient of OD230 : OD260 : OD280 was close to 1 : 2 : 1. Furthermore the ratio of nucleic acids to proteins (OD260/OD280) was supposed to be between 1.7 and 2. Concentrations were calculated using the law of Lambert-Beer:

$$E\lambda = \varepsilon\lambda \text{ x } c \text{ x } d$$

Eλ: Extinction at wavelength λ

ελ: Extinction coefficient at wavelength λ in m^2/mol

c: Substance concentration in solution in mol/m^3

d: Thickness of passed liquid in m

An extinction of 1 corresponds to 50 µg/ml double-stranded DNA.

2.2.5 DNA Restriction Analysis

Plasmid DNA was cleaved with restriction endonucleases for verification purposes after cloning and insert excisions. The plasmid DNA was analyzed *in silico* with the SnapGene™ 1.1.3. software. Restriction enzymes were chosen to either obtain a characteristic band pattern proofing successful cloning (restriction analysis) or to cut out inserts needed for subsequent cloning (preparative cloning). 5 µg of plasmid DNA was

incubated with 10 U of restriction enzyme in the corresponding buffer in 20 µl total volume. Enzymes and buffers were obtained from Thermo Fisher Scientific Bioscience GmbH. The solution was incubated for 90 min at 37°C. The restriction was assessed using DNA gel electrophoresis.

2.2.6 DNA Gel Electrophoresis

In DNA gel electrophoresis DNA fragments were separated in an agarose gel corresponding to their size. The pore size of the gel depends on the relative amount of agarose and determines fragment separation. For ideal separation 1 to 2% agarose was used in this work. The agarose gel was made of TAE buffer and agarose. After boiling up 2‰ HD-Green was added to the gel before polymerization. Before loading the DNA solution was mixed with TriTrack DNA-charging dye (6x). The gel was loaded into a chamber filled with 1 x TAE buffer to ensure electric conductivity. The DNA was separated in the gel towards the cathode by the application of voltage (90-150 V). GeneRuler™ express DNA ladder was used as a standard. The fragment pattern was documented using the Intas gel iX imager.

2.2.7 Gel Extraction of DNA

Gel extraction was used to isolate and purify DNA fragments after separation in gel electrophoresis (*cf.* 2.2.6). The fragments were used for subsequent experiments and therefore the gel was analyzed under blue light (380 to 400 nm) to prevent DNA denaturation. The fragment was cut out of the gel and purified according to the protocol of NucleoSpin® gel and PCR clean-up columns.

2.2.8 Polymerase Chain Reaction

The polymerase chain reaction (PCR) is a method for DNA amplification that can be used for various experimental aims. Different cases are explained in the following subchapters. All PCR types follow the same principle: The double helical structure of the DNA is broken up by heat, oligonucleotides (primer) framing the target sequence attach to their complementary sequence at a defined temperature (annealing) and enable the polymerase to read off the coding strand while synthesizing an inverse copy with the provided dNTPs

(elongation). After the passage of the polymerase the old and the new strand hybridize via hydrogen bonds between complementary base pairs (termination). Phusion high-fidelity polymerase was used as a polymerase. This polymerase has a 3' to 5' exonuclease activity which eliminates falsely integrated nucleotides (proof-reading). The cycle is repeated, and the DNA is amplified exponentially. Afterward, the DNA product was stored at 4°C. The PCRs were conducted with the thermocycler PeqStar 2x gradient. The following table shows the used ratios and an exemplary PCR program.

Reagent	**Amount**
Template DNA 100 ng	100 ng
High fidelity buffer	10 µl
2.5 µl forward primer	10 µM
2.5 µl reverse primer	10 µM
1 µl of 10 mM dNTPs	10 µM
0.5 µl fusion high-fidelity polymerase	1 U
Add ddH2O up to a total volume of 50 µl	x µl

Table 3 ***Ratio of reagents for PCR.***

Phase	**Temperature (°C)**	**Time**
Initial strand separation	92-98	5 min
~ 15-30 cycles:		
Strand separation	92-98	10 s
Annealing	50-60	15 s
Elongation	72	15-60 s/kb
Termination	72	5 min
Storage	4	∞

Table 4 ***Exemplary PCR program.***

2.2.8.1 Site-directed Mutagenesis PCR

The site-directed mutagenesis (SDM) is a method to introduce directed point mutations into the target cDNA using a modified primer. The primer is not completely complementary to the coding strand but encodes for the desired amino acid change framed by base triplets complementary to the coding strand. In the first round, two PCRs run separately, one with the forward and one with the backward primer only. In the second

round, the single-stranded PCR products were combined to form a double-stranded DNA. The SDM PCRs were set up the same way as the PCRs described previously. After the PCR program, the DNA was purified using the NucleoSpin® Gel and PCR clean-up columns and a part of the solution (5 µl) was analyzed via gel electrophoresis for verification purposes (2.2.6). The purified DNA was restricted by DpnI to improve cloning results. For DpnI restriction 2.8 µg of purified SDM PCR product, 30 U of DpnI, 2 µl Tango buffer 10x and 5 µl ddH_2O were mixed and incubated at 37°C for 2 h. The enzymatic restriction was inactivated for 20 min at 80°C.

2.2.9 Colony PCR

The colony PCR detects specific DNA sequences in bacterial colonies. This method was used to verify DNA ligation (2.2.11). An insert was cloned into a vector by ligation and subsequently transformed (2.2.1). Colonies were picked on the selective agar. The picked colony was dissolved in 20 µl of ddH_2O in a PCR tube by pipetting. The pipette tip was dropped off in a 2 ml SafeSeal® tube with 1.5 ml LB-medium. The PCR tube was incubated at 95°C for 5 min for lysis of the bacteria and release of DNA. Subsequently, 25 pmol primer 1, 25 pmol primer 2, 1 U DreamTaq polymerase, 5 µl/U of DreamTaq buffer, 4 µl/U of 25 mM $MgCl_2$, 1 µl/U 10 mM dNTP solution and 14 µl ddH_2O were mixed and added to the 20 µl bacterial solution for a final volume of 50 µl. The PCR was run correspondingly to the DreamTaq polymerase data sheet. Depending on the used primer the amplified sequence had a defined length if the insert was cloned successfully with the correct orientation. Colony PCR was evaluated via gel electrophoresis (2.2.6). A vector without an insert was loaded as a negative control. SafeSeal® tubes of positively tested colonies were incubated overnight (37°C), and DNA was extracted via Mini preparation (2.2.2).

2.2.10 PCR Clean-up

PCR clean-up was used to isolate and purify amplified DNA from remaining PCR reagents before further usage of the plasmid. If two DNA sequences (*e.g.*, restriction of insert out of backbone) had to be separated a gel extraction was performed instead (2.2.7). The clean-up was performed according to the protocol of NucleoSpin® Gel and PCR clean-up columns.

2.2.11 DNA Ligation

Ligation describes the reaction of connecting the 5' phosphate group of one nucleotide to the 3' hydroxyl group of the deoxyribose of the following nucleotide via a phosphodiester bond. In a total volume of 20 µl, 100 ng of the dephosphorylated vector was mixed with 1 U of T4 Ligase, 2 µl T4 ligase buffer, 0.2 µl of 50% (w/v) PEG4000 and an amount of phosphorylated insert depending on the length of the insert. The ratio of insert to vector backbone was 5 to 1. The amount of insert needed was calculated using the following formula:

$$\frac{5 \times mass\ vector\ (ng) \times length\ insert\ (bp)}{length\ vector\ (bp)} = \mathrm{x}\ ng\ insert$$

The mixture was incubated for 12 h at 4°C. Afterward the ligation was transformed in *E.coli* (2.2.1).

2.2.12 DNA Sequencing

DNA sequencing was performed by Microsynth Seqlab. Results were assessed using the SnapGene™ 1.1.3. software and ClustalW2 multiple sequence alignment. DNA samples were sent according to the requirements of Microsynth Seqlab. Oligonucleotides were provided if not available from the service provider.

2.2.13 DNA Phosphorylation and Dephosphorylation

The insert was phosphorylated, whereas the backbones were dephosphorylated to perform a ligation (2.2.11). 40 µl of purified PCR product was mixed with 2 U of Fast-AP thermosensitive alkaline phosphatase, 1 µl of Fast-AP buffer and 7 µl ddH_2O. The mixture was incubated for 2 h at 37°C. Fast-AP was heat-inactivated at 75°C for 5 min. The solution was mixed with 10 µl sixfold Orange G loading dye and cleaned up (2.2.7). In contrast, the inserts were supposed to carry anhydrides on 3' and 5' ends to enable proper ligase action. Therefore 150 µl PCR product was mixed with 20 U T4 polynucleotide kinase and 7.5 µl/U T4-DNA-ligase buffer and incubated for 30 min at 37°C. The enzyme was heat-inactivated at 75°C for 5 min. 6 x Orange G loading dye was added and phosphorylated PCR products were purified via gel extraction (2.2.7). Both products were used for ligation afterward (2.2.11).

2.3 Protein and Immuno-Biochemical Methods

2.3.1 Cell Lysis

To analyze intracellular or membrane-bound proteins via ELISA and Western blotting (WB) transfected or transduced cells were lysed with Jak2 lysis buffer. Jak2 lysis buffer was self-assembled according to the protocol above (2.1.3). Semi-adherent human embryonic kidney 293T (HEK293T) cells in a 10 cm dish were treated as follows: The SN of semi-adherent HEK-293T cells was harvested separately from cells. Cells were washed off the dish with 1 ml ice-cold PBS and transferred into a 1.5 ml tube. After centrifugation at 12000 g and 4°C for 5 min, the cells were washed in 1 ml PBS and centrifuged again. The PBS was discarded, the cells were resuspended in 200 µl of Jak2 lysis buffer and the tube was incubated for 90 min at 4°C. Afterward, the lysate was centrifuged for 20 min at 11,500 g at 4°C and transferred into a new tube. The SN containing the dissolved protein was transferred to a 1.5 ml tube. Protein quantification was conducted with a BCA assay (2.3.2).

2.3.2 Protein Quantification

The total protein amount of cell culture lysates (CL) was standardized to 2.5 µg/µl. Quantification was performed using the Pierce bicinchoninic acid (BCA™) protein assay kit. Each sample was quantified by the determination of the optical density at 450 nm using the Fluorometer Infinite® M200 PRO reader. For Western blot analysis the protein concentration was achieved by diluting the sample with 5 x Laemmli buffer and ddH_2O. For analysis via ELISA, samples were diluted with ddH_2O only.

2.3.3 Co-Immunoprecipitation

Co-immunoprecipitation is a method to concentrate proteins in cell culture. Proteins were captured with a primary antibody, that was bound via its F_c part to Protein A sepharose beads. 1 ml SN was collected 48 h after transient transfection (2.4.3), centrifuged (4°C, 450 x g, 5 min), and transferred to a new tube. The primary antibody was applied in a 1:1000 dilution and incubated overnight at 4°C under constant agitation. 30 µl Protein A Sepharose beads in IP buffer were washed three times in TBS (2700 g, 4°C, 2 min) and finally resuspended in 100 µl TBS. The SN with the primary antibody was

mixed with 100 µl Protein A TBS solution and incubated rotating at 4°C for 4 h. The antibody that had previously bound to the target protein was bound to Protein A Sepharose, centrifuged, and washed three times in TBS (5 min, 4°C, 2700 x g). Before Western blot analysis (2.3.4) the captured and concentrated protein was resuspended in 50 µl 2.5x Laemmli buffer and incubated for 10 min at 95 °C. Naive SN and SN after immunoprecipitation served as controls.

2.3.4 Western Blotting

Sodium dodecyl sulfate (SDS) polyacrylamide gel electrophoresis (PAGE) with subsequent Western blotting (WB) aims to detect proteins in cell culture supernatants and lysates.

The proteins were separated via a polyacrylamide gel and electric voltage (90 to 140 V) according to their molecular weight in Mini-PROTEAN tetra systems. Before loading the protein suspension was treated with Laemmli buffer according to the Laemmli protocol [84]. The protein weight was identified by the application of a standard of known weight. The gel consisted of two parts differing in pore size and pH value (discontinuous separation). In this work 10% gels were used when blotting mLTβ (32,329 Da + ~ 8 kDa due to glycosylation) and 12% gels were used when blotting mLTα (21,999 Da). Table 5 shows the composition of gels with different percentages.

All values in v/v % (ml)	**Collecting gel**	**10% separating gel**	**12% separating gel**
ddH_2O	57	39.996	32.996
Acrylamide	16.8	33	40
SGP	-	26	26
CGP	25	-	-
10% APS	1	1	1
TEMED	0.1	0.04	0.04
Total vol./ gel	2.983 ml	10 ml	10 ml

Table 5 ***Composition of separating and collecting gel;*** *All values refer to v/v % relative to the total volume (in ml) needed for one gel. Depending on the gel's percentage of acrylamide a different separating gel was combined with the collecting gel.*

Afterward, the proteins were horizontally transferred to either a polyvinylidene fluoride or nitrocellulose membrane. Polyvinylidene fluoride membrane was used when imaging the membrane with the ECL ChemoCam imager and the nitrocellulose membrane was used when imaging with the Odyssey Fc dual-mode imaging system. Before the transfer, the polyvinylidene fluoride membrane was activated in pure methanol for 2 min and washed for 1 min in transfer buffer. The Western blot was performed in a semi-dry method with the Trans-Blot® Turbo™ transfer system. Inside the chamber, four layers of Whatman paper soaked in transfer buffer ensured electric conductivity on both sides. The proteins were transferred by voltage (20 V, 3 A, 60 min) and afterwards, the membrane was blocked in skim milk TBS-T for 4 h at 4°C to prevent unspecific antibody bindings. Then the membrane was washed three times for 5 min in 15 ml TBS-T and the primary antibody was applied in Intercept® protein-free blocking buffer (1:1000). After overnight incubation at 4°C the membrane was washed as described previously and the secondary antibody was applied in skim milk TBS-T (1:5000) for 1 h. While the primary antibody was directed against the target protein, the secondary antibody was directed against the the primary antibody. The secondary antibody was linked to horseradish peroxidase (HRP), which catalyzed the oxidation of luminol causing a luminescent signal. The luminescence signal was detected and compared to PageRuler™ prestained protein ladder, which was used as the protein standard. Signal fire™ elite ECL reagent was employed as the luminol reagent when SN was analyzed and immobilon Western HRP substrate was used as the luminol reagent when CL was analyzed. CL of cells transfected with plasmids encoding for green fluorescent protein (GFP) was used as a negative control (NC) and a protein of known signal intensity as a positive control (PC).

For the detection of another protein or the same protein with a different primary antibody, a polyvinylidene fluoride membrane was stripped, blocked again, and incubated a second time. The primary antibody was detached by incubating the membrane in 50 ml of stripping buffer and 50 µl of β-mercaptoethanol at 60°C for 30 min. Then the stripping mixture was washed three times with 15 ml of TBS-T. The blocking and re-incubation with antibodies were conducted as described previously.

2.3.4.1 Western Blot Quantification

To quantify the shedding of the mLTβ variants, protein expression was quantified using the ImageJ 1.53e software. The protein expression of every culture was normalized relative to the culture with the lowest expression intensity. Next, the CL samples were diluted in lysis buffer, while the SN samples were diluted in DMEM+/+ medium. The dilution of SN samples was adjusted according to the calculated CL ratios to account for biological variations in transfection and protein expression.

2.3.5 ELISA

The enzyme-linked immunosorbent assay (ELISA) is a quantifying method for proteins. A 96-well plate was coated with a capture antibody. The target protein was bound by antibody and immobilized. The amount of protein in the sample was determined by adding a HRP-linked detection antibody, that either directly or indirectly detected the target protein by catalyzing a color switch reaction. The intensity of the color switch was quantified by spectrophotometry at 450 nm with the Fluorometer Infinite® M200 PRO reader. With a known standard, the O.D. could be correlated with the amount of protein per volume performing a regression analysis. ELISA data were evaluated using GraphPad Prism software. The mLTα and mLTβ ELISA were conducted according to the protocol of the ELISA kit.

2.4 Cell Biological Methods

2.4.1 Cultivation of adherent Cells

HEK293T and Phoenix-Eco cells are adherent. Cultures were kept in 10 ml DMEM+/+ medium in 10 cm TC dishes and incubated in a H_2O-saturated environment at 37°C and 5% CO_2 in the CO_2 incubator HERACell VIOS S250i. Every fourth day 6 x10^5 cells were split. The cells were detached by 2 ml of trypsin-EDTA and incubated for 5 min. The endopeptidase action was stopped by adding 2 ml of DMEM+/+. Afterward, the cells were centrifuged at 453 x g, RT for 5 min. Cell count and viability were determined according to the protocol of the TC10™ automated cell counter.

2.4.2 Cultivation of Ba/F3-gp130 Cells

Ba/F3-gp130 cells are murine pre-B-cells that are stably transduced with the gene encoding for the gp130 receptor. The cells were cultivated in 10 cm dishes in 10 ml DMEM+/+ with Hyper IL-6 and puromycin in a H_2O-saturated environment at 37°C and 5% CO_2 in the CO_2 incubator HERACell VIOS S250i. Hyper IL-6 is a fusion protein of Interleukin 6 and the soluble Interleukin 6 receptor and can activate every cell that carries the gp130 receptor. 10 ng/ml Hyper IL-6 for cell stimulation was applied in this work. Puromycin was applied in a concentration of 1.5 µg/ml to select cells that were retrovirally transduced with a pMOWS_puro vector.

2.4.3 Transfection of Eukaryotic Cells

Transient transfection of cDNAs into eukaryotic cells via lipofection enables analysis of specific proteins. For transfection into HEK293T cells, 2 $x10^6$ cells were seeded on a 10 cm dish with DMEM+/+ medium. After 24 h 5 µg of plasmid DNA was dissolved in 1 ml DMEM-/- and mixed with 10 µl TurboFect™ Transfection reagent and added to the cells after incubating for 20 min at RT. The cells and the lipoplex were incubated for 48 h (37°C, 5% CO_2). The protein expression was analyzed in CL and SN. Transfection of a pEGFP-plasmid served as a control for transient transfection, which was evaluated microscopically.

2.4.4 Retroviral Transduction of Ba/F3-gp130 Cells

In this work plasmid DNA is stably inserted into the genome of the Ba/F3-gp130 cells by retroviral transduction. A plasmid encoding for the target protein was packed into a retrovirus by transient transfection into Phoenix eco cells. The retrovirus was used to infect the Ba/F3-gp130 cells, and the plasmid was integrated into the genome by the reverse transcriptase of the retrovirus. Therefore, 8 $x10^5$ Phoenix Eco cells per well were seeded out in 6 well plates. After 24 h the cells were transfected with 1 µg of pMOWS_puro vector (*cf.* 2.4.3). The 2 ml DMEM+/+ medium was exchanged after another 6 h with 2 ml of 30% v/v fetal bovine serum (FBS) DMEM+/+. 24 h later retroviral supernatant was centrifuged (RT, 5 min, 453 x g) and 250 µl were mixed with 1 $x10^5$ Ba/F3-gp130 cells and 3 µl polybrene. This solution was centrifuged for 2 h at 453 x g. Afterwards, the cells were re-suspended in 5 ml DMEM+/+ supplemented with

20 ng/ml Hyper IL6 and transferred to a 6-well plate. After two days 1.5 µg/ml puromycin was added and hence positively transduced cells were selected. Transduced cells were screened for autonomous production of the target protein via Western blot (2.3.4).

2.4.5 Flow Cytometry

Flow cytometry is used to count cell populations sorted by the amount of target protein on the surface. The cells are counted by light absorption, light refraction and light emission when passing through a laser. In this work, Ba/F3-gp130 cells carrying different mutations of mLTβ on the cell membrane were counted. 5 x10^5 Ba/F3-gp130 cells were washed once in PBS and once in FACS buffer. Then cells were resuspended in 50 µl FACS buffer. The primary antibody directed against the target protein was added in a 1:100 dilution and incubated for 1 h at RT. The primary antibody was washed with FACS buffer, and the secondary antibody was added 1:500 in 50 µl FACS buffer and incubated in a dark environment for 1 h at RT. As a secondary antibody α-rabbit F_c Alexa Fluor® 488 was used. The cells were washed and resuspended in 500 µl FACS buffer. Afterward, the cell populations were analyzed with the Flowcytometer BD FACS Canto II. The data were assessed with FlowJo software.

2.4.6 Shedding Assay

A shedding assay was set up to analyze the influence of different molecules regarding ectodomain shedding of mLTβ over time. HEK293T cells were transfected in a 10 cm dish with pcDNA3.1_mLTβ_WT plasmid as described previously (2.4.3). 24 h later the cells were washed in 37°C PBS and detached with 2 ml of trypsin/EDTA. The peptidase action was stopped by adding 2 ml of DMEM+/+. The cell suspension was centrifuged (5 min, 453 x g, RT) and resuspended in 5 ml DMEM+/+. 1 ml per well cell suspension was seeded to five wells of a 6-well plate. In the sixth well, a zero value of non-transfected HEK293T cells was obtained for the subsequent analysis. After incubation for 24 h the cells were washed in 1 ml PBS. For the shedding stimulation, the cells were incubated in DMEM-/- to prevent protein contamination by dimethyl sulfoxide (DMSO) and FBS. For shedding induction 48.2 µM of PMA. The inhibitors GW280264X (GW) and GI254023X (GI) were used in a concentration of 3 µM while 10 µM were used for Marimastat. The inhibitors were applied for 30 min before PMA stimulation. As a negative control, DMSO

with a concentration of 2 µl/ml was used. GI was used as selective ADAM10 inhibitor, GW as mixed ADAM10 and ADAM17 inhibitor [69, 85] and MM as a broad-spectrum metalloproteinase inhibitor [86]. PMA is an activator of PKC [70] and ADAM activity depends on PKC phosphorylation. In the setup for the induced shedding assay, 100 µl SN was taken after 2, 4, 6 and 12 h and centrifuged (5 min, 453 x g, 4°C). When constitutive shedding was examined the same inhibitors and concentrations were used without adding the shedding inductor PMA. 100 µl SN was taken after 12, 24, 36 and 48 h and centrifuged (5 min, 453 x g, 4°C). For Western blot and ELISA analysis the samples were prepared as described in chapter 2.3.1..

3 Results

3.1 mLTβ Shedding

3.1.1 mLTβ Domains and Deletion Variants

A mLTβ monomer consists of four domains. The intracellular domain (M1-T27) (ICD) contains the protein's N-terminus. The following single-pass helical transmembrane domain (TM) anchors the cytokine to the cell membrane (S27-P48). The stalk region (Q49-P154) connects the C-terminal extracellular domain (A155-G304) (ECD) to the cell surface. The extracellular domain carries out the cytokine's function. Predominantly this monomer assembles with another mLTβ monomer and a mLTα monomer to form a functional heterotrimeric cytokine [87]. As mLTβ is a single-pass transmembrane protein we assumed that shedding takes place in the stalk of the protein (Q49-P154) within the juxtamembrane region, 10 to 35 amino acids from the cell surface. Still, more distant shedding sites are possible [75]. To identify the crucial amino acids in the 106 amino acids long stalk, three deletion variants (DVs) were cloned based on pcDNA3.1_mLTβ_WT. Every mLTβ DV missed amino acids in three different parts of the stalk. DV1 missed the amino acid D50 to Q66, DV2 missed amino acid Q66 to P135, and DV3 T87 to L153. To facilitate protein analysis and to ensure the detectability of the different mLTβ DVs, a Myc-tag was ligated to the C-terminal extracellular domain within the open reading frame. The plasmids were named pcDNA3.1_mLTβ_DV1_myc, pcDNA3.1_mLTβ_DV2_myc, pcDNA3.1_mLTβ_DV3_myc. Fig. 5 shows a model of the tertiary structure of the mLTβ monomer. The colored rectangles depict the directed deletions. Fig. 6 shows the primary structure of the mLTβ domains and the deleted sequences in DV1 to DV3. Cloning correctness was validated by Sanger sequencing depicted in Fig. 7. Additionally, the plasmids were enzymatically cleaved with SpeI and BamHI. The electrophoresis of cleaved plasmids is shown in Fig. 8 and verifies successful cloning as the fractions depict the *in silico* predicted pattern. Calculated molecular weights and glycosylation sites for evaluation of protein analysis are listed in Table 6.

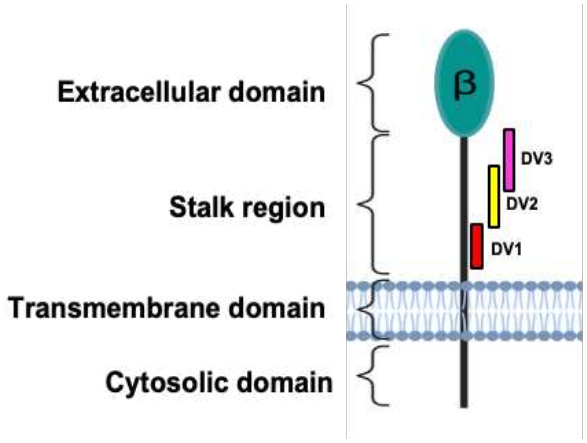

Fig. 5 ***Model of an mLTβ monomer****; colored rectangles depict directed deletions; red equals DV1, yellow equals DV2; purple equals DV3; created with biorender.com.*

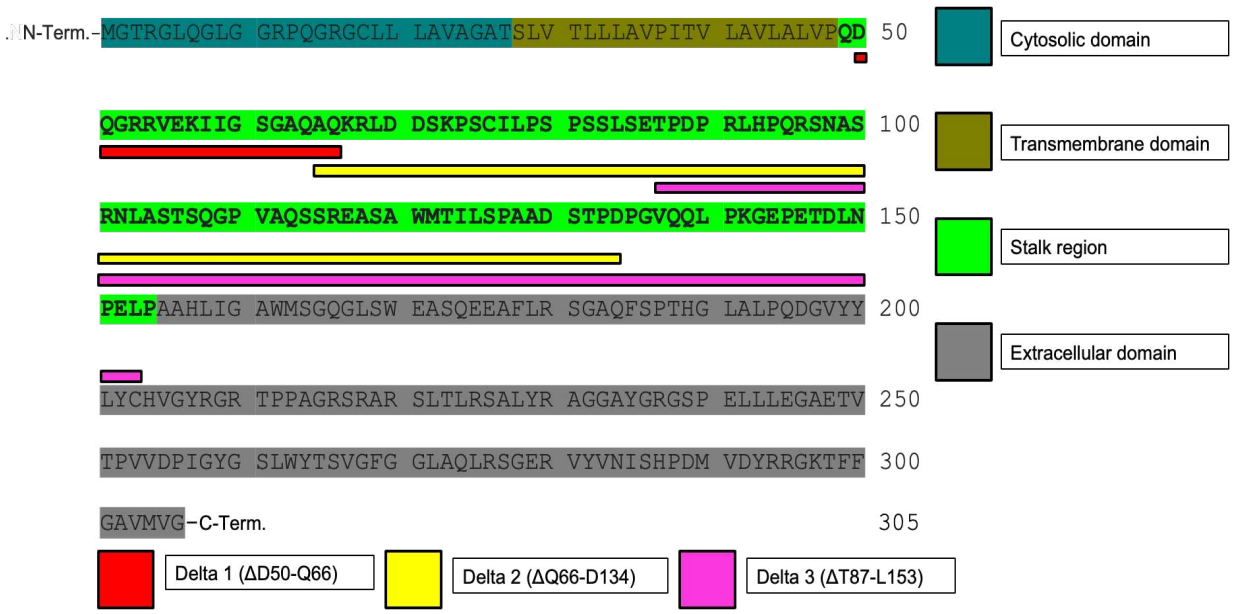

Fig. 6 ***mLTβ primary structure and deletion variants****; domains and directed deletion are highlighted by color; created with Microsoft Powerpoint.*

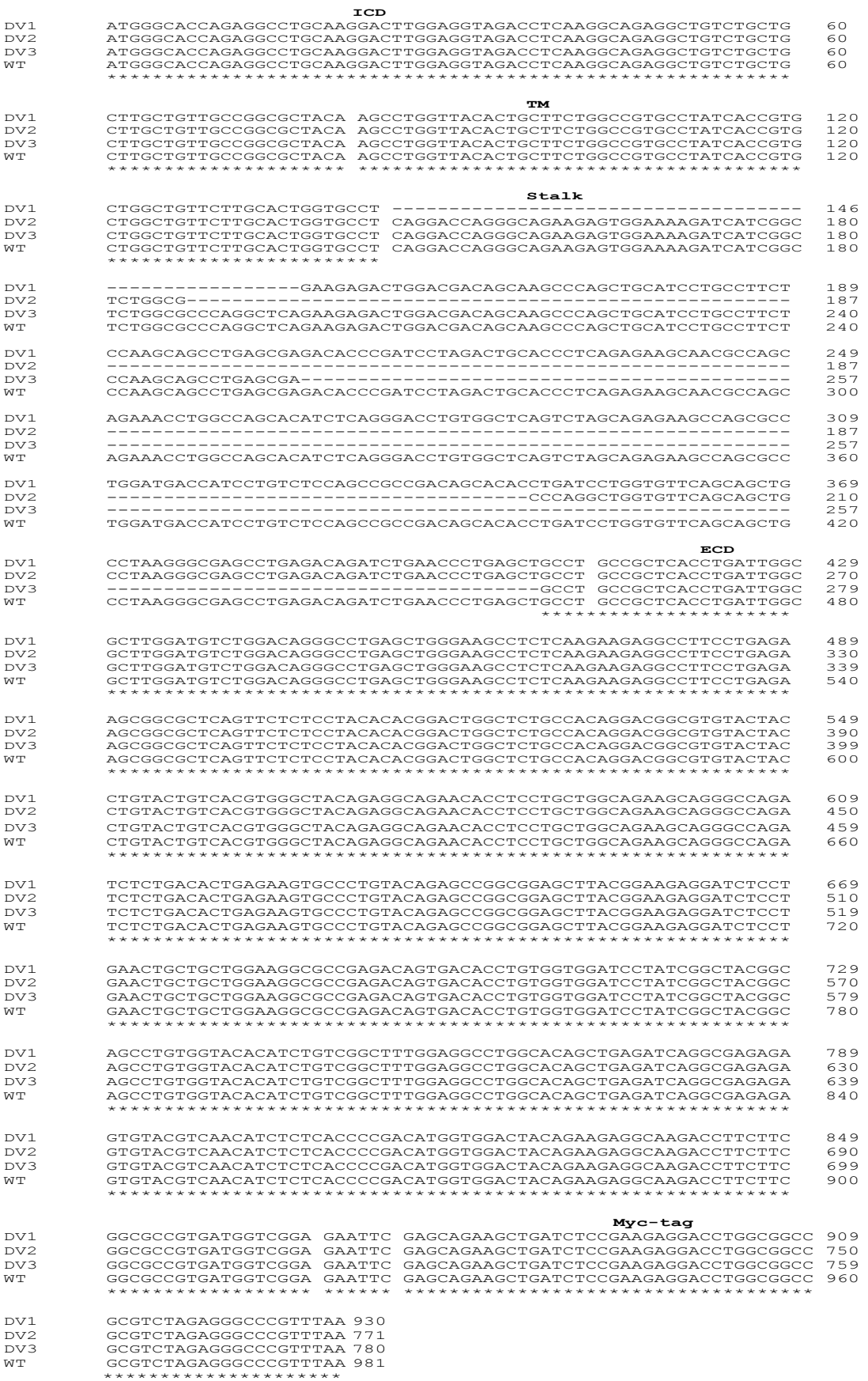

Fig. 7 ***pcDNA3.1 vector carries mLTβ_WT/ DV1/DV2 /DV3_myc****; Alignment of Sanger sequenced plasmids; only the open reading frame is shown; Aligned with ClustalOmega multiple sequence alignment; domains and ligated Myc-tag are separated by spaces and labeled.*

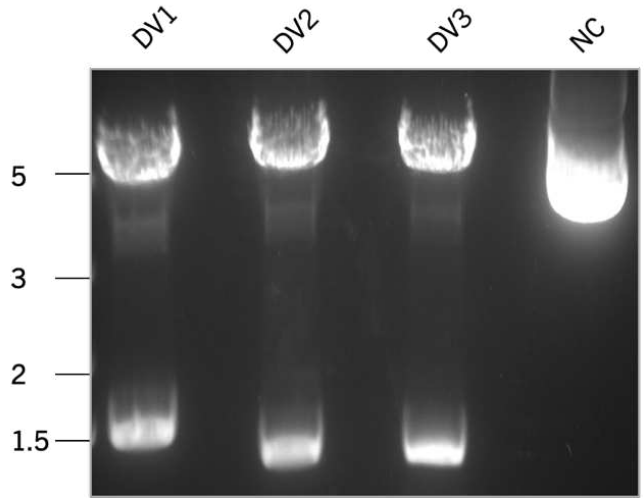

Fig. 8 ***Inserts DV1-DV3 are cloned into pcDNA3.1;*** *gel electrophoresis of restricted pcDNA3.1_mLTβ_DV1-3_myc + unrestricted pcDNA3.1_mLTβ_DV1_myc as NC; restriction with SpeI and BamHI; in silico calculated fragment sizes: DV1 4885bp + 1391 bp, DV2 4892 bp + 1222 bp, DV3 4892 bp + 1231 bp, NC 6276 bp; the unrestricted NC can be seen at ~4.5 kB because closed circular plasmids run through the gel faster than linear fragments; standard ladder in kB.*

mLTβ variant	**DV1**	**DV2**	**DV3**	**WT**
MW variant alone (in Da)	30809.93	25518.21	25194.8	32328.66
MW variant + Myc (in Da)	31995.26	26703.51	26380.1	33790.24
N glycosylation sites	2	1	1	2
O glycosylation sites	16	4	1	18
Total glycosylation sites	18	6	11	20

Table 6 ***Molecular weight of mLTβ WT and DVs and glycosylation sites****; calculated on www.healthtech.dtu.dk.*

3.1.2 mLTβ_DV1 (△D50-Q66) is Not Detectable in the Cell Culture Supernatant

To examine the characteristics of the different deletion variants regarding the expression and the release into the supernatant (SN), the plasmids were transfected into HEK293T cells, and the protein expression was analyzed via Western blotting. Fig. 9 A shows cell lysates (CL) of transfected HEK293T cells. Fig. 9 B shows the supernatant of the respective cells. Every variant is expressed and detectable. Wild-type mLTβ was used as positive control and pEGFP was used as negative control. Wild-type mLTβ and DV3 are expressed in the cell lysate and released into the supernatant at equal amounts. DV2 is expressed equally as much in cell lysate but less in the supernatant. DV1 is expressed in the cells but is not detectable in the supernatant. The results suggest that the deletion of

ΔD50-Q66 prevents the release of mLTβ into the supernatant while ΔQ66-D134 reduces it. The missing amino acids ΔT87-L153 do not influence the extracellular release of mLTβ.

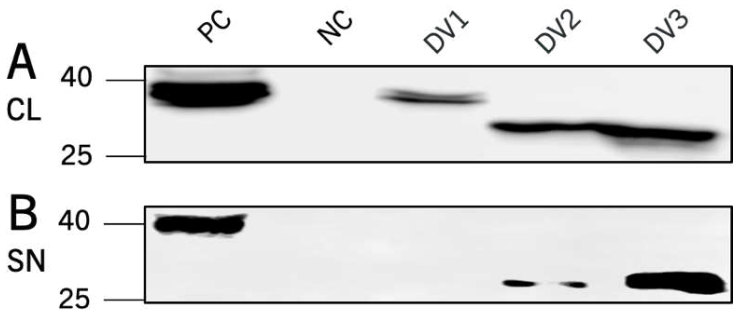

Fig. 9 ***mLTβ_DV1 (ΔD50-Q66) is not detectable in cell culture supernatant of HEK293T cells****, the depicted blots are representatives of three biological replicates (n= 3); A: CL of HEK293T cells transfected with pcDNA3.1_mLTβ_DV1-3_myc; pcDNA3.1_mLTβ_WT_myc used as PC; pEGFP used as NC B: untreated SN of cells blotted in A; α-myc WB; protein ladder in kDa.*

3.1.3 Ba/F3-gp130 Cells Stably Expressing mLTβ Deletion Variants

Ba/F3-gp130 cells stably expressing mLTβ and the deletion variants (DV) were generated to confirm the findings in HEK293T cells. Stable cells express proteins at constant levels and are thus less prone to biological variability. pMOWs_puro vectors encoding for mLTβ_WT, DV1, DV2 and DV3 were generated in a previous work of this group. Restriction analysis with SpeI and PmlI (Fig.) validated the cloning procedure and the orientation of the insert. The resulting plasmids were named pMOWs_puro_mLTβ_WT_myc, pMOWs_puro_mLTβ_DV1_myc, pMOWs_puro_mLTβ_DV2_myc and pMOWs_puro_mLTβ_DV3_myc.

Fig. A shows a Western blot of lysed retrovirally transduced Ba/F3-gp130 cells expressing Myc-tagged mLTβ WT, DV1, DV2 and DV3. Fig. 10 B shows the Western blot of the respective supernatant. mLTβ WT and mLTβ DV1 are strongly expressed, whereas the protein expression of DV2, and especially DV3, appears weak. No protein was detected in the supernatant. In HEK293T cells wild-type mLTβ and mLTβ DV2 and DV3 were detectable in the supernatant and general expression strength was higher (Fig. 9 B). pEGFP was used as positive control for microscopic evaluation of the transduction and as negative control for the Western blot. The Western blot was validated using samples of known intensities and heights.

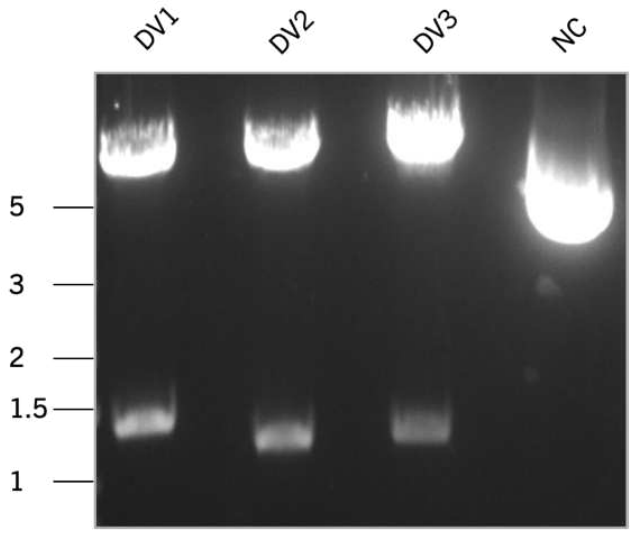

Fig. 10 ***Inserts DV1-DV3 are correctly cloned into pMOWs_puro vector****; gel electrophoresis of restricted pMOWs_puro_mLTβ_DV1-3_myc + unrestricted pMOWs_puro_mLTβ_DV1_myc as NC; restriction with SpeI and PmlI; in silico calculated fragment sizes: DV1 5383 bp + 1342 bp, DV2 5896 bp + 11173 bp, DV3 5389 bp + 1192 bp, NC 6725bp; the unrestricted negative control can be seen at ~4.8 kB because closed circular plasmids run through the gel faster than linear fragments; standard ladder in kB.*

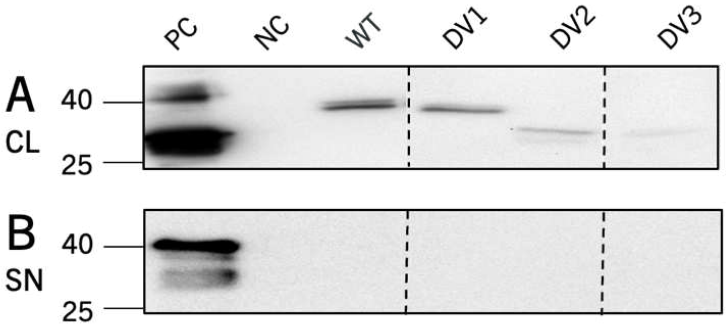

Fig. 11 ***Retrovirally transduced Ba/F3-gp130 cells express mLTβ WT but do not secret mLTβ DV1-3 into SN in detectable amounts; A:*** *CL of Ba/F3-gp130 cells retrovirally transduced with pMOWS_puro_mLTβ_DV1-3_myc and pMOWS_puro_mLTβ_WT_743_myc; pMOWS_puro_PEGFP used as NC;* ***B:*** *untreated SN of cells blotted in A; depicted blots are recompositions of lanes of the same blot; depicted blots are representatives of three biological replicates (n= 3); α-myc WB; protein ladder in kDa.*

The cellular concentration of Ba/F3-gp130 cells expressing mLTβ_WT_myc was increased to 5 x10^6/ml and the supernatant was analyzed after 2, 4, 6, 8, 12 and 24 h. Normally Ba/F3-gp130 cells were cultivated at a maximum density of 1.25 x10^3 cells/ml to avoid cellular stress. At any time mLTβ was not found in the SN but was detectable in the cell lysate (Fig. 10). As the target proteins are expressed in Ba/F3-gp130 cells (Fig. 11 A), and were also detectable in the supernatant of HEK293T cells (Fig. 9 B) the missing release of transduced proteins into the supernatant could be attributed to a cell-specific expression weakness and too little protein amounts rather than protein properties. Ba/F3-gp130 cells are unsuitable for the analysis of supernatant by Western blotting and cannot confirm the results ins HEK293T cells (*cf.* 3.1.2).

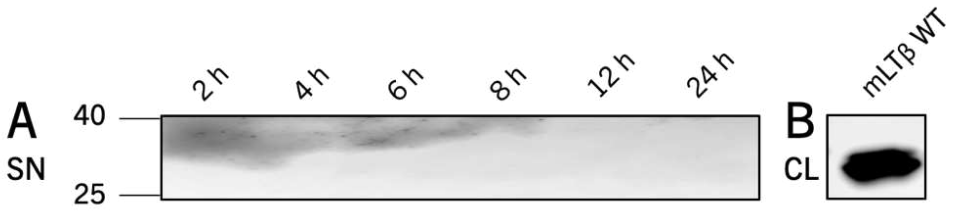

Fig. 10 ***mLTβ WT is not detectable in a BA/F3gp130 cells concentrated up to 5 x10^6/ml****; A: SN of BA/F3gp130 cells retrovirally transduced with pMOWS_puro_mLTβ_DV1-3_myc and pMOWS_puro_mLTβ_WT_743_myc B: untreated CL of cells whose SN was blotted in A; depicted blots are recompositions of lanes of the same blot; depicted blots are representatives of three biological replicates (n= 3); α-myc WB; protein ladder in kDa.*

3.1.4 Ba/F3-gp130 Cells Expressing mLTβ DV1 (△D50-Q66) Show Higher Amounts of Cell-surface mLTβ than Cells Expressing Wild-type mLTβ

Since Ba/F3-gp130 cells were weak in expression for wild-type mLTβ and DVs (Fig. 11 A) a more sensitive method was used to analyze the protein's properties. The Ba/F3-gp130 cells expressing mLTβ WT, DV1, DV2 and DV3 were subjected to flow cytometry. As depicted in Fig. 11 the amount of cell-surface mLTβ is higher for cells expressing mLTβ DV1 compared to cells expressing wild-type mLTβ. Ba/F3-gp130 cells expressing mLTβ DV2 and DV3 do not express mLTβ variants on their cell surface as they present the same signal as non-transduced Ba/F3-gp130 cells (NC). Ba/F3-gp130 cells expressing EGFP were used as positive control. While the protein expression for mLTβ WT of Ba/F3-gp130 is relatively low, the DV1 presents the highest amounts of target protein on the cell surface.

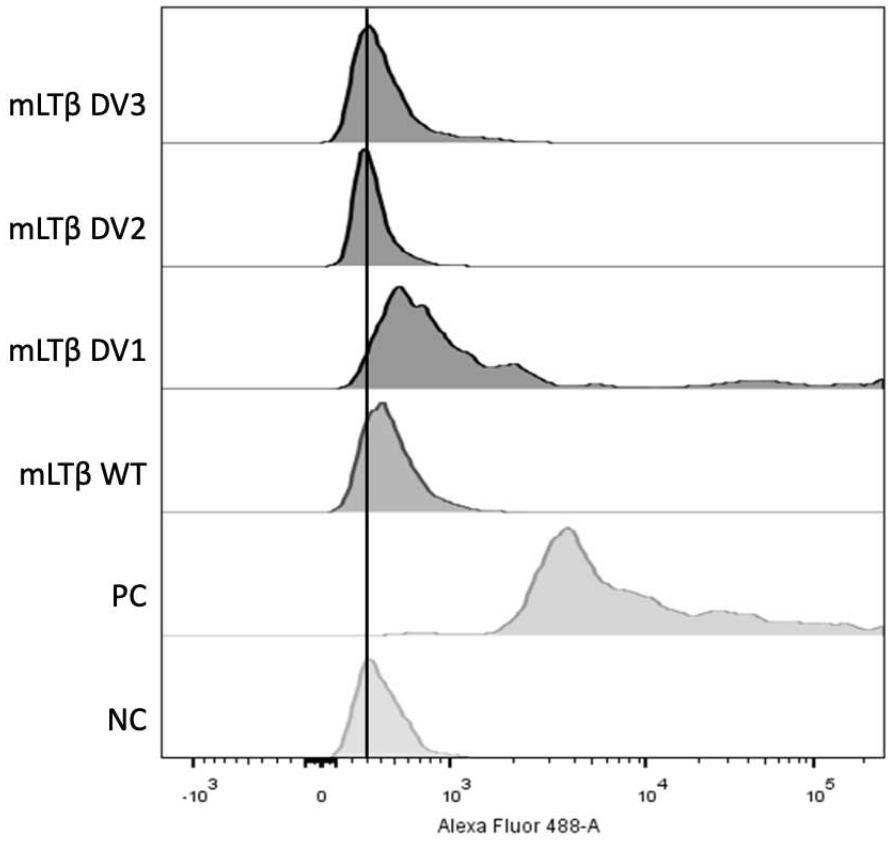

Fig. 11 ***Ba/F3-gp130 cells expressing mLTβ DV1 have a higher cell surface expression of mLTβ DV1 than cells expressing mLTβ WT, DV2 or DV3****; α-myc primary Ab, α-mouse Fc Alexa Fluor 488-A conjugated secondary Ab; the shown data is representative for three biological replicates (n= 3), x-axis shows the emission intensity, y-axis shows the number of cells; cell count is normalized (Ø 8812.75 cells).*

3.1.5 Charged Amino Acids in the mLTβ Shedding Site

The analysis of the mLTβ deletion variants in HEK293T and Ba/F3-gp130 cells suggested that the sequence from D50 to Q66 is crucial for the extracellular release of mLTβ (3.1.4). To identify the amino acids most important in this process, single amino acid mutations were introduced in the sequence from D50 to Q66 of wild-type mLTβ — the deleted sequence in mLTβ DV1. Experimental studies [88, 89] and database analysis [80] have characterized substrate properties specific to ADAM10 and 17. ADAM17 is proven to be a sheddase of mLTβ [11] while ADAM10 involvement is likely but not evident [90, 91]. Therefore, these properties were utilized to select the amino acids to be tested in this work. Roughly 40% of all shared substrates of ADAM10 and 17 C-terminally carry a leucine (L) directly neighboring the shedding site. In 25% a neutral alanine (A), proline (P), and basic arginine (R) are preferred by both proteases next to the N-terminus of the shedding site. Furthermore, amino acid charge and polarity are suspected to crucially influence shedding susceptibility by ADAM10 and 17. *E.g.*, the shedding of

activated leukocyte cell adhesion molecule (ALCAM; CD166) by ADAM proteases has been proven to be heavily influenced by negatively charged aspartic acids (D) within the stalk of the protein. The inhibitory effect is stronger the more negative the charge. A charge reversal to positively charged amino acids has a higher impact on the shedding susceptibility than mutation to a neutral charge [88]. ADAM10 and ADAM17 also differ in their function and substrate specificity: Constitutively active ADAM10 favors aromatic amino acids - especially tyrosine (Y) and phenylalanine (F) - on both termini and a demethylated lysine (K) on the N-terminus of the shedding site in roughly 15% of all its substrates. ADAM17 instead, has a specificity higher than 40% for valine (V) at the C-terminus neighboring amino acid site [89]. The extent to which these findings might influence the extracellular release of mLTβ was investigated in this work. Thereby, the involvement of ADAM10 and 17 as responsible proteases could be examined. By mutating selected single amino acids in the putative shedding site (D50 to Q66), the findings were transferred to mLTβ. Fig. 12 displays the introduced mutations.

mLTβ WT:	49-QDQGRRVEKIIGSGAQA-65
mLTβ CV1 (R53D;R54D):	49-QDQGDDVEKIIGSGAQA-65
mLTβ CV2 (R53D;R54D;K57D):	49-QDQGDDVEDIIGSGAQA-65
mLTβ CV3 (R54D;V55D):	49-QDQGRDDEKIIGSGAQA-65

Fig. 12 ***mLTβ CV and WT amino acid primary structure Q49-A65****; WT amino acids are highlighted in green; introduced charge reversals are highlighted in red.*

The three mLTβ charge variants (CVs) were cloned using site-directed mutagenesis (2.2.8.1). The pcDNA3.1_mLTβ_WT_myc plasmid was used as the template for mLTβ CV1 (R53D;R54D) and mLTβ CV3 (R54D;V55D). CV3 was generated by running one PCR each with the oligonucleotides R54DV55D-rv and R54DR55D-fw and afterward combining the products. CV1 was generated in the same manner with the oligonucleotides R53DR54D-rv and R53DR54D-fw. mLTβ CV2 (R53D;K57D) was generated with pcDNA3.1_mLTβ_CV1_myc as template and by applying the oligonucleotides K57D-rv and K57D-fw. Fig. 13 shows the cloning strategy. The plasmids were named pcDNA3.1_mLTβ_CV1_myc, pcDNA3.1_mLTβ_CV2_myc and pcDNA3.1_mLTβ_CV3_myc. Directed mutations and insert orientations were verified by restriction analysis and comparison to *in silico* pattern prediction (Fig. 14) as well as Sanger sequencing (Fig. 15).

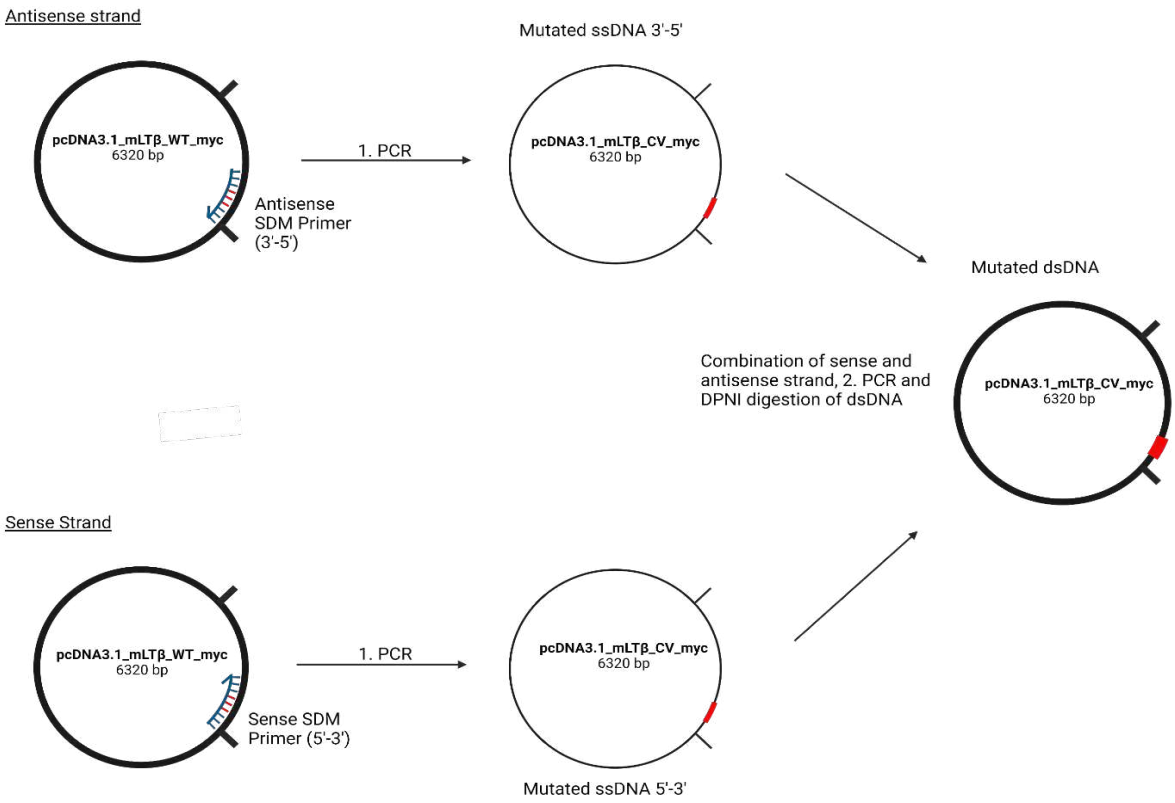

Fig. 13 ***Cloning of pcDNA3.1_mLTβ_CV1-3_myc****; PCR was run with pcDNA3.1_mlTβ_WT_myc template DNA and SDM primer depending on the CV. The resulting mutated ssDNA encoding for mLTβ_CV was combined, and PCR was run again to generate dsDNA; to secure the purity of the PCR product remaining template DNA was cleaved by DPNI restriction; created with biorender.com.*

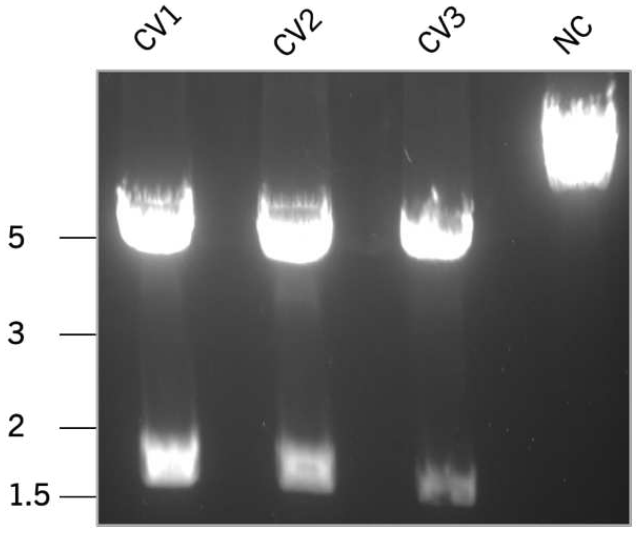

Fig. 14 ***mLTβ CV1 (R53D;R54D), CV2 (R53D;R54D;K57D), CV3 (R54D;V55D point mutations are introduced and orientated correctly****; gel electrophoresis of restricted pcDNA3.1_mLTβ_CV1-3_myc + unrestricted pcDNA3.1_mLTβ_CV1_myc as NC; restriction with SpeI and BamHI; in silico calculated fragment sizes: CV1, CV2, CV3: 4888 bp + 1432 bp, NC: 6320 bp.*

Fig. 15 ***mLTβ WT and CVs sequencing alignment****; Mutations introduced by SDM highlighted in red bracket; deletion of mLTβ_DV1_ΔD50-Q66 underlined in red; excerpt of sanger sequencing result of pcDNA3.1_mLTβ_CV1_myc, pcDNA3.1_mLTβ_CV2_myc and pcDNA3.1_mLTβ_CV3_myc.*

3.1.6 The Relative Amount of mLTβ Charge Variants in the Supernatant is Less Compared to Wild-type mLTβ

mLTβ CV plasmids were transiently transfected in HEK293T cells and the protein expressions were analyzed via Western blotting (Fig. 16). All three charge variants as well as wild-type mLTβ are detectable in the cell lysate as well as the supernatant. mLTβ WT, CV1 and CV3 are expressed at approximately the same level, while the expression of mLTβ CV2 is weaker.

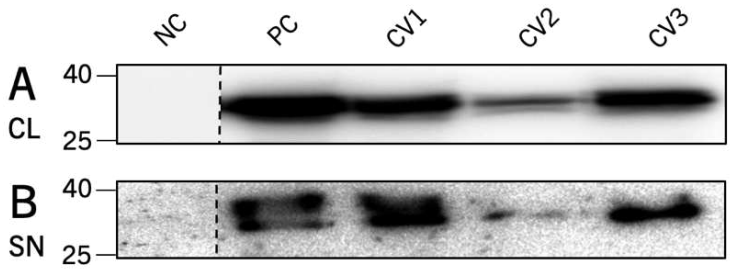

Fig. 16 ***mLTβ charge variants are expressed in HEK293T cells and released into SN; A:*** *CL of transiently transfected HEK293T cells,* ***B****: SN of the respective cells in A; the depicted blots are a recomposition of lanes of the same blot; mLTβ WT useed as PC; pEGFP used as NC; α-myc WB; shown blots are representatives of 5 biological replicates (n=5).*

The protein expressions in Fig. 16 A were quantified and standardized to the expression intensity of CV2, the variant with the weakest expression, in order to determine the different amounts of mLTβ in the supernatant for each charge variant (2.3.4.1). The standardized CL samples exhibit comparable expression rates in the cell lysates (Fig. 17 A). Consequently, the different amounts of mLTβ observed in the supernatant (Fig. 17 B) can be attributed to the introduced charge reversals in the positions R53, R54, V55 and K57. mLTβ DV1 was included as comparative zero value. CV1 shows larger amounts of mLTβ in the supernatant compared to CV2, yet it is lower than that of CV3. All three charge variants present less mLTβ in the supernatant than the wild-type. mLTβ DV1 is not detectable in the supernatant

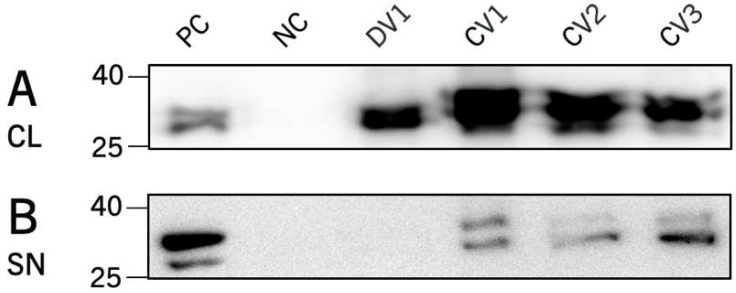

Fig. 17 ***All CVs present less mLTβ in SN than the wild-type****;* ***A****: Standardized CL samples shown in Fig. 16 A + CL of mLTβ_DV1_ΔD50-Q66 Fig. 16 A;* ***B****: Standardized SN samples shown in Fig. 17 B; α-Myc WB; shown blots are representatives of the three biological replicates (n= 3).*

Every standardized expression was quantified, and the relative amount of extracellularly released mLTβ was calculated for mLTβ WT, DV1, CV1, CV2 and CV3. After determining the average relative extracellularly released amount ($\bar{x}$) for every variant, the mean ratios were related to the ratio of mLTβ WT ($\bar{x}$ relative released amount mLTβ DV/CV / $\bar{x}$ released amount mLTβ WT). 61% of mLTβ WT detected in the CL was detected in the SN of respective cells. DV1 was not detected in the supernatant ($p<0.02$). 57% of the CV1 amount detected in CL was detected in SN meaning that mLTβ CV1 reaches 88% of the extracellularly realeased amounts compared to mLTβ WT (57%/ 61%; shed 12% less). 24% of the mLTβ CV2 detected in cell lysate was also detectable in the supernatant showing that mLTβ CV2 is transferred to its soluble form only 36% as much as wild-type mLTβ ($p<0.05$). Cells transfected with pcDNA3.1_mLTβ_CV3_R54DV55D_myc released 42% of mLTβ detected in the cell lysate into the supernatant resulting in a 62% extracellular release ratio relative to mLTβ WT. The ratios of every variant relative to mLTβ WT are presented in Table 7 and Fig. 18. The impact of charge reversals in the deleted region of DV1 on the transfer of bound or intracellular to soluble mLTβ are illustrated in Fig. 18. As described for other ADAM substrates, the extracellular release of mLTβ is affected by amino acid charge and polarity. The more negative the charge, the less protein is released extracellularly. However, the presence of valine has a higher impact than the amino acids charge. If the underlying and influenced mechanism is shedding through ADAM proteases or a different extracellular release mode, needs to be clarified in succeeding experiments.

n=	1	2	3	$\bar{x}$	Median	SD	$\bar{x}$ sample/ $\bar{x}$ WT
Values in %							
WT	61	93	48	67	61	23	100
DV1	1	0	1	0.66	1	0.57	0.1
CV1	74	45	57	59	57	14	88
CV2	29	19	25	24	25	5	36
CV3	52	57	17	42	52	22	62

Table 7 ***Charge reversals and valine mutations decrease the extracellular release of mLTβ;*** *Quantified relative extracellular amounts of mLTβ WT, DV1, CV1, CV2, CV3; signal intensity of mLTβ variants' SN relative to CL compared to WT.*

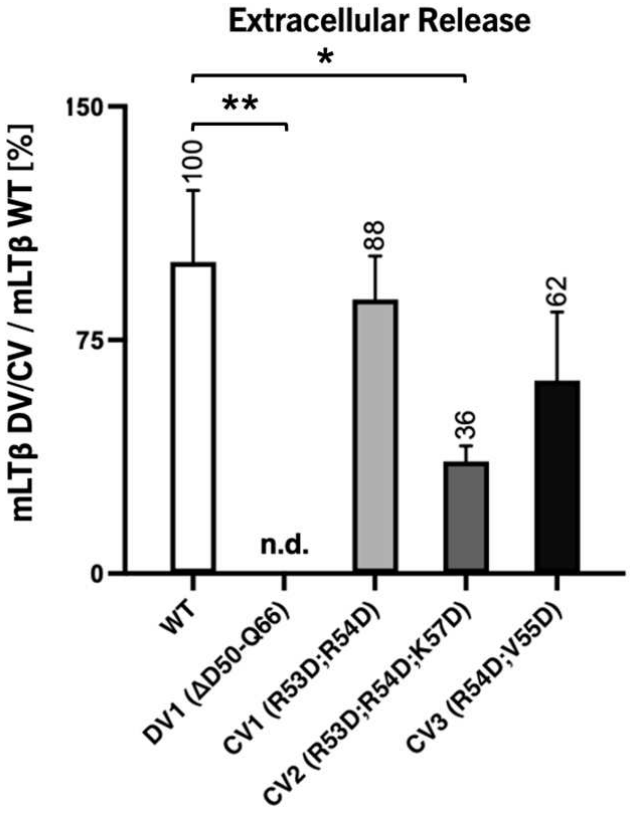

Fig. 18 ***mLTβ CVs show a lower SN to CL ratio compared to mLTβ WT****; depicted values are percentages of Table 7 right column "$\bar{x}$ sample/ $\bar{x}$ WT", * for p<0.05 ** for p<0.02.*

3.1.7 Generation of Stable Ba/F3-gp130 Cells Expressing mLTβ Charge Variants

To confirm valine 55 and amino acid charge as factors important for the extracellular release of mLTβ, Ba/F3-gp130 cells constitutively expressing mLTβ CV1, CV2, and CV3 were generated. Ba/F3-gp130 cells constitutively expressing mLTβ CVs can be subjected to flow cytometry for the identification of proteins expressed on the cell membrane. Therefore, subcloning of mLTβ CV inserts into a pMOWs_puro vector was performed. pcDNA3.1_mLTβ_CV1-3_myc plasmids were used as templates for each respective pMOWs_puro_mLTβ_CV1-3_myc plasmid. The mLTβ CV cDNA and the C-terminal Myc-tag were cut out using PmeI restriction. After separation and purification of the insert from the remaining pcDNA3.1 backbone via gel extraction and DNA purification the inserts were phosphorylated for higher ligation efficiency. The target pMOWs_puro vector was opened via PmeI restriction and dephosphorylated at the 5'-end and purified. Afterward, the inserts were ligated into the pMOWS_puro backbones via blunt-end ligation. Fig. 19 presents the cloning scheme.

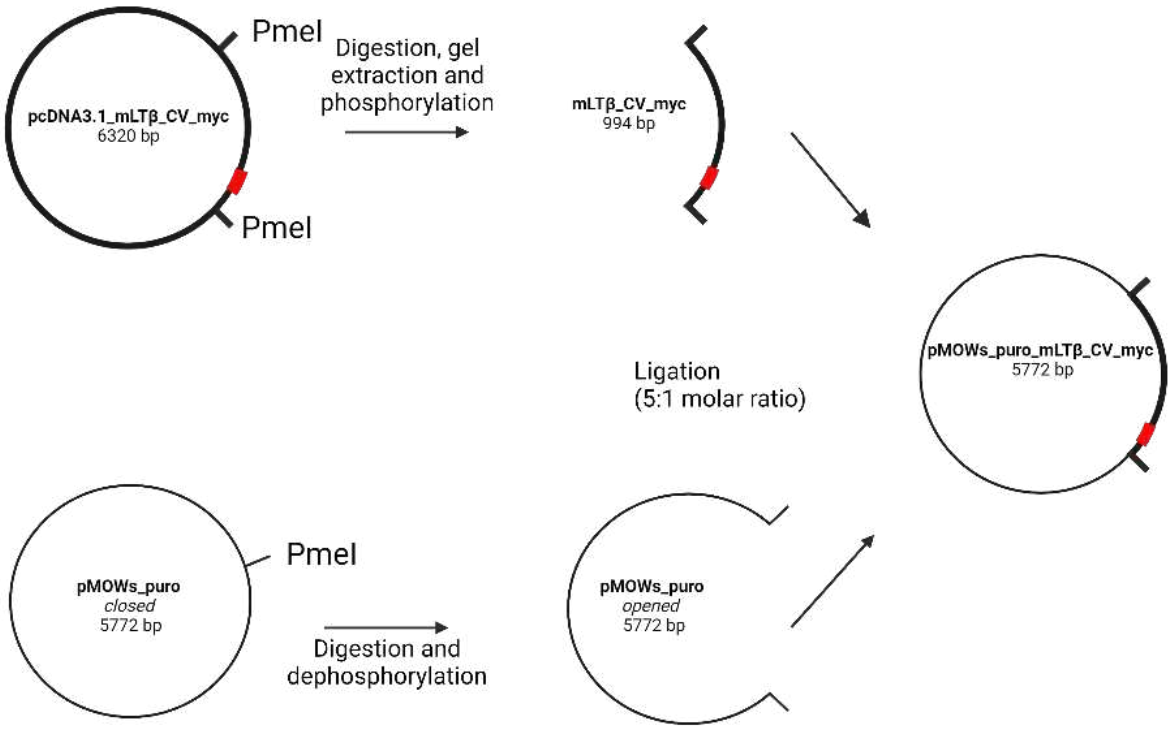

Fig. 19 ***Cloning strategy of pMOWs_puro_mLTβ_CV1-3_myc;*** *the mLTβ CV1-3 inserts with C-terminal Myc-tag were cut by PmeI; Insert and backbone were separated via gel electrophoresis and subsequent gel extraction; pMOWs_puro vector religand was opened with PmeI and dephosphorylated to prevent relegation, created with biorender.com.*

For the selection of successfully ligated plasmids, the ligation product was transformed into *E. coli* XL1-blue and incubated on an ampicillin selection agar. After 12 h colonies were picked, and a mini culture of every picked colony was incubated. DNA extraction was performed after verification of the plasmid and insert's orientation via colony PCR (cPCR). cPCR for the mLTβ CV1 vector was run with the primers DF85 and R53DR54D_rv, while the cPCR for the mLTβ CV2 vector was run with the primers DF86 and K57D_fw and the cPCR for the mLTβ CV3 vector was run with the primers DF85 and R54DV55D_rv. A religated pMOWs_puro vector without insert was used as negative control (mock). Unspecific annealing occurred but could be ignored by comparing the signal intensities and reevaluation by enzymatic restriction. The gel electrophoresis of the cPCR of pMOWS_puro_mLTβ_CV1_myc is displayed in Fig. 20 A. Numbers 10 and 22 were chosen (highlighted in red bracket) for subsequent retroviral transduction into Ba/F3-gp130 cells. The gel electrophoresis of the cPCR of pMOWS_puro_mLTβ_CV2_myc is shown in Fig. 20 B. Plasmid numbers eight and 21 were chosen. The gel electrophoresis of the cPCR of pMOWS_puro_mLTβ_CV3_myc is shown in Fig. 20 C. Plasmid numbers seven and 23 were chosen.

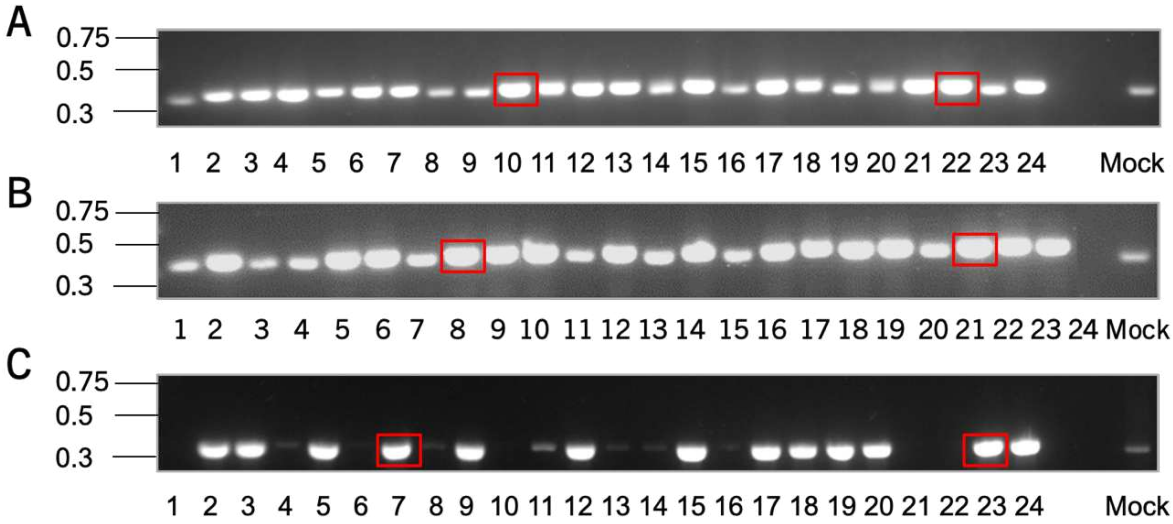

Fig. 20 ***pMOWS_puro mLTβ CV insert + myc tag are validated via cPCR;*** *gel electrophoresis of cPCR products of* ***A****: pMOWS_puro_mLTβ_CV1_myc,* ***B****: pMOWS_puro_mLTβ_CV2_myc,* ***C****: pMOWS_puro_mLTβ_CV3_myc transformed E.coli XL1-blue; used primers were DF85 and R54DV55D_rv; the expected fragment size are CV1: 300 bp, CV2: 328 bp, CV3: 333 bp; standard ladder in kB, chosen plasmids are highlighted in red brackets.*

For DNA amplification midi preparations of chosen plasmids were performed. Sanger sequencing and restriction analysis (Fig. 21) with HindIII confirmed successful cloning and the correct insert orientation.

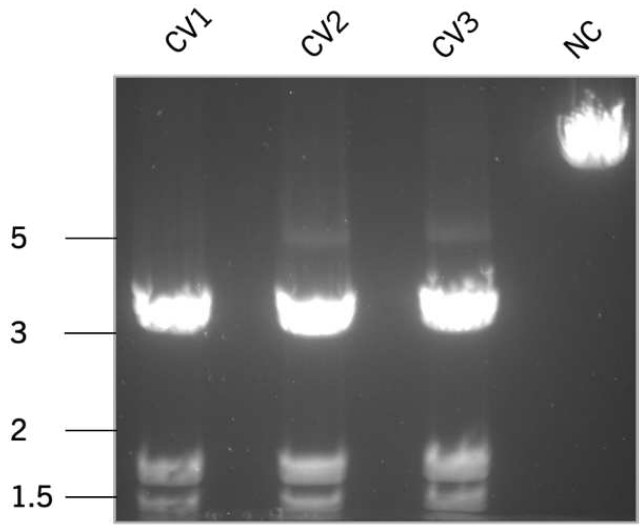

Fig. 21 ***Inserts pMOWS_puro_LTβ_CV1-3_myc are successfully cloned by blunt end ligation****; gel electrophoresis of restricted pMOWS_puro_mLTβ_CV1-3_myc + unrestricted pMOWS_puro_mLTβ_CV1 as NC; restriction with HindII; in silico predicted fragment sizes: CV1, CV2, CV3 3459 bp + 1818 bp + 1499 bp; NC 6776 bp; standard ladder in kB.*

Stably transduced Ba/F3-gp130 cells were generated by retroviral transduction. pMOWS_puro_mLTβ_CV1-3_myc were transfected into Phoenix eco cells. Virus-carrying supernatant was harvested, concentrated by centrifugation, and incubated with Ba/F3-gp130 cells. Ba/F3-gp130 cells were transduced with all three mLTβ CV cDNAs. Successfully transduced cells were selected with puromycin for two weeks. A Western blot of lysed retrovirally transduced Ba/F3-gp130 cells expressing Myc-tagged mLTβ WT, mLTβ CV1, mLTβ CV2 and mLTβ CV3 is shown in Fig. 22. Cell lysate of pEGFP transduced Ba/F3-gp130 cells was used as a negative control for Western blot and as positive control for the microscopic validation of the transduction. All mLTβ variants were expressed by the cells and detectable in the cell lysate but not in the supernatant. The Ba/F3-gp130 cells express less CV1 (R53D;R54D) and CV3 (R54D;V55D) than mLTβ WT and CV2 (R53D;R54D;K57D).

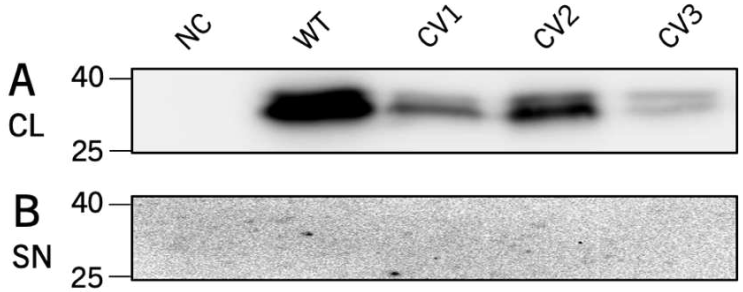

Fig. 22 ***Retrovirally transduced Ba/F3-gp130 cells express mLTβ CV1-3 but do not secret mLTβ CV1-3 into SN in detectable amounts****; A: CL of stable transduced Ba/F3-gp130 cells expressing myc tagged mLTβ charge variants; PEGFP used as NC in WB and as positive control in transduction, pMOWS_puro_mLTβ_myc used as PC; B: SN of respective samples from A; standard in ladder in kDa, α-myc.*

3.1.8 mLTβ CVs Have Higher Cell Surface Expression than mLTβ WT

Flow cytometry was performed on the Ba/F3-gp130 cells expressing mLTβ charge variants. The signal intensity at 488 nm excitation was slightly higher in cells expressing mLTβ CV2 (R53D;R54D;K57D) compared to cells expressing wild-type mLTβ WT. mLTβ CV3 (R54D;V55D) shows less cell-surface mLTβ than mLTβ CV2 (R53D;R54D;K57D) but more than wild-type mLTβ. mLTβ CV1 (R53D;R54D) shows as much cell-surface mLTβ as cells transduced with wild-type mLTβ. Ba/F3-gp130 cells expressing GFP were used as positive control, while non-transduced Ba/F3-gp130 cells with no mLTβ expression were used as the zero-value reference (NC) (Fig. 23). The results align with the Western blot analysis (Fig. 17), showing that extracellular release of mLTβ is inhibited by the CV3 and, more strongly, by the CV2 mutations. As the putative proteases are not inhibited in this experiment, the question regarding the underlying transfer mechanism of mLTβ remains unclear.

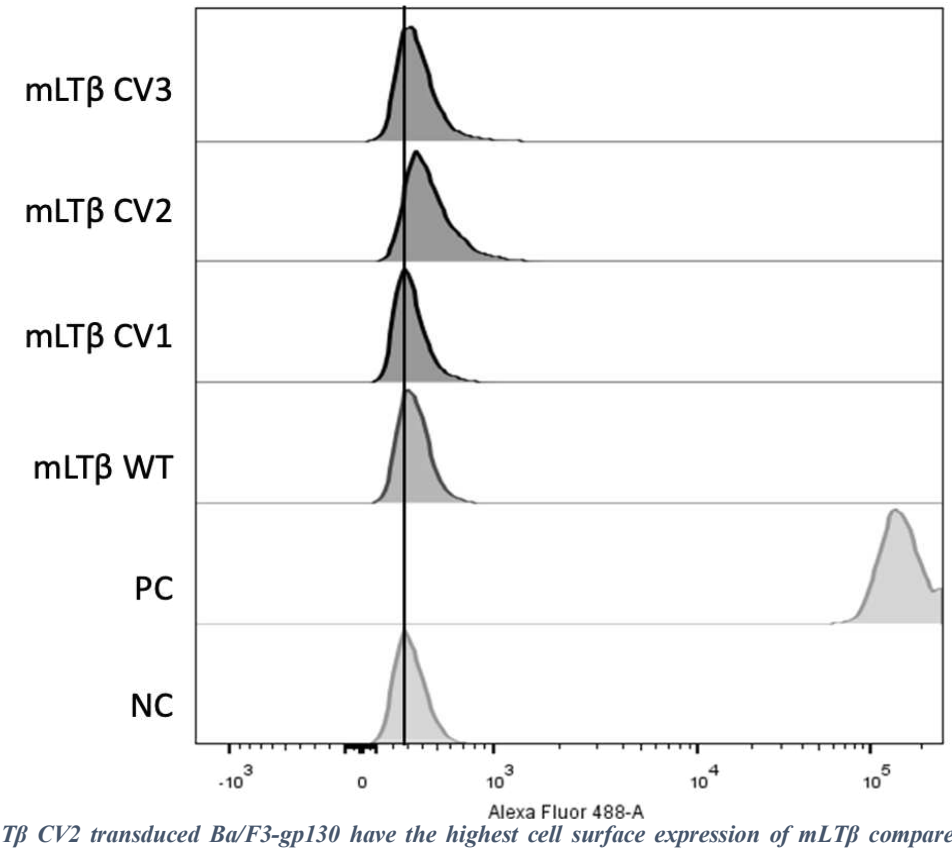

Fig. 23 ***mLTβ CV2 transduced Ba/F3-gp130 have the highest cell surface expression of mLTβ compared to cells expressing mLTβ WT, mLTβ CV1 and mLTβ CV3****; α-myc primary Ab, α-mouse Fc Alexa Fluor 488-A conjugated secondary Ab; the shown data is representative for three replicates, x-axis shows the emission intensity, y-axis shows the number of cells; cell count is normalized (Ø 13595 cells).*

3.2 Shedding Kinetics of mLTβ

Although the sequence and certain amino acids critical for the extracellular release of mLTβ were analyzed, the underlying mechanism—whether shedding via ADAM proteases or an alternative mode of transfer—remained uninvestigated. Therefore, a shedding assay was established (2.4.6) to examine shedding under constitutive and induced conditions within a time kinetic. HEK293T cells were transfected with mLTβ WT and treated with the shedding inductor PMA and/or the metalloproteinase inhibitors (GI, GW, MM) in different combinations to identify the responsible proteases. For constitutive shedding the supernatant was taken after 12, 24, 36 and 48 h. Induced shedding was examined at 2, 4, 6, 8, 12 and 24 h. The supernatant was analyzed via Western blot and ELISA.

3.2.1 Constitutive mLTβ Shedding

Western blot data reveals mLTβ in supernatant of HEK293T cells after 24 h. The mLTβ amount showed a continuous increase until 48 hours. In the supernatant of cells treated with GI (ADAM 10 inhibitor), GW (ADAM 10 and 17 inhibitor), MM (broad-spectrum metalloproteinase inhibitor) and DMSO mLTβ was detectable after 36 h. The DMSO and MM-treated cells did not exhibit a difference between 36 h and 48 h of incubation. The supernatant of GW and GI-inhibited cells only showed a small amount of protein in the supernatant after 36 h but increased strongly after 48 h, particularly when inhibited with GI. Fig. 24 B verifies specific mLTβ expression in all cells of the respective supernatant blotted in Fig. 24 A. The findings hind towards ADAM10 as the primary sheddase of

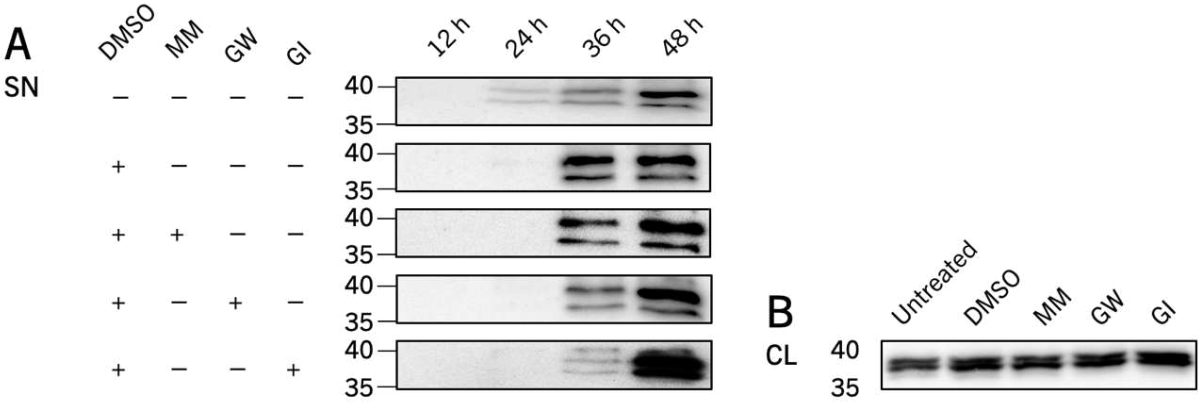

Fig. 24 ***mLTβ is detectable after 24 h under non-induced conditions and is inhibited by GI****; A: SN of HEK293T cells transfected with pcDNA3.1_mLTβ_WT incubated under conditions (untreated, DMSO, MM, GI, GW) in chronological order; B: CL of respective cells lysed after 48 h; α-myc; time (p) in h; standard ladder in kDa,.*

mLTβ under constitutive conditions as GI presents the strongest inhibitory effect. However, GW, MM and even DMSO without an inhibitory effect decreased the extracellular release of mLTβ. This could be attributed to further proteinases involved as well as experimental weaknesses. Overall, the signal intensities and differences between the inhibitors are too small for a clear statement regarding the responsible proteinases.

To specify the data presented in Fig. 24 the samples were subjected to an ELISA. Fig. 25 shows the averaged amount (n= 3) of mLTβ in the supernatant of HEK293T cells transfected wild-type mLTβ within a time kinetic. Samples of untreated, DMSO, GI and GW conditions were subjected to the ELISA. All values fluctuate around the overall average value of 1442 pg/ml. mLTβ was detectable under all conditions after 24 h. The amount did not increase or decrease over time under either condition, and no statistically significant differences were detected.

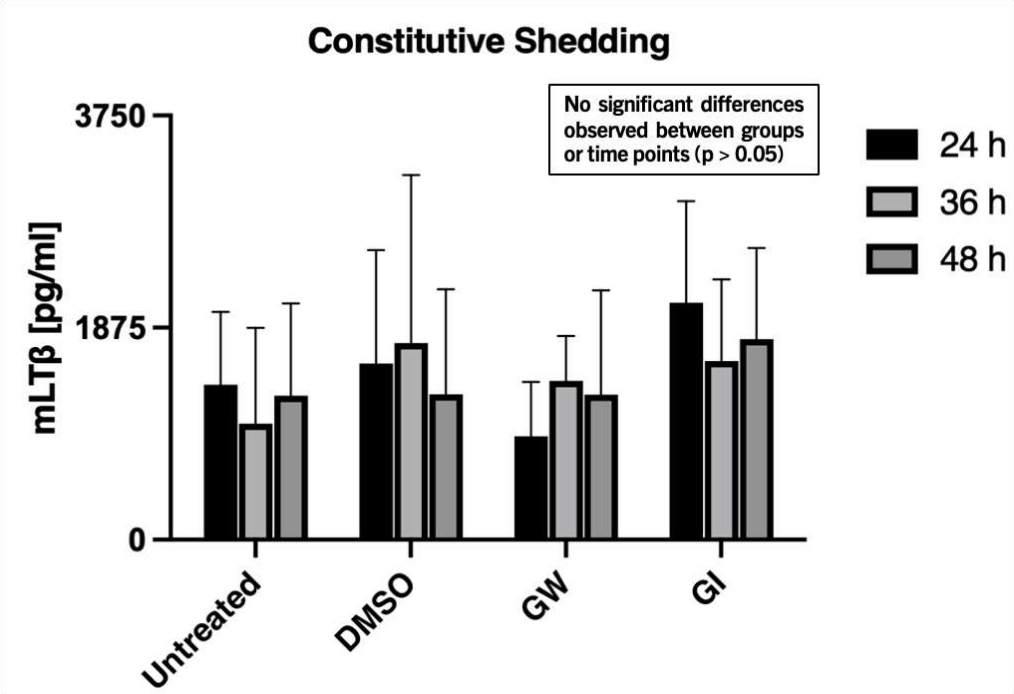

Fig. 25 ***GW and GI have no inhibitory effect on constitutive shedding of mLTβ****; competitive ELISA of SN of HEK293T cells transfected with pcDNA3.1_mLTβ_WT incubated under conditions (untreated, DMSO, MM, GI, GW) in chronological order, time in h, values are averaged out of the independent repetitions (n=3), statistical analysis showed no significant differences between treatments or time points (ANOVA, p > 0.05).*

Taken together, these results do not reveal a consistent or statistically supported trend. While the Western blot data suggests ADAM10 as a likely candidate, the ELISA data lack statistical significance and refute the trends shown by the Western blot data. Therefore, the experimental setup is insufficient for definitive identification of the proteolytic mechanism underlying the constitutive release of mLTβ.

3.2.2 Induced mLTβ Shedding

HEK293T cells transfected with pcDNA3.1_mLTβ_WT_myc from the same culture were incubated under different conditions. All conditions, except for the DMSO negative control, were treated with the respective inhibitor prior to stimulation with PMA. The supernatant of respective cells was subjected to Western blot (Fig. 26 A). The cells incubated with PMA (PC) presented mLTβ in the supernatant after 6 h and the amount of mLTβ steadily increased up to 24 h. In culture incubated with DMSO only (NC), mLTβ was detectable in the supernatant after 12 h. The same was observed for the cells treated with the broad-spectrum inhibitor MM. GW inhibition resulted in small amounts of mLTβ after 12 h which clearly increased after 24 h. In the GI-inhibited samples mLTβ became detectable after 24 h. Fig. 26 B shows the CL of the cells. The data suggests ADAM10 and 17 as the mLTβ sheddases.

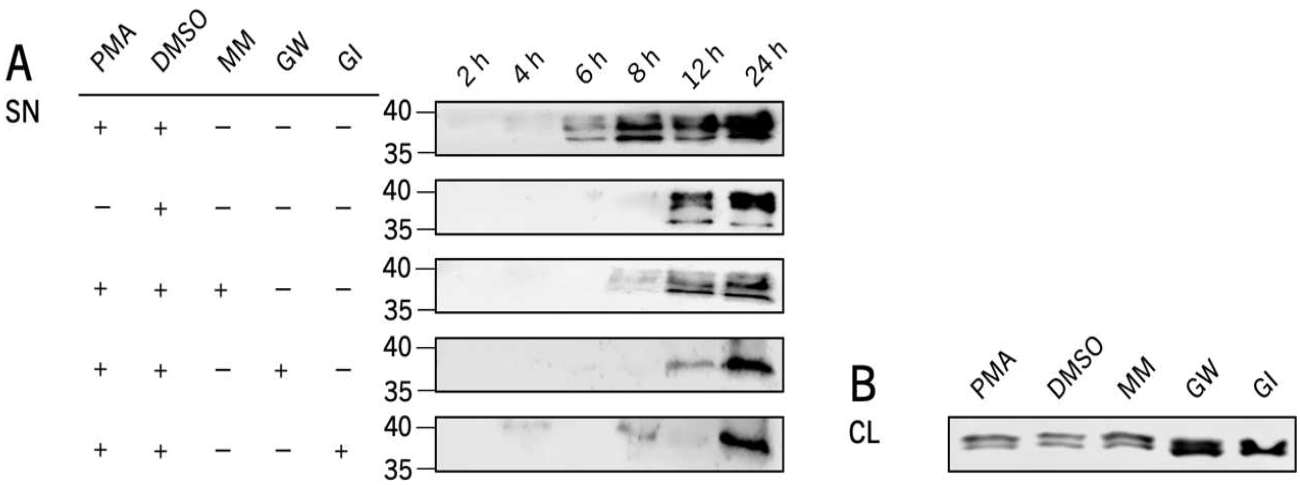

Fig. 26 ***mLTβ is inducibly shed within 6 h by ADAM 10 and 17****; A: SN of HEK293T cells transfected with pcDNA3.1_mLTβ_WT incubated under conditions (PMA only, DMSO, PMA + MM, PMA+ GI, PMA + GW) in chronological order; B: CL of respective cells lysed after 24 h; α-myc; time (p) in h; standard ladder in kDa.*

To determine whether these findings are statistically significant or not the samples blotted in Fig. 26 were subjected to an ELISA. The ELISA was repeated three times and protein amounts were averaged. After 6 h of stimulation, PMA-stimulated cells exhibit higher amounts of mLTβ than the unstimulated (DMSO) and the PMA-stimulated but GW-inhibited (GW + PMA) cells. Additionally, the mLTβ amount increases the most in the PMA-stimulated cells. After 4 h, the supernatant of GW and PMA incubated cells

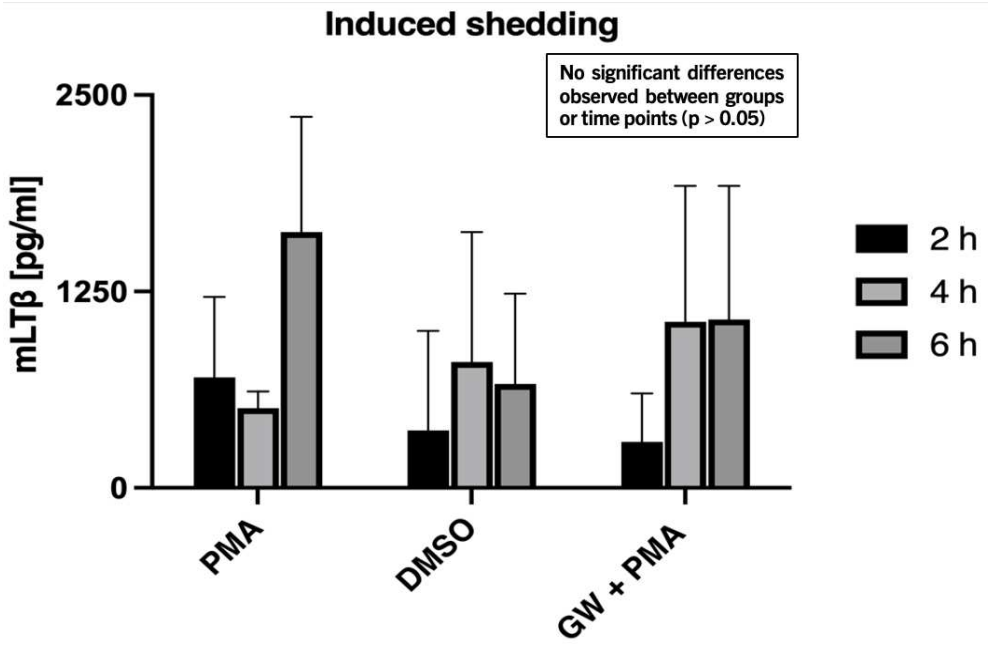

Fig. 27 ***ADAM10 and 17 inhibition (GW) has no significant effect on mLTβ shedding****; competitive ELISA of SN of PMA-stimulated HEK293T cells transfected with pcDNA3.1_mLTβ_WT incubated under conditions (PMA only, DMSO, GW) in chronological order, time in h, values are averaged out of the independent repetitions, statistical analysis showed no significant differences between treatments or time points (ANOVA, p > 0.05).*

(GW + PMA) contain more mLTβ than the PMA and DMSO-incubated cells. Meanwhile, the mLTβ amount does not increase after 4 h. After 4 and 6 h the GW + PMA cells have released more mLTβ than the cells without protease inhibition (DMSO) (Fig. 27).

The Western blot trends indicate that mLTβ shedding can be induced within 6 hours and support the involvement of ADAM10 and ADAM17 in this process. However, the ELISA data did not confirm these observations. No significant differences were detected between groups, and inhibition of proteases did not lead to a reduction of mLTβ in the supernatant.

3.3 The Influence of mLTβ on the Synthesis of mLTα

mLTβ and mLTα are structurally and functionally linked (*cf.* 1.2). In this work the influence of both cytokine domains on each other's synthesis was analyzed.

3.3.1 mLTα and mLTβ Are Linked to a HA Tag

To achieve simultaneous detection of both proteins on the same Western blot in succeeding co-transfection assays and to reduce the variances caused by different protein tags and antibody properties, the cDNAs of both proteins were fused with an identical tag. The mLTβ insert linked to a Myc-tag embedded in a pcDNA3.1 vector was switched to an HA tag embedded in a pcDNA3.1 vector. Fig. 28 and Fig. 29 show the cloning strategy of pcDNA3.1_mLTβ_WT_HA.

To facilitate the insertion of the mLTβ_WT insert into the pcDNA3.1_HA plasmid, in the first step a SpeI restriction site was introduced. Therefore, the mLTβ_WT insert was amplified with two specific primers. pcDNA3.1_SpeI_FP was designed to be fully complementary to the template and served as the forward primer. LTB_SpeI_RP was used as the reverse primer. The non-complementary end of the reverse primer encoded for a SpeI restriction site. Hence, the mLTβ insert was amplified and a SpeI site was added. The PCR product was purified and phosphorylated to improve subsequent ligation. The insert was ligated into a dephosphorylated pCR_Script HincII vector in order to generate sticky ends for the subsequent ligation into the pcDNA3.1 vector. The ligations were conducted in a 5:1 molar ratio (insert : backbone). Dephosphorylation improved cloning results by preventing the re-ligation of the opened vector.

Subsequently, the pCR-Script-SpeI_mLTβ_WT_SpeI was subjected to SpeI restriction. The sticky end SpeI_mLTβ_WT_SpeI insert was isolated, purified, phosphorylated, and ligated into an open, dephosphorylated pcDNA3.1 HA-tagged backbone with SpeI sites on both ends (Fig. 31). This plasmid backbone was cut out of the pcDNA3.1_mLTα_WT_HA via SpeI restriction before.

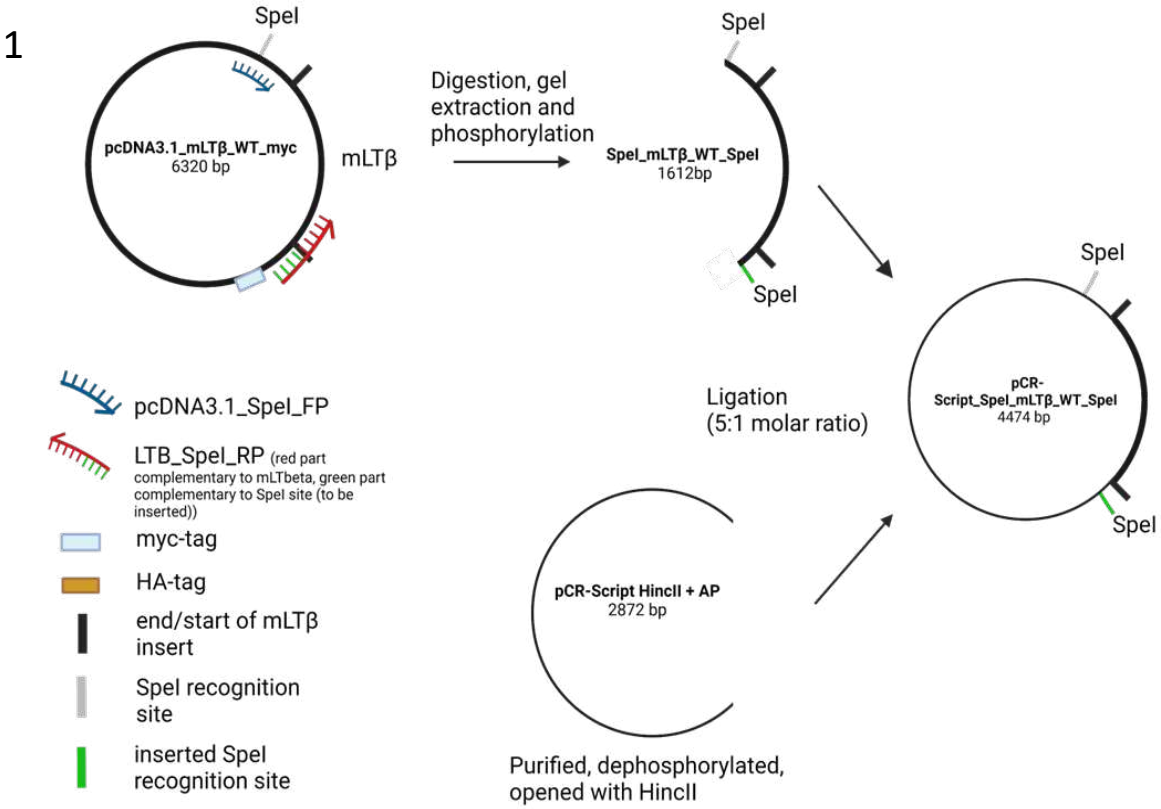

Fig. 28 ***Cloning strategy for mLTβ_WT insert amplification, SpeI site insertion and subsequent ligation into pCR-Script HincII vector***

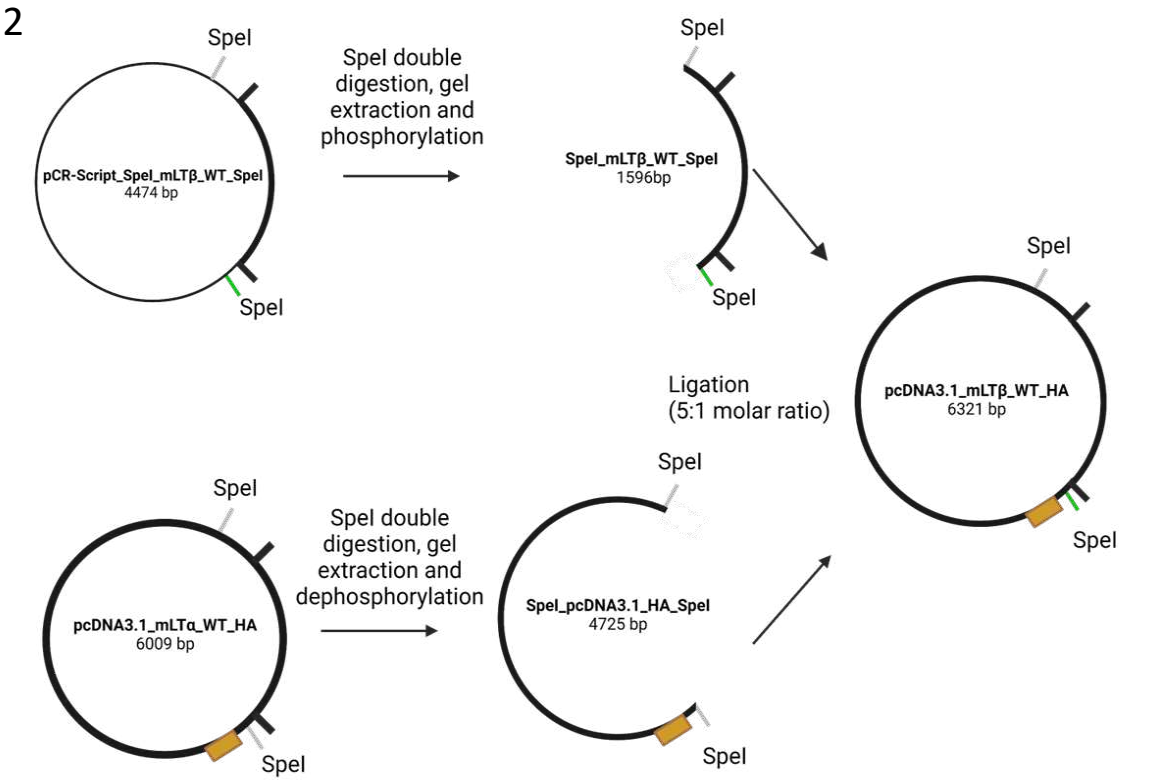

Fig. 29 ***Cloning strategy mLTβ_WT insert is ligated into HA tagged pcDNA3.1 vector at SpeI restriction sites****; labels are the same as in Fig. 28.*

Fig. 30 shows the gel electrophoresis of the restriction analysis of the cloned plasmid. Specific restriction enzymes were chosen to generate an unequivocal band pattern, which served to confirm the insert's insertion and orientation into the plasmid. Additionally, all plasmids were Sanger sequenced before further experiments. The plasmid was named pcDNA3.1_mLTβ_HA.

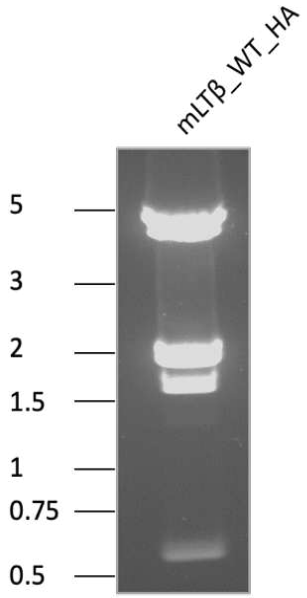

Fig. 30 ***The tag of mLTβ WT is switched from Myc to HA; gel electrophoresis of restricted pcDNA3.1_mLTβ_HA vector****; the plasmid was restricted with Eco147I, in silico calculated fragment sizes were 4315, 1491 and 515 bp; standard ladder in kB.*

3.3.2 Co-transfection of mLTα and mLTβ

To analyze the impact of mLTβ on the synthesis of mLTα, co-transfections of pcDNA3.1_mLTα_WT_HA and pcDNA3.1_mLTβ_WT_HA were performed in ratios from 0.25:1 to 4:1 (mLTβ: mLTα) using a constant 0.1% (v/v) of TurboFect™ transfection reagent in HEK293T cells. The total amount of transfected DNA was kept constant at 5 µg for all conditions, and any differences were filled with pEGFP. The amounts of each plasmid used are shown in Table 8. The Western blot of the CL and the SN of the co-transfected HEK293T is presented in Fig. 31.

Ratio (DNA amounts in µg)	**0.25:1**	**0.5:1**	**1:1**	**2:1**	**4:1**	**0:1 (mLTα only)**	**1:0 (mLTβ only)**	**NC (pEGFP)**
pcDNA3.1_mLTα_WT_HA	1	1	1	1	1	1	/	/
pcDNA3.1_mLTβ_WT_HA	0.25	0.5	1	2	4	/	1	/
pEGFP	3.75	3.5	3	2	/	4	4	5
TurboFect™ (in µl)	10	10	10	10	10	10	10	10

Table 8 ***Ratios of co- transfected mLTα:mLTβ plasmid****, amounts in µg, all transfections used 10 µl of TurboFect™ and carried a total of 10 µg of DNA.*

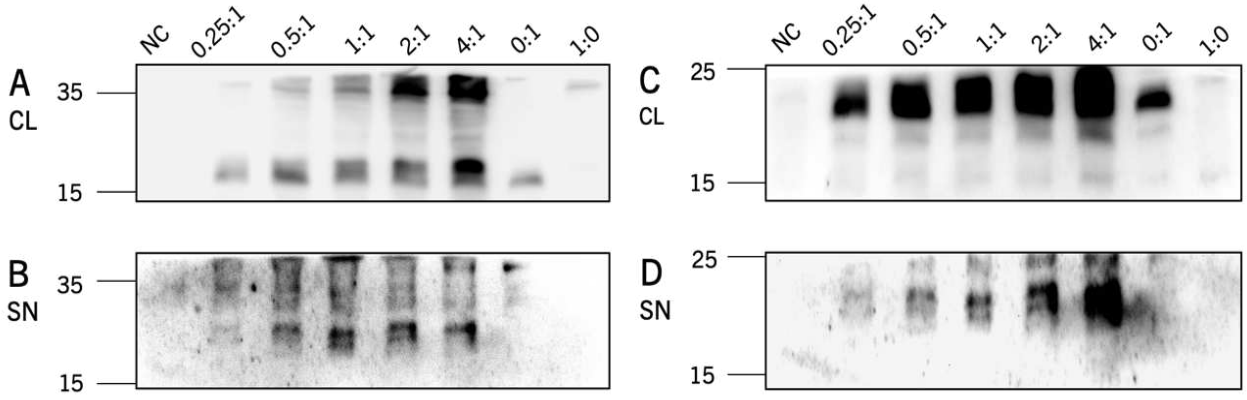

Fig. 31 ***The extracellular expression of mLTα increases with an increasing amount of mLTβ****; A: CL of HEK293T cells co-transfected with pcDNA3.1_mLTα_WT_HA and pcDNA3.1_mLTβ_WT_HA; B: SN of corresponding cells of A; C: Same Western blot as A cut at 25kDa; D: same Western blot as B cut at 25 kDa; pEGFP used as negative control (NC); X:Y describes ratio of transfected mLTβ to mLTα plasmids amounts; 5 µg total amount of DNA in every approach; standard ladder in kDa; mLTα at 22 kDa and mLTβ at 32 kDa; α-HA primary antibody; n= 3.*

As the amounts of transfected mLTβ plasmid increase from 0.25 µg to 4 µg, the mLTβ expression gradually increases in the cell lysate. The expression of mLTα at 22 kDa length does not increase as much as the mLTβ expression at 32 kDa length but still increases gradually (Fig. 31 A and C). In the supernatant, the same can be observed for

the mLTα expression while mLTβ does not increase with higher amounts of transfected mLTβ plasmid (Fig. 31 B and D).

The same samples were subjected to an ELISA. In contrast to the Western blot, which utilized an α-HA primary antibody, the ELISA employed a primary antibody directed directly against the target protein itself, rather than the HA protein tag making the quantification more accurate. All samples were obtained from independent co-transfections (n= 3) and quantified in the same ELISA. Measured amounts were averaged and diagrammed in Fig. 32.

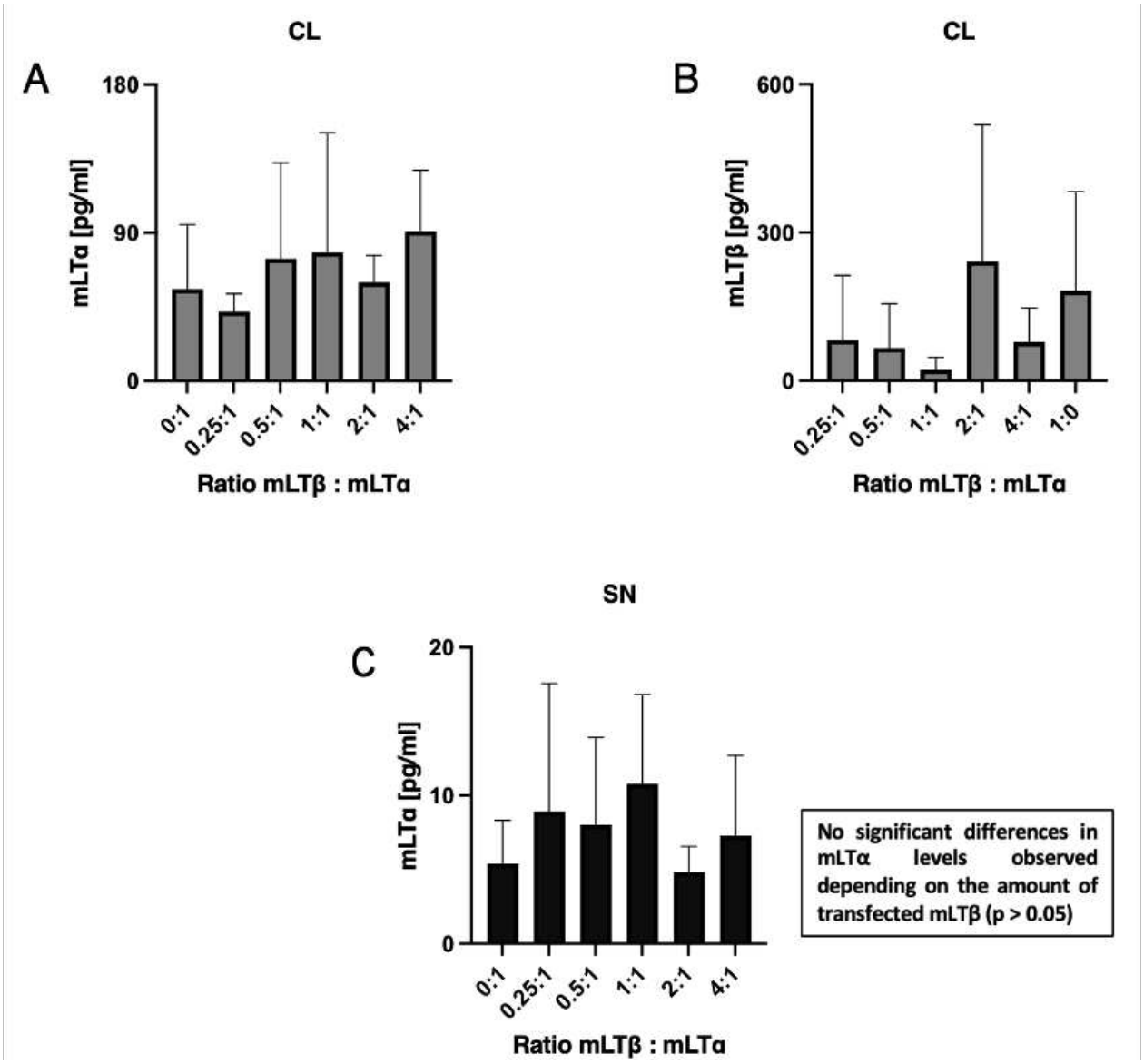

Fig. 32 ***Extracellular amounts of mLTα do not increase with increasing amounts of transfected mLTβ in ELISA analysis****, A: Quantification of mLTα in CL of HEK293T cells co transfected in different ratios with mLTα and mLTβ plasmids (constant 5 µg plasmid amount), competetive α-mLTα ELISA; B: Quantification of mLTα in SN of the cells from A, competetive α-mLTα ELISA; C: Quantification of mLTβ in the same samples of A, competetive α-mLTβ ELISA; mean and SD are depiceted (n=3).*

The averaged mLTα amounts in the cell lysate increase from 55.8 pg/ml in the mLTα single transfection (0:1) to 90.9 pg/ml in the 4:1 co-transfection (Fig. 32 A). The 0.5:1 co-transfected cells express 74.1 pg/ml mLTα while the 1:1 co-transfected cells express 78.1 pg/ml mLTα. Standard deviations range from 9.0 pg/ml (0.25:1) to 59.2 pg/ml (2:1). Except for the 0.25:1 (41.8 pg/ml) and 1:1 (59.8 pg/ml) co-transfection the amount of mLTα linearly increases with the co-transfected amount of mLTβ (R^2= 0.4982). In the supernatant mLTα amounts range from 5.3 pg/ml in the 0:1 ratio to 10.8 pg/ml in the 1:1 ratio. The 0.25:1, 0.5:1, 2:1 and 4:1 vary within this range. Standard deviations range from 1.4 pg/ml (2:1) to 7.1 pg/ml (0.25:1). The mLTα amount in supernatant also increases with the amount of co-transfected mLTβ. The linear relationship is less strong than in the CL (R^2= 0.2169) (Fig. 32 C). mLTβ in the cell lysate did not increase gradually as previously seen in Western blot (Fig. 31 A and B). Values ranged from 22.3 pg/ml (1:1) to 241.9 pg/ml (2:1) with standard deviations from 20.7 pg/ml (1:1) to 225.6 pg/ml (2:1). As no statistically significant differences were detected, a conclusion about the influence of transfected mLTβ on the synthesis of mLTα cannot be drawn. Potentially, a higher number of repetitions could prove a significant trend.

4 Discussion and Outlook

The TNF/TNFRSF is a group of cytokines and cognate receptors with a crucial influence on the immune system. Physiologically it is involved in regenerative processes in the liver [92], lymphoid organogenesis, and the maintenance of secondary lymphoid organs [43]. On the pathological side, it plays a role in the etiology of genetic [93, 94], autoimmune [20, 95], and oncological [23] diseases. LTα and LTβ are part of the TNF/TNFRSF. The lymphotoxins possess noteworthy characteristics. They exhibit their effects as soluble or membrane-bound cytokines and their effects can vary depending on the cells expressing them [13, 51]. Additionally, they can exert stand-alone effects or act in synergy with other TNF/TNFRSF members [45]. Moreover, the assembly of lymphotoxins as homo- or heterotrimers influences their molecular behavior [40]. Biologicals addressing the TNF/TNFRSF such as Etanercept, Infliximab, Adalimumab and Certolizumab have enabled therapeutic opportunities for diseases that were previously only unsatisfactorily treatable. The development required a precise molecular understanding of the cytokines and their corresponding receptors. Thus, a more detailed understanding of the LT system has the potential to design effective therapeutic strategies [96]. This work aimed to further analyze the properties of the lymphotoxins. The mLTβ amino acid sequence which enables the extracellular release was described. A corresponding kinetic was analyzed under induced and constitutive conditions. Meanwhile, the potentially responsible proteases were examined. Furthermore, the influence of mLTβ on the synthesis of mLTα was investigated.

4.1 mLTβ Shedding

mLTβ occurs in a membrane-bound and shed form while their functional differences are not fully understood. ADAM17 is the primary sheddase of mLTβ [13], but others may be involved. For the ADAMs no consensus substrate recognition sequence has been identified so far. Instead, interactions seem to be substrate-specific [89]. Some specificities have been studied for other ADAM17 substrates. For instance, CADM1 shedding is attenuated by o-glycosylation of hydroxyl groups [97], while the transfer of ErbB4 and ALCAM is mediated by alternative splicing, negative amino acid charge, and the distance from the cell membrane [88]. Contradictorily, shedding of the human IL6R is potentiated in the SNP D358A, substituting alanine for negatively charged aspartic acid

adjacent to the shedding site [98]. Peptide library analysis of 474 ADAM17 and ADAM10 substrates showed protease preferences for certain amino acids neighboring the shedding site but no indispensable sequence [80]. While membrane proximity [99] and the processing of ADAM17 by rhomboid-like pseudoproteases [100] have been proven as general control mechanisms, not all regulatory elements of the proteases have been identified. One aim of this work was to reveal further relevant factors in the context of mLTβ.

To narrow the interaction site of mLTβ and its putative sheddases, deletion variants were generated. Previous studies found that in other ADAM substrates the protein stalk is crucial for shedding [101, 102]. Therefore, three putative sequences in the mLTβ stalk were deleted, and their effects were tested. The results revealed that the amino acids D50 and Q66 are crucial for the extracellular release of mLTβ. Each deletion variant lacked a part of the protein stalk that connects the functional (A155-G306) to the transmembrane domain (S28-P48). mLTβ DV2 (ΔQ66-P135) and mLTβ DV3 (ΔT87-L153) were detectable in the cell lysate and the supernatant of HEK293T cells. mLTβ DV1 (ΔD50-Q66) was only detectable in the cell lysate ($p<0.02$). Potentially, because it lacks the interaction site for proteolytical cleavage from the cell's membrane. While other mechanisms of extracellular release cannot be ruled out. Analysis of Ba/F3-gp130 cells supported these findings because cells expressing mLTβ DV1 exhibited higher residual mLTβ levels on the cell membrane compared to cells expressing wild-type mLTβ. Ba/F3-gp130 cells expressing mLTβ DV2 and Ba/F3-gp130 cells expressing mLTβ DV3 did not show increased cell surface expression compared to Ba/F3-gp130 expressing wild-type mLTβ (Fig. 11). However, this confirmation requires critical consideration since p-values were greater 0.05 and mLTβ was not detectable in the supernatant of the cells but only in the cell lysate (Fig. 11). To ensure the validity of the methodological approach, mLTβ transduced Ba/F3-gp130 cells were concentrated up to 5 $x10^6$ cells/ml. Within 24 h, no protein was detected in the supernatant (Fig. 10), not even in the cells expressing wild-type mLTβ. This indicates that the protein synthesis was insufficient to examine the protein expression in Ba/F3-gp130 cells via Western blot. The total protein amount in the supernatant was constantly below the detection limits. Concentrating the supernatant via ultrafiltration or immunoprecipitation should be evaluated in subsequent studies.

Tertiary protein structure is heavily influenced by its charge and is suspected to be a key factor for the substrate recognition by ADAMs. This was demonstrated for the ADAM

substrate ALCAM (CD166). Positively charged amino acids at the interaction site increase shedding, while neutral and especially negatively charged amino acids attenuate shedding [88]. Additionally, ADAM17 prefers aliphatic amino acids, such as valine (V), in the P1 position, while ADAM10 favors aromatic amino acids, such as phenylalanine (F), at the same position [80, 89]. Looking at the mLTβ stalk region these properties can be found in the essential DV1 region. The positively charged amino acids R53, R54, K57 and the aliphatic V55 were tested in three combinations (CV1-3) by substitution of negatively charged aspartic acid (D). All three CVs showed altered supernatant-to-cell lysate ratios in the amount of the mLTβ compared to the wild-type protein. R53, R54, K57 and especially V55 are important for the extracellular release of mLTβ. The mLTβ CVs confirmed that amino acid charge is a relevant factor for the extracellular release of mLTβ. In mLTβ CV2, three positively charged amino acids (2 × R, 1 × K) were replaced with three negatively charged amino acids (3 × D). As a result, mLTβ CV2 was transferred only at 36% of the rate of wild-type mLTβ WT ($p<0.05$) (Fig. 18). Furthermore, the mLTβ transfer rate is positively correlated with the positive charge in the shedding site. This can be seen by the comparison of the shedding of mLTβ CV1 (R53D;R54D) to mLTβ CV2 (R53D;R54D;K57D), where mLTβ CV1 is transferred more than mLTβ CV2 (88 vs. 36% compared to mLTβ WT shedding; Fig. 18). Moreover, the data suggests that valine 55 is more important than the amino acids charge in this region. mLTβ CV3 (R54D;V55D), which misses aliphatic V55 but retains the positively charged amino acids R53, is transferred 26% less than CV1 (88% vs. 62% compared to mLTβ WT shedding; Fig. 18). Even though, mLTβ CV3 carries one positively charged amino acid more than mLTβ CV1. In conclusion, all tested combinations show altered transfer rates indicating that the regulation of the transfer of mLTβ follows a pattern like other ADAM substrates, such as CD166 or the IL-6R. Still, a higher number of repetitions is needed to prove statistical significance for the observations regarding mLTβ CV1 and CV3. Flow cytometry analysis on Ba/F3-gp130 cells point towards the same conclusion, although also missing statistic significance (Fig. 23). Cells that express mLTβ CV2 show the highest amount of residual protein on the cellular surface, followed by cells expressing mLTβ CV3. mLTβ CV1 expressing cells show no difference compared to the mLTβ WT.

Like the Ba/F3-gp130 cells expressing mLTβ DVs, Ba/F3-gp130 cells expressing mLTβ CVs do not express proteins in the supernatant in sufficient amounts. Considering another cell line for stable mLTβ DV/CV transduction and subsequently analyzing protein

expression via Western blot and flow cytometry would be useful to clarify the equivocal findings.

The design of deletion and charge variants leads to conclude three relevant factors, which might be involved in the regulation of the extracellular release of mLTβ. Firstly, the crucial sequence is located within the first 16 amino acids of a 106 amino acid stalk indicating that proximity to the cell membrane is important. Secondly, similar to what was observed for the ADAM17 substrates ErbB4 and ALCAM, the charge of amino acids influences the transfer of mLTβ [88], potentially by ADAM17. Hereby applies, the more negative the charge the less likely the transfer. Thirdly, valine seems to be a crucial amino acid within this site. To gain further insights into transfer of mLTβ and identify ADAMs as the key players, follow-up experiments are proposed. The influence of the o-glycosylations within the Q49 to Q66 region could provide further information as glycosylations might sterically hinder sheddases or influence the stability of the mLTβ ectodomain. Furthermore, the influence of the distance between the cell membrane and the DV1 region should be looked at more closely. Therefore, a flexible polypeptide linker that does not interact with ADAM could be inserted between the transmembrane and stalk region to confirm substrate recognition based on membrane proximity. In follow up experiments an antibody targeting the DV1 region should be evaluated as option to selectively and temporarily suppress the extracellular release of mLTβ. Therapeutic approaches targeting ADAMs have long been considered interesting targets due to their pleiotropic functions and effects[103]. Nevertheless, side effects, toxicity and low bioavailability led to failures in clinical trials [104, 105]. Developing a substrate-specific inhibitory molecule that targets only one ADAM17 substrate may reduce side effects while maintaining a high therapeutic efficacy. All in all, the findings increase the possibility to understand the functional differences between bound and soluble mLTβ and to exploit its therapeutic potential.

4.1.1 ADAM 10 and 17 Play a Role in mLTβ Shedding

Constitutive mLTβ shedding was detectable after 24 hours in HEK293T cells in Western blot. Treatment with the ADAM10 and ADAM17 inhibitor GW appeared to delay mLTβ detection in the supernatant until 36 hours. Similarly, treatment with the selective ADAM10 inhibitor GI resulted in minimal mLTβ levels at 36 hours, with increased levels observed after 48 hours (Fig. 24). These observations suggest ADAM10 and ADAM17

as sheddases of mLTβ. Notably, GI exhibited a more pronounced inhibitory effect, indicating that ADAM10 might be the primary protease involved under constitutive conditions. Application of the broad-spectrum inhibitor Marimastat also led to reduced amounts of mLTβ in the supernatant, supporting the involvement of ADAM10 and ADAM17, but potentially also other MMPs, in this process (Fig. 24). These findings warrant further investigation to determine statistical signifance. It is also important to note that the inhibitory effects of GI and GW observed in Western blot analyses (Fig. 24) were not consistently reflected in ELISA data (Fig. 25) which did not show significance either.

Under PMA-stimualted conditions mLTβ was detectable in the supernatant after 2 h. The shedding induction in cells with a broad inhibition of metalloproteinases (MM) presented postponed shedding for six additional hours as it was detectable after 12 h compared to non-inhibited cells after 6 h. However, selective inhibition of ADAM17 and ADAM10 using GW had a stronger effect. Similarly, when ADAM10 was selectively inhibited with GI, induced mLTβ shedding was also incapacitated. mLTβ was detectable after 24 h under both conditions (Fig. 26). As previously presented, mLTβ became detectable after 24 hours in the constitutive setting, putatively mediated by ADAM10. Therefore, no induced shedding can be assumed for the 24-hour time point. Considering that ADAM10 is characterized as a non-inducible MMP, while ADAM17 is known to be inducible, these findings hind towards ADAM17 as the major sheddase of mLTβ under stimulated conditions. This aligns with previous studies [13, 69, 71]. The more effective inhibition of ADAM17 by GI than by GW imposes contradictions and might be due to biological variances or overall inhibitor effectiveness. GI is a hundredfold more selective for ADAM10 but still conveys an inhibitory effect on ADAM17 [69]. To definitively exclude the involvement of ADAM10 in induced shedding and ADAM 17 in constitutive shedding , the experiments could be repeated using cells genetically deficient for the respective protease. Additionally, the broad-spectrum metalloproteinase inhibition with Marimastat suggests that induced mLTβ shedding is not exclusively mediated by ADAM17 but may also involve other proteinases. Findings via Western blot were supplemented by ELISA analysis of induced shedding. The GW-inhibited approach always presented higher mLTβ amounts than the non-stimulated approach (DMSO) and lower amounts than the non-inhibited approach (PMA only) except after 4 h. Shedding was detectable after 2 h (Fig. 27). The inhibition of shedding through GW confirms that ADAM10 and especially ADAM17 are responsible for mLTβ shedding and that this

process starts at least 2 h, rather than 6 h shown by Western blot, after stimulation. Still, the ELISA data failed to provide statistical significance. All in all, a higher number of repetitions and sample size is necessary to obtain explicit and unequivocal results regarding the shedding of mLTβ.

Since at least two proteases are involved, an important aspect for further experiments is to explore whether mLTβ has a common shedding site for all its proteases, or if each protease has a distinct shedding site and mechanism. Initially, the shedding assays could be extended with mLTβ DV1, to refute or support the existence of other shedding sites outside this region. Understanding its shedding site specificity is crucial because it impacts the feasibility of a suppression of the mLTβ shedding. If each protease has a solitary site, then inhibiting one protease may not lead to a complete suppression of shedding, as other proteases could potentially compensate for and rescue the shedding process. This could have implications for *in vivo* scenarios. If the shedding of one pharmacologically silenced protease is rescued by another, no effect is to be expected. On the other hand, this could also imply therapeutic advantages such as organ-specific shedding suppression because induced and constitutive shedding are mediated by different proteases and could be targeted differentially. Potentially unfavorable aspects such as rheumatic attacks [13] can be alleviated while favorable effects such as liver cell regeneration [49] remain intact.

In conclusion, further experiments should test the suppression of shedding by the blockage of the DV1 site. It would be interesting to test the effects of the specific suppression in induced and constitutive mLTβ shedding *in vivo*. Thereby functional differences between bound and shed and induced or constitutive mLTβ shedding could be identified.

4.2 mLTβ Needs mLTα and Influences its Expression

The ligands of the TNFSF act together [1], functionally depend on each other [40], and share structural characteristics [6]. The three ligands in the TNFSF, TNFα, LTβ and LTα, are all encoded at 6p21.33 in the human and at 17, 18.59 cM in the murine genome, all located within 12 kb of genomic DNA [106, 107]. This genetic and functional proximity suggests that these cytokines might influence each other's expression.

Studies have shown that mice deficient for LTα and/or TNFα have proven an impact on the synthesis of other TNFSF members, although the specific effect remains uncertain [108, 109]. Still, LTβs functional need for LTα suggests a positive correlation in their biosynthesis [40].

In this work, the expression of mLTα increased progressively with the amount of co-transfected mLTβ. Higher amounts of co-transfected mLTβ plasmid led to increased mLTα protein levels, even though the amounts of transfected mLTα plasmid were the same (Fig. 31 A-D). The elevation of mLTα can be seen in the cell lysate and supernatant while the gradual increase of mLTβ is only observable in cell lysate but not in supernatant. The ELISA data revealed trends but not significances.

mLTα assembles with $mLT\beta_2$ in the endoplasmic reticulum before it is transported to the membrane [26] and released into the supernatant. This process is regulated by the proteases involved. A potential saturation of these proteases might influence the absence of a significant elevation of mLTβ. Still, this finding lacks a clear explanation and seems contradictory. mLTα monomers that do not assemble with mLTβ to a form a membrane-bound $mLT\alpha_1\beta_2$ heterotrimer, can be secreted into the supernatant as mLTα homotrimer. The observations indicate that both utilizations of mLTα monomers may be enhanced. Functionally, this suggests that elevated mLTβ levels, which primarily activate the LTβR, could indirectly influence TNFRI and TNFRII activation, contributing to crosstalk within the TNF/TNFRSF signaling pathways. The ELISA data point into the same direction. mLTα concentrations rose from 55.8 pg/ml to 90.9 pg/ml in the cell lysate (CL) (R^2 = 0.4982) and from 5.3 pg/ml to 10.8 pg/ml in the supernatant (R^2 = 0.2169) (Fig. 32). While these data suggest a positive correlation between mLTα levels and increasing amounts of co-transfected mLTβ, the results did not reach statistical significance. Similarly, Western blot analyses indicated trends consistent with the ELISA findings; however, these too lacked statistical significance. To strengthen the validity of these observations, future experiments should increase the number of biological replicates and increase the amount of protein analyzed.

Taken together, mLTβ might be a stimulating factor for the synthesis of mLTα. Many factors (*e.g.* enhanceosomes, coactivators, epigenetic modifications) influence the evolutionary highly conserved promotor of the TNF/LT gene locus that presents a cell type- and stimulus-specific expression regulation [110, 111].

One additional factor could be the resulting cytokines themselves. Additional research is required to verify this conclusively. As the immune system cannot tolerate the aberrant function of mLT$\alpha_1\beta_2$ the interdependent regulation of two different gene products can be considered an immunological safety measure to prevent generalized fragility [26]. This underscores the importance and therapeutic potential of the TNFR/TNFSF, especially its LT subfamily.

4.3 Conclusion

In this study, the essential sequence for the extracellular release of mLTβ was located between the amino acids D50 and Q66. Within this sequence, the amino acids R53, R54, V55, and K57 were identified as particularly relevant. The charge properties of these amino acids are a regulating factor. Negatively charged amino acids lead to a decreased amounts of mLTβ in the supernatant. More importantly, the non-polar amino acid, valine at position 55, is confirmed as a relevant element for the extracellular release of mLTβ. Additionally, the proximity to the cell membrane might be a decisive factor.

Under different conditions, two proteases, ADAM10 and ADAM17, are involved in the transfer of membrane-bound mLTβ to its soluble form. Constitutive mLTβ shedding was detectable after 24 hours, likely mediated by ADAM10, whereas induced shedding appeared after 2 hours and was presumably mediated by ADAM17. A subordinated role can be presumed for other matrix metalloproteinases and should be considered in further studies. Subsequent experiments should also reconsider the number of repetitions and amount of protein analyzed to receive more detailed and significant information. Moreover, it would be a useful extension of this work to develop an antibody that targets the mLTβ DV1 (ΔD50-Q66) site and prevents shedding. This mLTβ-specific suppression of protease activity might have the potential to reduce adverse effects that led to the failure of therapeutic ADAM inhibition in the past. Furthermore, it should be investigated whether the proteases involved all interact with mLTβ at the same amino acid position and how they can be differentially pharmacologically addressed. Thus, in addition to the functional differentiation of bound and shed mLTβ, the effect of constitutive as opposed to induced shedding could be further specified *in vivo* through respective ADAM10 and/or 17 gen knockouts.

This study also examined mLTβ as a stimulatory factor for the expression of mLTα. An increase in intracellular mLTβ plasmid levels led to a rise in synthesized and secreted mLTα, even though the amount of transfected mLTα plasmid remained constant. This suggests that LTβ might indirectly signal through the LTα receptors, TNFRI and TNFRII. Moreover, LTβ requires LTα monomers for its proper structural conformation to signal via its LTβR. The expression enhancement of mLTα by mLTβ could be an immunological safety mechanism and would contribute to the complex regulation of the immune response and plasticity of the TNF/TNFRSF. However, additional experiments are required to validate the significance of this observation.

All in all, this study identified key amino acid sequences involved in the extracellular release of mLTβ, shed light on the roles of ADAM10 and ADAM17 in this process, and examined the regulatory relationship between mLTβ and mLTα.

5 Bibliography

1. Hehlgans T, Pfeffer K. The intriguing biology of the tumour necrosis factor/tumour necrosis factor receptor superfamily: players, rules and the games. *Immunology.* 2005;115(1):1-20.
2. Peter C. Heinrich, Müller M, Lutz Graeve. Löffler/Petrides Biochemie und Pathobiochemie. Springer, Berlin, Heidelberg; 2014. XXIX, 1073 p.
3. Lackie J. A Dictionary of Biomedicine. Oxford University Press: Oxford University Press; 2010.
4. Liu Y, Zhao M, Qu H. Identification of cytokine-induced cell communications by pan-cancer meta-analysis. *PeerJ.* 2023;11:e16221.
5. Dostert C, Grusdat M, Letellier E, Brenner D. The TNF Family of Ligands and Receptors: Communication Modules in the Immune System and Beyond. *Physiol. Rev.*. 2019;99(1):115-60.
6. Locksley RM, Killeen N, Lenardo MJ. The TNF and TNF receptor superfamilies: integrating mammalian biology. *Cell.* 2001;104(4):487-501.
7. Chan FK, Chun HJ, Zheng L, Siegel RM, Bui KL, Lenardo MJ. A domain in TNF receptors that mediates ligand-independent receptor assembly and signaling. *Science.* 2000;288(5475):2351-4.
8. Yu X, James S, Felce JH, Kellermayer B, Johnston DA, Chan HTC, Penfold CA, Kim J, Inzhelevskaya T, Mockridge CI, Watanabe Y, Crispin M, French RR, Duriez PJ, Douglas LR, Glennie MJ, Cragg MS. TNF receptor agonists induce distinct receptor clusters to mediate differential agonistic activity. *Commun. Biol.*. 2021;4(1):772.
9. Dempsey PW, Doyle SE, He JQ, Cheng G. The signaling adaptors and pathways activated by TNF superfamily. *Cytokine Growth Factor Rev.*. *2003*;14(3-4):193-209.
10. Hehlgans T, Männel DN. The TNF-TNF receptor system. *Biol. Chem.*. 2002;383(10):1581-5.
11. Reddy P, Slack JL, Davis R, Cerretti DP, Kozlosky CJ, Blanton RA, Shows D, Peschon JJ, Black RA. Functional analysis of the domain structure of tumor necrosis factor-alpha converting enzyme. *J. Biol. Chem.*. 2000;275(19):14608-14.
12. Peschon JJ, Slack JL, Reddy P, Stocking KL, Sunnarborg SW, Lee DC, Russell WE, Castner BJ, Johnson RS, Fitzner JN, Boyce RW, Nelson N, Kozlosky CJ, Wolfson MF, Rauch CT, Cerretti DP, Paxton RJ, March CJ, Black RA. An essential role for ectodomain shedding in mammalian development. *Science*. 1998;282(5392):1281-4.
13. Young J, Yu X, Wolslegel K, Nguyen A, Kung C, Chiang E, Kolumam G, Wei N, Wong WL, DeForge L, Townsend MJ, Grogan JL. Lymphotoxin-alphabeta heterotrimers are cleaved by metalloproteinases and contribute to synovitis in rheumatoid arthritis. *Cytokine*. 2010;51(1):78-86.
14. Sonar S, Lal G. Role of Tumor Necrosis Factor Superfamily in Neuroinflammation and Autoimmunity. *Front. Immunol.*. 2015;6(364).
15. Masters SL, Anna Simon, Ivona Aksentijevich, Kastner DL. Horror Autoinflammaticus: The Molecular Pathophysiology of Autoinflammatory Disease. *Annu. Rev. Immunol.*. 2009;27(1):621-68.
16. Steiner JD, Annibal A, Laboy R, Braumann M, Göbel H, Laasch V, Müller RU, Späth MR, Antebi A, Kubacki T. A novel TNFRSF1A mutation associated with TNF-receptor-associated periodic syndrome and its metabolic signature. *Rheumatology (Oxford)*. 2023;62(10):3459-68.

17. Tauzin S, Debure L, Moreau J-F, Legembre P. CD95-mediated cell signaling in cancer: mutations and post-translational modulations. *Cell. Mol. Life Sci.*. 2012;69(8):1261-77.
18. Ferrari S, Giliani S, Insalaco A, Al-Ghonaium A, Soresina AR, Loubser M, Avanzini MA, Marconi M, Badolato R, Ugazio AG, Levy Y, Catalan N, Durandy A, Tbakhi A, Notarangelo LD, Plebani A. Mutations of CD40 gene cause an autosomal recessive form of immunodeficiency with hyper IgM. *Proc. Natl. Acad. Sci. U.S.A.*. 2001;98(22):12614.
19. Veerasubramanian PK, Wynn TA, Quan J, Karlsson FJ. Targeting TNF/TNFR superfamilies in immune-mediated inflammatory diseases. *J. Exp. Med.*.2024;221(11).
20. de Souza HSP, Fiocchi C. Immunopathogenesis of IBD: current state of the art. *Nat. Rev. Gastroenterol. Hepatol.*. 2016;13(1):13-27.
21. Fukuda K, Miura Y, Maeda T, Hayashi S, Kikuchi K, Takashima Y, Matsumoto T, Kuroda R. LIGHT regulated gene expression in rheumatoid synovial fibroblasts. *Mol. Biol. Rep.*. 2024;51(1):356.
22. Tsokos GC, Lo MS, Reis PC, Sullivan KE. New insights into the immunopathogenesis of systemic lupus erythematosus. *Nat. Rev. Rheumatol.*. 2016;12(12):716-30.
23. Croft M, Benedict CA, Ware CF. Clinical targeting of the TNF and TNFR superfamilies. *Nat. Rev. Drug Discov.*. 2013;12(2):147-68.
24. Upadhyay V, Fu Y-X. Lymphotoxin signalling in immune homeostasis and the control of microorganisms. *Nat. Rev. Immunol.*. 2013;13(4):270-9.
25. Androlewicz MJ, Browning JL, Ware CF. Lymphotoxin is expressed as a heteromeric complex with a distinct 33-kDa glycoprotein on the surface of an activated human T cell hybridoma. *J. Biol. Chem.*. 1992;267(4):2542-7.
26. Browning JL, Dougas I, Ngam-ek A, Bourdon PR, Ehrenfels BN, Miatkowski K, Zafari M, Yampaglia AM, Lawton P, Meier W. Characterization of surface lymphotoxin forms. Use of specific monoclonal antibodies and soluble receptors. *J Immunol.*. 1995;154(1):33-46.
27. Mauri DN, Ebner R, Montgomery RI, Kochel KD, Cheung TC, Yu GL, Ruben S, Murphy M, Eisenberg RJ, Cohen GH, Spear PG, Ware CF. LIGHT, a new member of the TNF superfamily, and lymphotoxin alpha are ligands for herpesvirus entry mediator. *Immunity.* 1998;8(1):21-30.
28. Wang J, Chun T, Lo JC, Wu Q, Wang Y, Foster A, Roca K, Chen M, Tamada K, Chen L, Wang C-R, Fu Y-X. The Critical Role of LIGHT, a TNF Family Member, in T Cell Development. *J Immunol.*. 2001;167(9):5099-105.
29. Sen R, Baltimore D. Inducibility of kappa immunoglobulin enhancer-binding protein Nf-kappa B by a posttranslational mechanism. *Cell.* 1986;47(6):921-8.
30. Häussinger D, Bode J, Buschmann T, Choi SS, Diehl AM, Drasdo D, Eglinger J, DeFrances MC, Fürst G, Gasbarrini A, Knoefel W, Kordes C, Gebhardt R, Michalopoulos GK, Hoehme S, Petersen BE, Hovhannisyan A, Pfeffer K, Schmelzle M, Sawitza I. *Liver Regeneration*. Dieter H, editor: De Gruyter; 2011.
31. Wilson NS, Dixit V, Ashkenazi A. Death receptor signal transducers: nodes of coordination in immune signaling networks. *Nat. Immunol.*. 2009;10(4):348-55.
32. Probert L. TNF and its receptors in the CNS: The essential, the desirable and the deleterious effects. *Neuroscience.* 2015;302:2-22.
33. Brenner D, Blaser H, Mak TW. Regulation of tumour necrosis factor signalling: live or let die. *Nat. Rev. Immunol.*. 2015;15(6):362-74.
34. Faustman D, Davis M. TNF receptor 2 pathway: drug target for autoimmune diseases. *Nat. Rev. Drug Discov.*. 2010;9(6):482-93.

35. Park YC, Ye H, Hsia C, Segal D, Rich RL, Liou H-C, Myszka DG, Wu H. A Novel Mechanism of TRAF Signaling Revealed by Structural and Functional Analyses of the TRADD-TRAF2 Interaction. *Cell.* 2000;101(7):777-87.
36. Grech AP, Gardam S, Chan T, Quinn R, Gonzales R, Basten A, Brink R. Tumor Necrosis Factor Receptor 2 (TNFR2) Signaling Is Negatively Regulated by a Novel, Carboxyl-terminal TNFR-associated Factor 2 (TRAF2)-binding Site. *J. Biol. Chem.*. 2005;280(36):31572-81.
37. Ware CF, VanArsdale TL, Crowe PD, Browning JL. The ligands and receptors of the lymphotoxin system. *Curr. Top. Microbiol. Immunol.*. 1995;198:175-218.
38. Consortium TU. UniProt: the universal protein knowledgebase in 2021. *Nucleic Acids Res.*. 2020;49(D1):D480-D9.
39. Liu SW, Sun F, Rong SJ, Wang T, Wang CY. Lymphotoxins Serve as a Novel Orchestrator in T1D Pathogenesis. *Front. Immunol.*. 2022;13:917577.
40. Williams-Abbott L, Walter BN, Cheung TC, Goh CR, Porter AG, Ware CF. The lymphotoxin-alpha (LTalpha) subunit is essential for the assembly, but not for the receptor specificity, of the membrane-anchored LTalpha1beta2 heterotrimeric ligand. *J. Biol. Chem.*. 1997;272(31):19451-6.
41. Kucka K, Lang I, Zhang T, Siegmund D, Medler J, Wajant H. Membrane lymphotoxin-α(2)β is a novel tumor necrosis factor (TNF) receptor 2 (TNFR2) agonist. *Cell Death Dis.*. 2021;12(4):360.
42. Ware CF. Network communications: lymphotoxins, LIGHT, and TNF. *Annu. Rev Immunol.*. 2005;23:787-819.
43. Fütterer A, Mink K, Luz A, Kosco-Vilbois MH, Pfeffer K. The Lymphotoxin β Receptor Controls Organogenesis and Affinity Maturation in Peripheral Lymphoid Tissues. *Immunity.* 1998;9(1):59-70.
44. Koni PA, Sacca R, Lawton P, Browning JL, Ruddle NH, Flavell RA. Distinct roles in lymphoid organogenesis for lymphotoxins alpha and beta revealed in lymphotoxin beta-deficient mice. *Immunity.* 1997;6(4):491-500.
45. Scheu S, Alferink J, Pötzel T, Barchet W, Kalinke U, Pfeffer K. Targeted Disruption of LIGHT Causes Defects in Costimulatory T Cell Activation and Reveals Cooperation with Lymphotoxin β in Mesenteric Lymph Node Genesis. *J. Exp. Med.*. 2002;195(12):1613-24.
46. Rennert PD, James D, Mackay F, Browning JL, Hochman PS. Lymph node genesis is induced by signaling through the lymphotoxin beta receptor. *Immunity.* 1998;9(1):71-9.
47. Banks TA, Rouse BT, Kerley MK, Blair PJ, Godfrey VL, Kuklin NA, Bouley DM, Thomas J, Kanangat S, Mucenski ML. Lymphotoxin-alpha-deficient mice. Effects on secondary lymphoid organ development and humoral immune responsiveness. *J. Immunol.*. 1995;155(4):1685-93.
48. Gommerman JL, Browning JL. Lymphotoxin/light, lymphoid microenvironments and autoimmune disease. *Nat. Rev. Immunol.*. 2003;3(8):642-55.
49. Anders RA, Subudhi SK, Wang J, Pfeffer K, Fu YX. Contribution of the lymphotoxin beta receptor to liver regeneration. *J. Immunol.*. 2005;175(2):1295-300.
50. Fausto N. Involvement of the innate immune system in liver regeneration and injury. *J. Hepatol.*. 2006;45(3):347-9.
51. Tumanov AV, Koroleva EP, Christiansen PA, Khan MA, Ruddy MJ, Burnette B, Papa S, Franzoso G, Nedospasov SA, Fu YX, Anders RA. T cell-derived lymphotoxin regulates liver regeneration. *Gastroenterology.* 2009;136(2):694-704 e4.
52. Behnke K, Zhuang Y, Xu HC, Sundaram B, Reich M, Shinde PV, Huang J, Modares NF, Tumanov AV, Polz R, Scheller J, Ware CF, Pfeffer K, Keitel V, Häussinger

D, Pandyra AA, Lang KS, Lang PA. B Cell-Mediated Maintenance of Cluster of Differentiation 169-Positive Cells Is Critical for Liver Regeneration. *Hepatology*. 2018;68(6):2348-61.
53. Tumanov AV, Grivennikov SI, Shakhov AN, Rybtsov SA, Koroleva EP, Takeda J, Nedospasov SA, Kuprash DV. Dissecting the role of lymphotoxin in lymphoid organs by conditional targeting. *Immunol. Rev.*. 2003;195:106-16.
54. Behnke K. Moleküle der TNF/TNFR Superfamilie: Rolle bei der Immunabwehr und Leberregeneration. Heinrich-Heine-Universität, Düsseldorf 2014.
55. Fu Y-X, Chaplin DD. Development and maturation of secondary lymphoid tissues. *Annu. Rev. Immunol.*. 1999;17(1):399-433.
56. Pfeffer K, Matsuyama T, Kündig TM, Wakeham A, Kishihara K, Shahinian A, Wiegmann K, Ohashi PS, Krönke M, Mak TW. Mice deficient for the 55 kd tumor necrosis factor receptor are resistant to endotoxic shock, yet succumb to L. monocytogenes infection. *Cell.* 1993;73(3):457-67.
57. Yamada Y, Kirillova I, Peschon JJ, Fausto N. Initiation of liver growth by tumor necrosis factor: deficient liver regeneration in mice lacking type I tumor necrosis factor receptor. *Proc. Natl. Acad. Sci. U.S.A.*. 1997;94(4):1441-6.
58. Yamada Y, Webber EM, Kirillova I, Peschon JJ, Fausto N. Analysis of liver regeneration in mice lacking type 1 or type 2 tumor necrosis factor receptor: requirement for type 1 but not type 2 receptor. *Hepatology.* 1998;28(4):959-70.
59. Wolfsberg TG, Straight PD, Gerena RL, Huovila A-PJ, Primakoff P, Myles DG, White JM. ADAM, a widely distributed and developmentally regulated gene family encoding membrane proteins with a disintegrin and metalloprotease domain. *Dev. Biol.*. 1995;169(1):378-83.
60. Seals DF, Courtneidge SA. The ADAMs family of metalloproteases: multidomain proteins with multiple functions. *Genes Dev.*. 2003;17(1):7-30.
61. Blobel CP. ADAMs: key components in EGFR signalling and development. *Nat. Rev. Mol. Cell Biol.*. 2005;6(1):32-43.
62. Bode W, Gomis-Rüth FX, Stöckler W. Astacins, serralysins, snake venom and matrix metalloproteinases exhibit identical zinc-binding environments (HEXXHXXGXXH and Met-turn) and topologies and should be grouped into a common family, the 'metzincins'. *FEBS Lett.*. 1993;331(1-2):134-40.
63. Edwards DR, Handsley MM, Pennington CJ. The ADAM metalloproteinases. *Mol. Asp. Med.*. 2008;29(5):258-89.
64. Nakayama K. Furin: a mammalian subtilisin/Kex2p-like endoprotease involved in processing of a wide variety of precursor proteins. *Biochem. J.*. 1997;327 (Pt 3)(Pt 3):625-35.
65. Schlöndorff J, Becherer JD, Blobel CP. Intracellular maturation and localization of the tumour necrosis factor alpha convertase (TACE). *Biochem. J.*. 2000;347 Pt 1(Pt 1):131-8.
66. Tellier E, Canault M, Rebsomen L, Bonardo B, Juhan-Vague I, Nalbone G, Peiretti F. The shedding activity of ADAM17 is sequestered in lipid rafts. *Exp. Cell Res.*. 2006;312(20):3969-80.
67. Chalaris A, Rabe B, Paliga K, Lange H, Laskay T, Fielding CA, Jones SA, Rose-John S, Scheller J. Apoptosis is a natural stimulus of IL6R shedding and contributes to the proinflammatory trans-signaling function of neutrophils. *Blood.* 2007;110(6):1748-55.
68. Adrain C, Zettl M, Christova Y, Taylor N, Freeman M. Tumor necrosis factor signaling requires iRhom2 to promote trafficking and activation of TACE. *Science.* 2012;335(6065):225-8.

69. Ludwig A, Hundhausen C, Lambert MH, Broadway N, Andrews RC, Bickett DM, Leesnitzer MA, Becherer JD. Metalloproteinase inhibitors for the disintegrin-like metalloproteinases ADAM10 and ADAM17 that differentially block constitutive and phorbol ester-inducible shedding of cell surface molecules. *Comb. Chem. High Throughput Screen.*. 2005;8(2):161-71.
70. Hahn D, Pischitzis A, Roesmann S, Hansen MK, Leuenberger B, Luginbuehl U, Sterchi EE. Phorbol 12-myristate 13-acetate-induced ectodomain shedding and phosphorylation of the human meprinbeta metalloprotease. *J. Biol. Chem.*. 2003;278(44):42829-39.
71. Le Gall SM, Maretzky T, Issuree PD, Niu XD, Reiss K, Saftig P, Khokha R, Lundell D, Blobel CP. ADAM17 is regulated by a rapid and reversible mechanism that controls access to its catalytic site. *J. Cell Sci.*. 2010;123(Pt 22):3913-22.
72. Saad MI, Jenkins BJ. The protease ADAM17 at the crossroads of disease: revisiting its significance in inflammation, cancer, and beyond. *FEBS J.*. 2024;291(1):10-24.
73. Chalaris A, Adam N, Sina C, Rosenstiel P, Lehmann-Koch J, Schirmacher P, Hartmann D, Cichy J, Gavrilova O, Schreiber S, Jostock T, Matthews V, Häsler R, Becker C, Neurath MF, Reiss K, Saftig P, Scheller J, Rose-John S. Critical role of the disintegrin metalloprotease ADAM17 for intestinal inflammation and regeneration in mice. *J. Exp. Med.*. 2010;207(8):1617-24.
74. Brodowicz T, Wiltschke C, Budinsky AC, Krainer M, Steger GG, Zielinski CC. Soluble HER-2/neu neutralizes biologic effects of anti-HER-2/neu antibody on breast cancer cells in vitro. *Int. J. Cancer*. 1997;73(6):875-9.
75. Lichtenthaler SF, Lemberg MK, Fluhrer R. Proteolytic ectodomain shedding of membrane proteins in mammals-hardware, concepts, and recent developments. *EMBO J.*. 2018;37(15).
76. Chalaris A, Garbers C, Rabe B, Rose-John S, Scheller J. The soluble Interleukin 6 receptor: generation and role in inflammation and cancer. *Eur. J. Cell Biol.*. 2011;90(6-7):484-94.
77. Reiss K, Saftig P. The "a disintegrin and metalloprotease" (ADAM) family of sheddases: physiological and cellular functions. *Semin. Cell Dev. Biol.*. 2009;20(2):126-37.
78. Scheller J, Chalaris A, Garbers C, Rose-John S. ADAM17: a molecular switch to control inflammation and tissue regeneration. *Trends Immunol.*. 2011;32(8):380-7.
79. Smith TM, Jr., Tharakan A, Martin RK. Targeting ADAM10 in Cancer and Autoimmunity. *Front. Immunol.*. 2020;11:499.
80. Tucher J, Linke D, Koudelka T, Cassidy L, Tredup C, Wichert R, Pietrzik C, Becker-Pauly C, Tholey A. LC–MS Based Cleavage Site Profiling of the Proteases ADAM10 and ADAM17 Using Proteome-Derived Peptide Libraries. *J. Proteome Res.*. 2014;13(4):2205-14.
81. Walsh G. Biopharmaceutical benchmarks 2018. *Nat Biotechnol.*. 2018;36(12):1136-45.
82. Baran P, Hansen S, Waetzig GH, Akbarzadeh M, Lamertz L, Huber HJ, Ahmadian MR, Moll JM, Scheller J. The balance of interleukin (IL)-6, IL-6·soluble IL-6 receptor (sIL-6R), and IL-6·sIL-6R·sgp130 complexes allows simultaneous classic and trans-signaling. *J. Biol. Chem.*. 2018;293(18):6762-75.
83. Ketteler R, Glaser S, Sandra O, Martens UM, Klingmüller U. Enhanced transgene expression in primitive hematopoietic progenitor cells and embryonic stem cells efficiently transduced by optimized retroviral hybrid vectors. *Gene Ther.*. 2002;9(8):477-87.

84. Laemmli UK. Cleavage of structural proteins during the assembly of the head of bacteriophage T4. *Nature*. 1970;227(5259):680-5.
85. Hundhausen C, Misztela D, Berkhout TA, Broadway N, Saftig P, Reiss K, Hartmann D, Fahrenholz F, Postina R, Matthews V, Kallen KJ, Rose-John S, Ludwig A. The disintegrin-like metalloproteinase ADAM10 is involved in constitutive cleavage of CX3CL1 (fractalkine) and regulates CX3CL1-mediated cell-cell adhesion. *Blood*. 2003;102(4):1186-95.
86. Rasmussen HS, McCann PP. Matrix metalloproteinase inhibition as a novel anticancer strategy: a review with special focus on batimastat and marimastat. *Pharmacol. Ther.*. 1997;75(1):69-75.
87. UniProt Consortium. UniProtKB - P41155 (TNFC_MOUSE) [Internet]. *UniProt*; 2021 [updated 2021 Jun 2; cited 2025 Jul 24]. Available from: https://www.uniprot.org/uniprot/P41155
88. Iwagishi R, Tanaka R, Seto M, Takagi T, Norioka N, Ueyama T, Kawamura T, Takagi J, Ogawa Y, Shirakabe K. Negatively charged amino acids in the stalk region of membrane proteins reduce ectodomain shedding. *J. Biol. Chem.*. 2020;295(35):12343-52.
89. Caescu CI, Jeschke GR, Turk BE. Active-site determinants of substrate recognition by the metalloproteinases TACE and ADAM10. *Biochem. J.*. 2009;424(1):79-88.
90. Zingoni A, Vulpis E, Loconte L, Santoni A. NKG2D Ligand Shedding in Response to Stress: Role of ADAM10. *Front. Immunol.*. 2020;11:447.
91. Waldhauer I, Goehlsdorf D, Gieseke F, Weinschenk T, Wittenbrink M, Ludwig A, Stevanovic S, Rammensee HG, Steinle A. Tumor-associated MICA is shed by ADAM proteases. *Cancer Res.*. 2008;68(15):6368-76.
92. Häussinger D, Bode J, Buschmann T, Choi SS, Diehl AM, Drasdo D, Eglinger J, DeFrances MC, Fürst G, Gasbarrini A, Knoefel W, Kordes C, Gebhardt R, Michalopoulos GK, Hoehme S, Petersen BE, Hovhannisyan A, Pfeffer K, Schmelzle M, Sawitza I. *Liver Regeneration.* Häussinger D, editor. Berlin/Boston: Walter de Gruyter GmbH & Co. KG; 2011 2011.
93. Salzer U, Chapel HM, Webster ADB, Pan-Hammarström Q, Schmitt-Graeff A, Schlesier M, Peter HH, Rockstroh JK, Schneider P, Schäffer AA, Hammarström L, Grimbacher B. Mutations in TNFRSF13B encoding TACI are associated with common variable immunodeficiency in humans. *Nat. Genet.*. 2005;37(8):820-8.
94. Hughes AE, Ralston SH, Marken J, Bell C, MacPherson H, Wallace RGH, van Hul W, Whyte MP, Nakatsuka K, Hovy L, Anderson DM. Mutations in TNFRSF11A, affecting the signal peptide of RANK, cause familial expansile osteolysis. *Nat. Genet.*. 2000;24(1):45-8.
95. Braun A, Takemura S, Vallejo AN, Goronzy JJ, Weyand CM. Lymphotoxin beta-mediated stimulation of synoviocytes in rheumatoid arthritis. *Arthritis Rheum.*. 2004;50(7):2140-50.
96. Albarbar B, Dunnill C, Georgopoulos NT. Regulation of cell fate by lymphotoxin (LT) receptor signalling: Functional differences and similarities of the LT system to other TNF superfamily (TNFSF) members. *Cytokine Growth Factor Rev.*. 2015;26(6):659-71.
97. Shirakabe K, Omura T, Shibagaki Y, Mihara E, Homma K, Kato Y, Yoshimura A, Murakami Y, Takagi J, Hattori S, Ogawa Y. Mechanistic insights into ectodomain shedding: susceptibility of CADM1 adhesion molecule is determined by alternative splicing and O-glycosylation. *Sci Rep.*. 2017;7:46174.
98. Garbers C, Monhasery N, Aparicio-Siegmund S, Lokau J, Baran P, Nowell MA, Jones SA, Rose-John S, Scheller J. The interleukin-6 receptor Asp358Ala single

nucleotide polymorphism rs2228145 confers increased proteolytic conversion rates by ADAM proteases. *Biochim Biophys Acta*. 2014;1842(9):1485-94.
99. Lipper CH, Egan ED, Gabriel KH, Blacklow SC. Structural basis for membrane-proximal proteolysis of substrates by ADAM10. *Cell.* 2023;186(17):3632-41.e10.
100. Lu F, Zhao H, Dai Y, Wang Y, Lee CH, Freeman M. Cryo-EM reveals that iRhom2 restrains ADAM17 protease activity to control the release of growth factor and inflammatory signals. *Mol. Cell.* 2024;84(11):2152-65.e5.
101. Garbers C, Jänner N, Chalaris A, Moss ML, Floss DM, Meyer D, Koch-Nolte F, Rose-John S, Scheller J. Species specificity of ADAM10 and ADAM17 proteins in interleukin-6 (IL-6) trans-signaling and novel role of ADAM10 in inducible IL-6 receptor shedding. *J. Biol. Chem.* 2011;286(17):14804-11.
102. Müllberg J, Oberthür W, Lottspeich F, Mehl E, Dittrich E, Graeve L, Heinrich PC, Rose-John S. The soluble human IL-6 receptor. Mutational characterization of the proteolytic cleavage site. *J. Immunol.* 1994;152(10):4958-68.
103. Moss ML, Minond D. Recent Advances in ADAM17 Research: A Promising Target for Cancer and Inflammation. *Mediators Inflamm.*. 2017;2017:9673537.
104. Yan S, Zhao Y, Yang Y, Liu B, Xu W, Ma Z, Yang Q. Progress of ADAM17 in Fibrosis-Related Diseases. *Mediators Inflamm.*. 2025;2025:9999723.
105. Cathcart JM, Cao J. MMP Inhibitors: Past, present and future. *Front Biosci (Landmark Ed)*. 2015;20(7):1164-78.
106. Medicine NLo. National Library of Medicine Gene database [web page]. National Center for Biotechnology Information; 2023 [cited 2023 08/04]. Available from: https://www.ncbi.nlm.nih.gov/gene.
107. Browning JL, Ngam-ek A, Lawton P, DeMarinis J, Tizard R, Chow EP, Hession C, O'Brine-Greco B, Foley SF, Ware CF. Lymphotoxin beta, a novel member of the TNF family that forms a heteromeric complex with lymphotoxin on the cell surface. *Cell*. 1993;72(6):847-56.
108. Liepinsh DJ, Grivennikov SI, Klarmann KD, Lagarkova MA, Drutskaya MS, Lockett SJ, Tessarollo L, McAuliffe M, Keller JR, Kuprash DV, Nedospasov SA. Novel lymphotoxin alpha (LTalpha) knockout mice with unperturbed tumor necrosis factor expression: reassessing LTalpha biological functions. *Mol. Cell Biol.*. 2006;26(11):4214-25.
109. Alexopoulou L, Pasparakis M, Kollias G. Complementation of lymphotoxin alpha knockout mice with tumor necrosis factor-expressing transgenes rectifies defective splenic structure and function. *J. Exp. Med.*. 1998;188(4):745-54.
110. Falvo JV, Tsytsykova AV, Goldfeld AE. Transcriptional control of the TNF gene. *Curr Dir Autoimmun.*. 2010;11:27-60.
111. Liu H, Sidiropoulos P, Song G, Pagliari LJ, Birrer MJ, Stein B, Anrather J, Pope RM. TNF-α Gene Expression in Macrophages: Regulation by NF-κB Is Independent of c-Jun or C/EBPβ. *J. Immunol.*. 2000;164(8):4277-85.